THE GEOTECHNICAL CHARACTERISTICS OF A FRAGMENTED SHALE

by

Robert H. Caswell

Submitted in partial fulfillment
of the requirements for the degree of
Master of Applied Science

Department of Civil Engineering

School of Graduate Studies

University of Ottawa

Ottawa, Canada

October, 1982.

To the memory of my father

ABSTRACT

Mechanical shales, such as Queenston Shale, have a tendency to deteriorate rapidly when exposed to the elements, and thus, are poor foundation and building materials. In fragmented conditions, their shear behaviour resembles that of sand.

Large-scale triaxial tests were performed on fragmented Queenston Shale. CID compression tests were performed on natural and weathered specimens of the shale, in saturated and dry states. The shale was found to be resistant to weathering and acid treatment. Weathered material had more or less the same shear behaviour as the natural material. Saturated material had a 10 to 30 % lower value in shear strength (in terms of deviator stress) when compared to dry material. The difference is attributed to increased grain breakage as a result of internal forces created by saturation. The shear strength of saturated, powdered Queenston Shale was 60 % lower than the shear strength of saturated fragmented material. The saturated shear strength of the powdered Queenston Shale is believed to be the same as the dry shear strength. Saturation appears to affect the volume change component of the shear strength and not the pure shear one.

The elastic parameters, K and G were determined from the compression tests under monotonic loading conditions. The shear modulus is dependent on the mean normal stress and is the same for saturated and dry cases. The bulk modulus is constant for all types of the material.

The tangent modulus parameters of fragmented Queenston Shale were calculated from the test results. The parameter β is approximately zero, while the parameter m is different for dry and saturated conditions.

ACKNOWLEDGEMENTS

The author is indebted to Dr. W. J. Thompson, original Thesis Supervisor, for suggesting the project, and for his guidance and financial assistance during the first half of this research project.

The author would like to extend his sincere appreciation to Dr. B. H. Fellenius, Thesis Supervisor, for his interest, time, guidance, and financial assistance during the last half of this research project.

Dr. B. Trak and Dr. C. Papantonopoulos, Professors of the Department of Civil Engineering, are thanked for their interest and advice towards the completion of this project.

Dr. B. Rust, Chairman of the Department of Geology, is thanked for his interest and assistance towards the performance of laboratory tests for this study.

The Domtar Construction Material Co. is thanked for its permission and cooperation towards the acquisition of testing material.

Grateful appreciation is extended towards Mr. R. J. Moore for his inovative ideas regarding the testing apparatus and for his assistance in laboratory work. Gratitude is also expressed to Mr. R. Brunet and Mr. W. Dick for their skillful assistance with the laboratory testing programme.

Sincere thanks are also extended to my mother for her encouragement and skillful typing of this manuscript.

TABLE OF CONTENTS

LIST OF FIGURES

LIST OF TABLES

LIST OF PLATES

NOTATION

Since much of the equipment used in this study was calibrated in Imperial units, most S.I. values used in this text are soft conversions.

a_o	initial cross-sectional area of specimen
AW	acid treated specimen
b	grain shape factor
C_u	coefficient of uniformity
D	initial diameter of specimen
e	void ratio
e_o	initial void ratio
E	Young's modulus
F_j	intragranular force
F_{zi}	component of intragranular force in the z direction
G	shear modulus
H	depth of a layer
I	invariant of stress
J	invariant of principal stress
K	bulk modulus
K_c	stress ratio
m	modulus number
M	tangent modulus
M	compression modulus of rubber
n_s	surface concentration
N	normal component of contact force
N	dry natural specimen

NW	saturated natural specimen
p'	$1/3(\sigma'_1+\sigma'_2+\sigma'_3)$
P	applied stress
P_r	reference stress
P_{ij}	contact force
PD	dry powdered specimen
PW.	dry powdered specimen
q'	$(\sigma'_1-\sigma'_3)$
R	friction force
t	rolling stress
T	tangential component of contact force
u	displacement
v	specific volume
w	water content
x, y, z	coordinate axes (z-vertical)
25D	dry weathered specimen
25W	saturated weathered specimen
β	stress exponent
γ	shear strain
δ	vertical settlement
ε	strain
ε_1	major principal strain
ε_3	minor principal strain
ε_a	axial strain

$\varepsilon_v, \varepsilon_{vol}$	volumetric strain
$(\varepsilon_1 - \varepsilon_3)$	deviatoric strain
λ	slope of failure line, normal consolidation line
λ	Lambe's constant
μ	coefficient of friction
μ	Lambe's constant
ν	Poisson's ratio
σ	normal stress
σ_{conf}	confining stress
σ_m	mean normal stress
σ_1	major principal stress
σ_3	minor principal stress
σ_{1c}	major principal consolidation stress
σ_{3c}	minor principal consolidation stress
σ_{oct}	octahedral normal stress
τ	shear stress
τ_{oct}	octahedral shear stress
ϕ	angle of internal friction
ϕ	diffraction angle
ϕ_{dry}	angle of internal friction for dry condition
ϕ_{sat}	angle of internal friction for saturated conditions

Chapter 1

Introduction

1.1 Objective

Approximately 75 % of all rocks exposed at the surface of the earth are sedimentary. Shales comprise a large portion of these outcrops, and are encountered in many large scale, civil engineering projects. Construction in such areas results in foundation work in rock of unreliable strength and unpredictable deformability behaviour. Construction involving rockfill derived from shale materials experiences similar problems of uncertainty with respect to design parameters.

The purpose of this study is to establish the stress-strain and strength characteristics of a fragmented mechanical shale, Queenston Shale, as observed in a large conventional triaxial test apparatus. These parameters should be useful for the analysis of stability and deformability of rockfills composed of this or similar materials.

1.2 Definitions

Mechanical shales are formed by the compression of sediments originating from the products of the breakdown of pre-existing rocks. The classification "mechanical shale" refers to the major trend in the compositon of the rock and needs not imply that mechanical shales are entirely without some cementing materials (Pettijohn 1975). Mechanical shales are weak when compared to cemented shales and igneous rocks, because the bonds of the former are not as strong as the crystalline bonds of the later group.

In addition to inherent weakness, mechanical shales slake when exposed to water and air. Slaking is a term which describes the desintegration of rock, usually shale, upon alternate drying and wetting.

Freezing and thawing, and chemical or biochemical deterioration can also contribute to desintegration of shales and most rocks. Often breakdown is the result of a combination of the four processes. Small organisms and plants alter minerals within rock, eventually leading to a breakdown of the rock. Acids, produced by the combination of infiltrated water and certain compounds within some rocks, destroy crystalline bonding. Freezing and thawing of water in cracks within rock produce local failure as a result of the stresses created by the expansion of ice. Alternate cycles of wetting and drying produce capillary and thermal stresses that break up rock. In addition, if a rock contains an expansive mineral, such as montmorillonite, saturation induces fracture stresses.

1.3 Occurrence and Uses

Mechanical shales outcrop, or are located close to the surface in many areas of North America. The Cretacious shales of Central Alberta and Eastern British Columbia, the Brunswick shales of New Jersey and Southern New York, and the Ordivician shales of Southern Ontario fall in this generalization.

In Alberta, strip mining and dam construction result in large volumes of fragmented, mechanical shales. In both cases, the rock is obtained by ripping and blasting.

The fragmented shale arising from mining operations is usually of little commercial value, and must be disposed of. The disposal presents a major problem for mining companies, because of the low strength of the rock and its potential for rapid deterioration with time. The normal procedure in open pit operations is to dump the rock in large piles at mined-out areas of the pit, or in the case of underground mining, to truck the material to available disposal sites. Spoil piles or tips formed from such rock often incurred long term stability problems, because consideration was only given to design parameters based on initial or fresh conditions, and not to the possibility that the competence of the rock might diminish with time, (Pit Slope Manual 1977).

Similar stability problems could occur in dam and embankment construction using mechanical shales as building materials. Such a situation would occur where there was a lack of sound rock and the economic advantages of using local rock outweighed the alternatives. The shales would then acquire commercial value.

When economic worth is implied, fragmented rock is known as rockfill. Rockfill fragments can range in size from 15 mm to 1 m or more, depending on the purpose.

The stability of dams and spoil heaps requires obtaining a realistic estimate of the shear strength of the material utilized. However, the shear strength is not necessarily the most important parameter for all types of geotechnical engineering designs. For example, large building construction, such as in

Piscataway Township, New Jersey are more concerned with settlement predictions than shear strength, (Jumikis and Jumikis 1975).

The economic repercussion of differential settlements emphasizes the need to properly predict settlements, while the failure of large mine tips, such as at Aberfan, Wales in 1966, points up the importance of ensuring the stability of man-made slopes through proper shear strength investigations.

CHAPTER 2

LITERATURE REVIEW

2.1 Background

Since the emergence of Soil Mechanics as an applied science in the early 1920's, the study of rockfill has been associated with the examination of the behaviour of cohesionless materials, which has been centered mainly on the behaviour of sand. The study of rockfill assumed a secondary standing to that of sand, because its behaviour was less of an engineering problem and, as long as structures were small, was easier to predict. In addition, the great cost of building testing equipment large enough to handle large pieces of rock led to the sparseness of reasearch in this area.

Most work on rockfill, up to date, has been connected with the behaviour of rockfill dams. According to Steele (1951), the design of rockfill dams originated in California soon after the discovery there of gold in 1848. They were generally of small proportions and daringly designed. The highly steeped slopes of these early dams have stood solidly for over 100 years with only the slightest trace of bulging near the bases of their downstream slopes.

Traditional rockfill is a strong building material and its behaviour resembles that of most cohesionless materials. Like sand, rockfill is free draining. In fact, the behaviour of both sand and rockfill are so similar that it seems necessary to include in this chapter a review of literature pertaining to the study of the nature of sands. The chapter is divided into three main sections: the behaviour of sand, the behaviour of rockfill, and strength theories for rockfill.

2.2 Behaviour of Sand

Early investigations into the behaviour of sands were mainly concerned with fundamental problems such as settlement characteristics and shear strength.

Terzaghi (1925) was the first to explain the principle behind the piping phenomenon that can occur in dams built on foundations composed of sand.

Casagrande (1936a) introduced the concept of critical void ratio in describing flow of cohesionless materials, that is to say a continuous deformation at constant shearing stress. In his other works, Casagrande (1936b) described the dependence of the angle of shearing resistance on the initial void ratio of some sands. Dense sands were found to have higher ϕ values than loose ones.

Terzaghi and Peck (1948) tested loose and dense sands in the triaxial apparatus at confining pressures of less than 1 MPa. They observed that under shearing loose sands behaved similarly to normally consolidated clays, that is, decreased in volume, while dense sands behaved as overconsolidated clays, that is, expanded in volume or exhibited dilatancy. Terzaghi and Peck (1948) presented charts for estimating allowable soil pressure for footings on sand on the basis of results of standard penetration test.

Taylor (1948) stated that the drained shear strength of sand was unaffected by the presence of water. In order to explain the influence of the void ratio on the angle of friction of a sand, Taylor (1948) suggested that part of the shear stress required to cause failure of a dense sand was used in providing the energy required to permit the sand to expand against the confining pressure. This investigator suggested that the shearing resistance was the combined result of two factors: friction and a volume change component, which he called interlocking. Taylor (1948) expanded on this theory by developing an expression for the shear stress required to provide energy for expansion for a sample in a direct shear test. Subsequently, Bishop (1954) derived an expression to determine the portion of the applied deviator stress, in a triaxial compression test, which had to be applied to provide energy for sample expansion. Rowe (1962) presented a similar expression to correct the deviator stress for effects of volume change. The three expressions are found in Appendix D.

It was not until the early 1960's that studies were made into the behaviour of sand subjected to stresses beyond the conventional range. De Beer (1965) conducted compression and penetration tests on a dense sand at pressures up to 350 MPa. This investigator found that a dense sand, located at high foundation depth, behaved more and more as a loose sand. The sand showed high relative settlement under the footing, more or less, of the same order as the settlement of a footing at the surface on a very loose sand.

Vesic and Clough (1968) defined a pressure range terminology as follows: Low Pressures, 0 to 1 MPa; Elevated Pressures, 1 to 10

MPa; High Pressures, 10 to 100 MPa; Very High Pressures, 100 MPa to 1 GPa; and Ultra High Pressures, those beyond 1 GPa. Vesic and Clough (1968) concluded that the nature of sand deformation varied with the pressure range. At Very Low Pressures, there was very little crushing. However, because the sand particles were free to move with respect to each other, dilatancy effects were quite significant. As the normal stress increased, crushing became more pronounced and the dilatancy effects gradually disappeared. The investigators found that crushing of the particles was most intense in the Elevated Pressure range, before a breakdown stress was reached. This stress, Vesic and Clough (1968) defined as the stress needed to eliminate all effect of the initial void ratio of sand. Beyond the breakdown stress, the investigators inferred that sand behaved essentially as a linear deformable solid, with a modulus of deformation, E, proportional to the mean normal stress. In addition, the failure characteristics for the High Pressure range were defined by a constant angle of internal friction equivalent to the angle of internal friction, obtained from the Low Pressure range after dilatancy effects were subtracted. Vesic and Clough (1968) observed that, in the Low Pressure range, E increased as the one half power of the mean normal stress. After that range, it increased as the one third power until the breakdown stress was reached.

A number of studies were made in the elevated pressure range by Hirschfeld and Poulos (1963), Hall and Gordon (1963), and by Lee and Seed (1967a). All investigators reported on the structural breakdown of the tested materials when sheared in triaxial compression at high confining stress. Their studies showed curved Mohr-Coulomb envelopes with curvatures pronounced for dense sands. The curvature of the envelopes can be regarded as normal for most geotechnical materials.

Lee and Seed (1967a) indicated that sand was relatively incompressible at low pressures. At high pressures there was considerable volume change due to crushing of the grains, and subsequently, compression continued for a considerable period of time. An increase in confining pressure had three effects: it reduced the brittle characteristics of the stress strain curve, it increased the strain to failure, and it decreased the tendency to dilate. The investigators concluded that the strain and volume change characteristics of dense sand at high confining pressures were not unlike those of loose sand at low pressures, reflecting De Beer's (1965) findings. In addition, Lee and Seed (1967a) found that the volume changes, which accompanied the shearing deformation, tended to produce samples with the same void ratio at failure. This fact was true for all confining pressures, even though the initial void ratios were vastly different. The failure envelopes were curved up to confining pressures of 4 MPa. Beyond this value, they tended to flatten out and, when projected back, passed through the origin. Application of the Bishop (1954) expression for dilatancy for the low pressure range flattened the failure envelopes.

Lee and Seed (1967b) also studied the effect of moisture on the behaviour of sand by testing an angular sand in drained triaxial compression. Tests were performed on dry and saturated specimens. The deviatoric strength of the saturated material was observed to be 30% to 35% lower than the dry strength. Similar tests on well rounded, uniform Ottawa sand showed no significant change in deviatoric strength between dry and saturated conditions. Lee and Seed (1967b) concluded that the presence of microcracks in the angular particles was at the root of the lower strength of the saturated material. Their rational was that the microcracks in the angular particles were areas of high stress concentration. When water entered the fissures, as a result of the capillary action created, it increased the stress level at these points. Air trapped by the water became pressurized and decreased the capillary tension, which holds the fissures closed. This process caused crushing of the particles to occur more easily when the sand was saturated, as opposed to the dry case, in which the breakdown of the grains was caused by external forces only. The actual tension present is a function of the vapour pressure in equilibrium with capillary water. Similar conclusions were reached by Terzaghi and Peck (1948) and Van Eeckhout (1976).

2.3 Behaviour of Rockfill

According to Leps (1970), the design of rockfill dams up until the late 1940's was based, not on diagnostic testing of the strength of rockfill, but on the satisfactory performance of many prototype fills, together with the application of broad reasoning and engineering intuition. This empirical approach to design had led to satisfactory results. At that time, rockfill was believed to be a satisfactory building material because of rock's inherent massive strength, which was assumed to apply to its fragments. However, because the strength of rockfill was unknown, the degree of stability of dams could not be determined.

Characterization of rockfill behaviour was based on past performance, as published in case histories. For example, Terzaghi and Peck (1948) mentioned that dumped rockfill should be generously watered ("sluiced"), while it was being placed. They pointed out that there was a wide divergence of opinion about the reasons for the beneficial results. They demonstrated the negative results of dry dumping, by citing the case of Cogswell Dam in southern California. The 280 feet dam was built by dry dumping in lifts of 25 feet. Infiltration at the 80% stage of completion caused the crest to settle by 8 to 16 feet.

It was not until the late 1950's and the early 1960's with the advent of higher and larger dams that investigations into the safety of the design had to be performed by quantifying the strength of rockfill.

Early developments in shear testing of rockfill materials were centered on triaxial type apparatus. This kind of apparatus was first developed for soil testing by Leo Jurgenson (1934) and subsequently, improved by Fidler and Watson, graduate students under the guidance of Taylor and Casagrande respectively, between 1936 and 1940. Concurrently, the U.S. Bureau of Reclamation, under the guidance of Loyd W. Hamilton, developed a similar apparatus capable of measuring pore pressures. The first triaxial cell test apparatus for rockfill was constructed in 1947-48 by Earl B. Hall, who was then working in the soils laboratory of the Corps of Engineers, South Pacific Division, at

Los Angeles (Leps 1970).

The next study into the mechanical behaviour of rockfill was undertaken by Holtz and Gibbs (1956). The investigators tested, in the triaxial apparatus, cylindrical specimens varying in size from 35 mm by 75 mm (1 3/8 in by 3 in) to 230 mm by 570 mm (9 in by 22 1/2 in) at three different strain rates with the cell pressure ranging from 100 kPa to 700 kPa. Holtz and Gibbs (1956) concluded that the rate of testing had practically no effect upon the shear test results for all the specimen sizes.

Lee and Farhoomand (1967) studied the compressibility of granular soil and the effects of particle crushing at high pressures, as applied to the design of gravel drains and soil filters for use in high earth dams. Isotropic and anisotropic triaxial compression tests were performed on a number of sands and gravels. The confining pressures applied in the study were within the range of 2 MPa (300 psi)* to 14 MPa (2000 psi). The tests were small scale, the maximum particle size being 20 mm (3/4 in) and the maximum specimen size, 70 mm by 150 mm (2 3/4 in by 6 in). Some of the investigators' conclusions are quoted here.

1. Uniformly graded, granular soils were quite compressible under applied stress.

2. Compression was usually accompanied by particle breakage and the two phenomena were interrelated.

3. Coarse cohesionless soils compressed more and showed more particle crushing than fine soils.

4. Soils with angular particles compressed more and showed more particle crushing than soils with rounded particles.

---

* Regarding SI conversions see Notation.

5. Uniform soils compressed and crushed more than graded soils with the same maximum grain size.

6. Under any particular load, compression and particle crushing continued at an ever-decreasing rate for an indefinite period of time.

7. Both compression and particle breakage appeared to be accelerated by the addition of water and to increase with: a) increasing grain size of uniform soil, b) increasing uniformity of particles, d) decreasing strength of individual particles, e) increasing confining pressures, and f) increasing shear stress at one confining pressure.

8. Since all soil particles crushed and became finer under load, the investigators' data indicated that a soil which met the filter requirements for a certain foundation material before compression also met the filter requirements for the altered foundation state following compression.

9. For the soil tested, there appeared to be a unique relationship between the volume change and the major principal stress which was completely independent of a K_c ratio, introduced by Lee and Farhoomand (1967) and defined as σ_{1c}/σ_{3c}. However, no such relationship was observed with respect to crushing. In the case of crushing, the higher the K_c ratio, the greater was the degree of particle crushing.

Ladanyi (1967) disputed Lee and Farhoomand's (1967) conclusion regarding the relationship between volume change and major principal stress and described it as a statistical curiosity.

Leps (1970) compiled the results of triaxial compression tests, performed on different rockfills up to the year 1969. The compilation contained data from 15 different rockfill materials with maximum particles ranging in size from 20 mm (3/4 in) to 200 mm (8 in). Leps (1970) recomputed the results of the triaxial tests to show friction angles as a function of normal pressures across the failure plane, as deduced from the use of the Mohr diagram. Leps' (1970) conclusions are summarized in the following seven points.

1. An increase in relative density resulted in an increase in friction angle.

2. Improving the gradation by making it well graded, providing it was not done with the addition of finer particles, was found to increase the friction angle at any given normal pressure.

3. Particle breakage was a function of the mean intensity of particle contact force and of the unconfined compressive strength of the rock particles.

4. With reference to particle shape, the more angular the particle, the stronger was the shear strength of the material.

5. Saturated rock, in all aspects, was less strong than dry rock.

6. Failure strains for higher confining pressures were usually two to three times those strains for the lateral pressures below 70 kPa (10 psi).

7. The shearing strength of rockfill, measured by tan ϕ, varied markedly as a function of normal pressure across the failure plane, being high at low pressures and substantially smaller as normal pressures increased.

Hall and Gordon (1963) performed triaxial tests with high pressure equipment on granular specimens of diameters 150 mm and 300 mm. Confining pressures were within the range of 900 kPa to 4500 kPa. The investigators found that the slope of the Mohr failure envelope decreased with increasing lateral pressure. They attributed the decrease to the degradation of particles during shear at high chamber pressures. They found that well-graded specimens, under similar conditions, suffered less crushing than uniformly graded specimens.

Marsal (1965, 1967) investigated the behaviour of materials composed of rock fragments and granular soils of alluvial origin with high contents of gravel and boulders. The research involved triaxial and one dimensional compression tests on large specimens of dimensions 113 cm by 250 cm and 115 cm by 67 cm respectively. The confining pressures for the triaxial test ranged from 500 kPa to 2500 kPa. Highly compacted rockfill exhibited dilatancy at low confining stresses of 700 kPa or smaller. All loose specimens developed compactancy during shear. Within the low pressure range of confinement (smaller than 700 kPa) the deviator stress-strain curves showed marked peaks for dense rockfill. This phenomenon disappeared with increasing confining pressures. On the other hand, similar curves for loose samples showed the deviator stress increasing to a maximum value and levelling off as the strain increased. The Mohr-Coulomb envelope was curved for confining stresses smaller than 3000 kPa (400 psi). The angle of internal friction was greater, the lower the confining stress. Particle breakage occurred above 700 kPa (100 psi) and increased with increasing lateral pressure. Particle breakage changed the grain size distribution and appreciably affected the deformation characteristics of the material tested. Particle breakage was more intense at lower stresses and approached a constant value at high stresses. The degree of particle breakage was dependent on the gradation of the material, the crushing strength of the grains, and the stress level. From friction tests on saturated and dry specimens of rock, Marsal (1973) concluded that the coefficient of friction was not affected by saturation.

Charles and Watts (1980) measured the influence of confining pressure on the angle of shearing resistance for a number of rockfills at low and medium confining pressures. The results of drained triaxial compression tests on heavily compacted well-graded samples of a wide range of rockfills all showed failure envelopes with pronounced curvature at low stresses. In addition, the investigators found that the crushing strength of all the tested materials decreased (up to 50%) when saturated.

Marachi et al. (1972) investigated the scale effect in shear testing of laboratory rockfill specimens. The investigators modelled the grain size distribution of field material and formed laboratory specimens with smaller particles, consisting of grain size distribution curves exactly parallel to that of the field material. The testing program consisted of three series of CID triaxial compression test on typical rockfill materials. Each series consisted of at least four tests on samples having diameter of 900 mm (36 in), 300 mm (12 in), 70 mm (2 3/4 in). The test for each specimen size were performed using effective confining pressures of 200 kPa (30 psi), 1000 kPa (140 psi), 3000 kPa (420 psi), and 5000 kPa (650 psi). A summary of their results follows.

1. According to Marachi et al. (1972) the modelling technique provided a useful method for predicting the strength and deformation characteristics of field rockfill materials through extrapolation. However, they did not mention any scaling method for extrapolation.

2. Isotropic consolidation characteristics of specimens with parallel grain size curves were the same.

3. The angle of internal friction was affected by the size of the particles in the test specimen. At any given confining pressure, the angle of internal friction for the 900 mm specimen was about 1° to 1.5° lower than that of the 300 mm specimen and 3° to 4° lower than the 70 mm specimen. This trend remained unaffected by the confining pressure or the material type.

4. The volume change during drained triaxial compression tests was smallest for the 70 mm specimens. The volume change of the 900 mm specimens had a tendency to be greater than that of the 300 mm specimens. Particle shape had a much greater effect on the volume change characteristics during shear than mineralogy.

5. The axial strain at failure increased as the maximum particle size increased.

6. The axial and volumetric strains at failure increased as the confining pressure increased, although the trend indicated that this effect would be small beyond 5000 kPa (650 psi). The angle of internal friction decreased as the confining pressure

increased, but again the trend indicated that this would not be appreciable beyond 5000 kPa. This maximum pressure corresponded to Vesic and Clough's (1968) breakdown stress in sands, and was the stress at which rockfill started to behave as a linearly deformable solid.

7. Materials, composed of well-graded and well rounded particles, were superior in their mechanical properties to uniformly-graded angular rockfill materials and thus, more suitable for use in high dams.

Point No. 7. contradicts Leps' (1970) 4th conclusion about the best rockfill being angular. The disagreement can best be resolved by examining the pressures to which the rockfill was subjected. Leps' (1970) study was at low stresses, a range where particle breakage was minimal, and where angularity of fragments provided more strength because of interlocking. At high stresses, angular particles underwent more breakage because of the high contact forces acting on knife edge areas. Like the angular sand studied by Lee and Seed (1967b), the shear strength of highly stressed rockfill was reduced by saturation. Lee and Seed (1967b) established that the presence of microcracks in the angular particles caused the reduction of strength.

Tests reported in the literature survey have established that rock was weaker when saturated. Van Eeckhout (1976) described five mechanisms that could be responsible for the reduction of strength. These were: a) fracture energy reduction, b) pore pressure increase, c) friction reduction, d) chemical and corrosive deterioration, and e) capillary tension. Fracture energy reduction occurs in any rock (or rock fragment) in the presence of liquids (water) due to the decrease of surface energy, according to Griffith's Theory (1921). This theory attributes the brittle fracture of a material to the existence of innumerable cracks and flaws, and that in compression large tensile stresses exist near the ends of certain critically oriented cracks, (Jaeger 1972). Local pore pressure increase reduces strength by the principle of effective stress, affecting rounded and angular particles in the same way. Friction reduction has been discounted by Taylor (1948) and by most researchers because the coefficient of friction is not affected by saturation (Marsal 1973). Chemical and corrosive deterioration does not apply to rockfill, unless the materials contain chemicals which are acid forming when combined with water. This is uncommon, however. Capillary tension decrease combined with a high portion of saturated fissures is likely the main cause in the difference in behaviour of angular and rounded rockfill, when saturated. This conclusion was reached by Lee and Seed (1967b) and was already suggested by Terzaghi and Peck (1948) in their explanation of the deterioration of dessicated clay, subjected to rapid saturation. The strength of saturated rockfill, both in crushing and in shear, is reduced due to a combination of capillary tension decrease, local pore pressure increase, and the reduction of fracture energy.

2.4 Strength Theories for Rockfill

The mechanical behaviour of rockfill, as described in the preceding section, can be analyzed by the use of three theories. The first is a statistical theory, based on particle behaviour, presented by Marsal (1973). The second theory is based on critical state soil mechanics and can be derived from the works of Roscoe, Schofield, and Wroth (1958). The third theory is the more traditional theory of elasticity.

2.4.1 Marsal (1973)

Marsal's work on large rockfill dams during the 1960's led him to develop a theory of failure for granular masses (Marsal 1973). The investigator approached the problem by considering the particle nature of the soil as opposed to the behaviour of the whole. Thus, the foundation of Marsal's theory is the estimation of the contact forces between particles. This estimation is accomplished by statistical means.

2.4.1a Average Contact Force

Marsal aims at establishing the contact forces on particular grains in terms of effective stresses, acting on the sample. This aim is accomplished by relating the effective stresses acting on any plane through the rockfill mass to the intragranular forces acting across the intersected areas of the grains. From the requirements of static equilibrium, the x, y, and z components of the intragranular forces are the vector sums of the components of the contact forces acting on that remaining portion of the whole grain, that is cut by the plane. The contact and intragranular forces are seen in Fig. 2.1.

The contact forces are dependent on the dimension and shape of the grains, the mechanical properties, which may vary from particle to particle, and the arrangement of the grains themselves. The arrangement requires static equilibrium. Static equilibrium is based on the number of contacts per particle and on the eccentricities of the granular forces from the centre of the grains. These are random variables.

The intragranular forces are dependent on the mean effective stresses and the intersected areas of the grains. The intersected areas are random variables and a frequency distribution must be established for them based on statistical methods. Further complication arises if a soil is nonuniform, being composed of several different fractions. In that case, the intersected area is the sum of that portion of the areas of each fraction, depending on the volume concentration of the fraction. The intersected area depends on the void ratio and the shape of the particles. It is equal to the porosity times the cross-sectional area, as determined by Windisch and Soulie (1970).

The intragranular force is equal to the average contact force times the number of contacts on that portion of the grain cut by the intersecting plane. Also, the intragranular force is equal to the average effective stress acting on the plane times the area of the intersected grain divided by the total area of the plane. The forces and stresses are vectors and must be treated as such in any operation. The average contact force is equal to the intragranular force, divided by the number of contacts. The intragranular force is dependent on the intersected area. Both the number of contacts and the intersected areas are random variables, and mean values must be used. The mean values are obtained from assumed frequency curves.

2.4.1b Frictional Resistance

The shear strength of a granular soil is the result of friction forces developed at the grain surfaces, which oppose the sliding and the rolling between grains. Both of these factors depend on the relationship between the tangential, T, and normal, N, components of the contact force, P, acting on a contact of a particular grain. The force R, available to resist the action T, is proportional to N.

$$R = \mu N$$

where μ is the interparticle friction. Because

$$P = \sqrt{T^2 + N^2}$$

and since, at the limit condition of equilibrium, T = R, the friction force, R, is given by

$$R = \mu P / \sqrt{(1 + \mu^2)}$$

This expression has to be adjusted for calculation of the available sliding resistance along the plane, which coincides with the direction of the relative movement between particles or mean free path. This plane is dependent on the type of test. In the triaxial test, the angle of this plane is equal to the arc-cotangent of the absolute value of the ratio of the radial strain to the axial strain. Essentially, the expression for the available sliding resistance, R, remains the same.

The rolling of the grains is caused by moments exerted by the weight of the grains and reduces the ability of the soil to resist shear forces at the contacts. The moment is caused by the intragranular force along the plane of the mean free path and its moment arm about the centroid of the particle. The moment arm is a statistical parameter. The intragranular force is related to the shear stress along the plane by the factor n_s, the surface concentration. This factor is obtained experimentally, and is the number of grains cut by the plane per unit area. Thus, the rolling stress is

$$t = b\tau$$

where τ is the shear stress along the mean free path; and b is a factor that takes into account the grain shape, the existence of idle particles, and the number of contacts on a particular plane.

The mean value of the frictional resistance is the difference between the available sliding friction and the rolling stress. Thus, it depends on the gradation and shape of the particles, the friction between grains, the statistical distribution of the contact forces, and the shear and normal stresses, acting on a plane parallel to the mean path of the particles.

2.4.2 Critical State Theory

Roscoe et al. (1958) developed the critical state concept for remoulded saturated clays. The theory, which has since been applied successfully to describe real clays in "in situ" conditions by Tavenas and Leroueil (1977), can be outlined as follows. When tested under triaxial compression conditions of either full drainage or no drainage, remoulded satured clay has a characteristic yield surface which contains a constant void ratio line (critical state line) in (p',e,q') space. Loading paths converge to this line at high strains. With the knowledge of the position of the critical state line and yield surface, it is possible to predict the ultimate state of any soil sample, when stresses are imposed upon it. The initial conditions of the sample and the drainage conditions must be known. According to Atkinson and Bransby (1978), two state boundaries define the behaviour of remoulded saturated clay in (p', v, q') space. These are the Roscoe surface and Hvorslev surface. The Roscoe surface links the normal consolidation line with the critical state line in (p', v, q') space. It is a curved surface which is followed by the test path of both drained and undrained tests on normally consolidated and lightly overconsolidated clays. The Roscoe surface is a state boundary in that it delineates between states that a sample can achieve and that can never achieve. The Hvorslev surface is the locus of failure points of overconsolidated samples in drained and undrained tests. The complete state boundary surface is seen in Fig. 2.2.

Roscoe et al. (1958) also investigated the behaviour of of silts, sands, glass beads, and steel balls. Atkinson and Bransby (1978) re-examined Roscoe's et al. (1958) data, and established, from compression curves, that it was impossible to achieve normally consolidated samples for sands. They suggested that both loose and dense samples acted as if they had been subjected to preconsolidation pressures, even though the samples had been set up at zero stress. Thus, sands are regarded as heavily overconsolidated. Since the slope of the critical state line is the same as the normal consolidation line, sands exist on the left (dry) side of the critical state line. Test paths are limited by a state boundary surface similar to the Hvorslev surface. Because sands are highly overconsolidated, experimental difficulties are encountered in achieving uniform stress and strain conditions in triaxial specimens at large deformations. These large deformations are required to bring the stresse of the specimens to critical state line. According to Atkinson and Bransby (1978), the simple shear test apparatus provides the best data for estimating the critical state line for sands. Unfortunately, very few studies have been conducted in the behaviour of sands in terms of the critical state concept, and most of the analyses are based, more or less, on postulation. According to Atkinson and Bransby (1978), the Hvorslev surface for sands should be thought of only as a state boundary surface, beyond which samples cannot progress. There is no guarantee that paths followed during testing will necessarily coincide with the Hvorslev surface, and indeed, the undrained path is somewhat below the Hvorslev surface.

At the present, no data on rockfill exists, to which critical state has been applied. Nevertheless, from the examination of experimental data on one dimensional compression and isotropic compression of rockfill by Marsal (1973) and Lee and Farhoomand (1967), it might be suggested that rockfill is heavily overconsolidated, and like sands, the slope of what may be called the normal consolidation line of rockfill, λ, is small. To make any conclusions regarding the application of the critical state concept to rockfill materials would be premature, except that rockfill behaviour in triaxial and one dimensional compressional tests is similar in some respects to that of sand.

2.4.3 Elasticity in Geotechnical Engineering

Widespread use of the theory of elasticity for predicting stresses within soil masses came into practice with the application of Boussinesq's (1885) equations for the distribution of stresses within a linear elastic half-space. This use was further fostered by the interpretations of Westergaard and Newmark (Taylor 1948). Prior to these analytical representations, the use of elasticity had been restricted in civil engineering to the analysis of statically indeterminate structures of steel. Although soils do not behave as linear elastic materials, the rationale for use of elastic theory has been the availability of solutions to problems, for which the boundary conditions correspond, approximately, to the boundary conditions for soil engineering problems of interest. The lack of available alternatives has also been a reason for its use.

According to Perloff (1975), in the cases of cohesionless soils, the elastic modulus depends markedly upon confinement. An analysis may be carried out by means of numerical methods, such as the finite element technique. Elastic parameters are used and are based upon the stress level at points within the medium.

A similar concept was suggested by Coste and Parayre (1962), who studied the variation of the deformation modulus of a sand from the Loire river as a function of both the mean normal pressure and the deviator. Experiments showed that E increased as a function of the mean normal stress and decreased as a function of the ratio of the deviator stress to the maximum deviator stress. Coste and Parayre's study had been influenced by Ladanyi (1960), who had published a detailed theoretical analysis of the relationships between stresses and strains of granular soils during shear. Ladanyi's (1960) analysis included dividing elastic and plastic deformation into spherical and deviatoric components. The investigator suggested that the stress-strain relationship of a granular soil could be described by two functions. One function is dependent on the principal stress ratio, σ_1/σ_3, the shear strain, γ, and the mean normal stress, σ_m; the other, on the volumetric strain, ϵ_{vol}, the shear strain, and the mean normal stress.

According to Taylor (1948), direct application of elasticity should not be applied when shear stresses are near failure shear stresses, or if the stresses decrease.

On the other hand, Perloff (1975) states that, when the boundary conditions of analytical models approximate the "in situ" boundary conditions, the stress distribution, interpreted from field measurements, correspond reasonably well to that predicted by linear analysis.

Penman, Burland, and Charles (1971) state that satisfactory predictions can often be made by means of elastic theory, provided the elastic parameters for the soil are chosen as representative for the stresses to be encountered. Such predictions become much more unreliable when large local failure zones develop or when significant rotations in principal stress directions occur.

Elasticity can also be applied for settlement calculations for granular soils as found in Janbu's (1967) Theory.

This theory can be considered as a non-linear elastic theory, at least as the first loading path is concerned. Janbu (1967) formulated a method of settlement calculations based on the tangent modulus concept. The tangent modulus can be represented by an empirical relation of the form

$$M = mP_r\left(\frac{P}{P_r}\right)^{1-\beta}$$

where M is the tangent modulus of elasticity, m is a modulus number, P is the applied stress, P_r is a reference stress (100 kPa), and β is a stress exponent.

By plotting the logarithm of P versus the logarithm of ϵ, the strain, the constants m and β may be obtained. The value $1/m\beta$ is the ε intercept at the reference stress of 100 kPa. The constant β is the tangent of the angle defining the slope of the line represented in the log-log plot. The parameters m and β uniquely define the deformation behaviour of a soil material. For instance, m and β can be used to calculate vertical settlements as given by the following formulae:

$$\varepsilon = \frac{1}{m\beta}\left[\left(\frac{P_2}{P_r}\right)^{\beta} - \left(\frac{P_1}{P_r}\right)^{\beta}\right]$$

where ε is the strain in the vertical direction, P_1 is the original stress, P_2 is a new applied stress, and P_r is the reference stress.

and

$$\delta = \int_0^H \varepsilon dz$$

where δ is the vertical settlement and H is the depth at which settlement is computed.

Clough and Woodward (1967) formulated the stress-strain characteristics for soils in terms of the shear modulus (G) and the bulk modulus (K). They state that the use of these parameters has some advantages over the use of the Young's modulus, E, and Poisson's ratio, ν, because the value of K may be expected to be nearly independent of the strain magnitudes, while the value of G decreases with increasing strain. Dealing directly with the values of G and K has the advantage that the value of G may be reduced appropriately to represent non-linear behaviour and failure, while the value of K is maintained constant. On the other hand, if the value of E is reduced to represent non-linear behaviour and failure while the value of ν is maintained constant, the values of both G and K are reduced in the same ratio as the value of E. The use of G and K, thus, offers the advantage of improved representation of the bulk compressibility. The values of G and K are uniquely related to the values of E and ν, and the values of either pair of parameters may be calculated if the values of the others are known.

As far as the state-of-the-art concerning the application of elasticity in soil mechanics, Kavazanjian and Mitchell's (1980) work on the time-dependent deformation behaviour of San Francisco bay mud can be considered as the most developed. In the model, the bulk modulus, K, and shear modulus, G, are replaced by tensor operators. These may depend on stress, strain, time, stress history or any other parameter used to define the state of an element. Following work by Bjerrum (1967), deformation is divided into immediate and delayed components. Thus, the volumetric and deviatoric behaviour are both subdivided into immediate and delayed parts.

In order to use the general model to predict the behaviour of laboratory triaxial specimens, Kavazanjian and Mitchel (1980) developed a finite difference consolidation program that predicts deformations and pore pressure. The program required 14 parameters to predict the stress-strain-time behaviour of a cohesive soil. All the parameters can be obtained from triaxial compression tests. Kavazanjian and Mitchell's (1980) work confirms the use of elasticity as means of describing the behaviour of a geotechnical material.

The theory of elasticity is used extensively in rock mechanics to describe deformation behaviour, although difficulties arise because of the presence of discontinuities in the rock mass. These problems, however, are not insurmountable, as demonstrated by Lo and Hori (1979). The investigators analyzed the deformation behaviour of sedimentary rocks from five different geological formations in terms of cross-anisotropic elasticity. The mechanical properties were assumed to be isotropic in bedding planes but anisotropic in orthogonal planes. Typically, five independent parameters describe each rock. These parameters were all obtained by performing uniaxial compression tests on variously oriented samples. Lo and Hori (1979) observed, from the stress-strain curves of the samples that all the rocks were essentially elastic up to stresses of half of the failure stress. The five elastic parameters were used by Lo and Hori (1979) to predict deformation of underground structures in rocks from the same formations.

The basic assumption in the theory of elasticity is proportionality between stress and strain. The main question, therefore, is the degree to which this proportionality holds in rockfill under the loadings, which are to be applied. Most cases of shear testing of rockfill yields stress-strain curves that show an approximately linear relation in the early part of the test, furnishing an indication of the application of elasticity. Whether proportionality holds, if the load is increased, is questionable. Even if hysteresis is ignored, a permanent set is usually observed. Certainly, if the load is increased beyond a certain yield stress, the original proportionality no longer holds. It is in the small strain range that elasticity can be reasonably assumed. A detailed expose of the theory of elasticity is presented in Appendix A.

2.5 Discussion

The literature survey has confirmed that the shear behaviour of rockfill is similar to that of sand and other granular materials. Dense sand, under conditions of high confinement, has a behaviour similar to loose sands; that is, it experiences a high degree of compression, as opposed to dilation, and it has a smooth stress-strain curve with no pronounced peaks.

All investigators have reported that the Mohr-Coulomb failure envelope of any rockfill material is curved. Rockfill has a distinctive range of shear behaviour dependent on the confinement. Well-graded, rounded rockfill is better suited for constuction purposes than uniformly-graded, angular rockfill.

Saturation decreases the shear strength of rockfill. The coefficient of friction of rock fragments, saturated and dry, is the same, thus, indicating that saturation does not affect the frictional component of the shear strength of a rockfill material. Saturation most likely causes a volumetric effect , which contributes to a decrease of the overall shear strength.

At first glance, Marsal's (1973) theory is inovative and comprehensive, and his approach new and refreshing, although requiring considerable knowledge of statistics. Marsal's (1973) data act as a conclusive proof of his theory. However, on examination of his theory, it is found that many obscure assumptions are used, both statistical and physical. In addition, the material parameters like surface concentration, while easy to obtain in principle, are, in fact, obtained only after tedious and time consuming work.

Critical state theory, as applied to rockfill, is somewhat exciting in concept, because it could prove that the theory is all encompassing and that the mechanical behaviour of clay, sand, and rock could be described by the same model. However, it is barely established for sands and not at all for rockfill.

No soil material is perfectly elastic and isotropic. The practical application of the theory of elasticity is limited in soil mechanics because it does not consider ultimate states. However because of its simplicity, it is still the most widely used theory for design in soil mechanics. In addition, the ease with which "elastic parameters" are obtained from standard tests fosters the widespread use of elasticity. However, these parameters are not necessarily realistic parameters that describe the material. It is only with feed-back from actual field investigations that proper design parameters can be established.

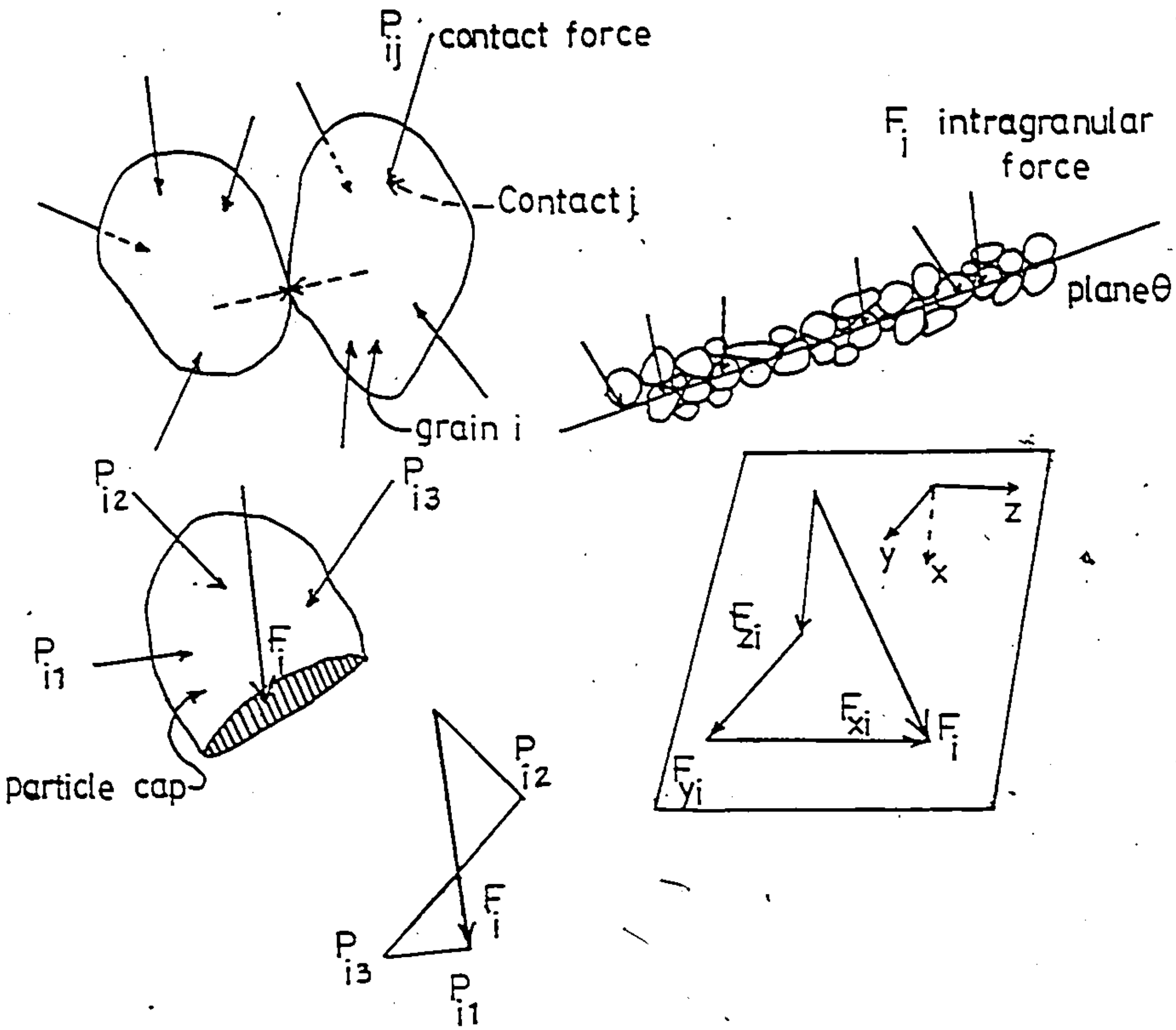

Figure 2.1 Contact and intragranular forces.

(from Marsal 1973)

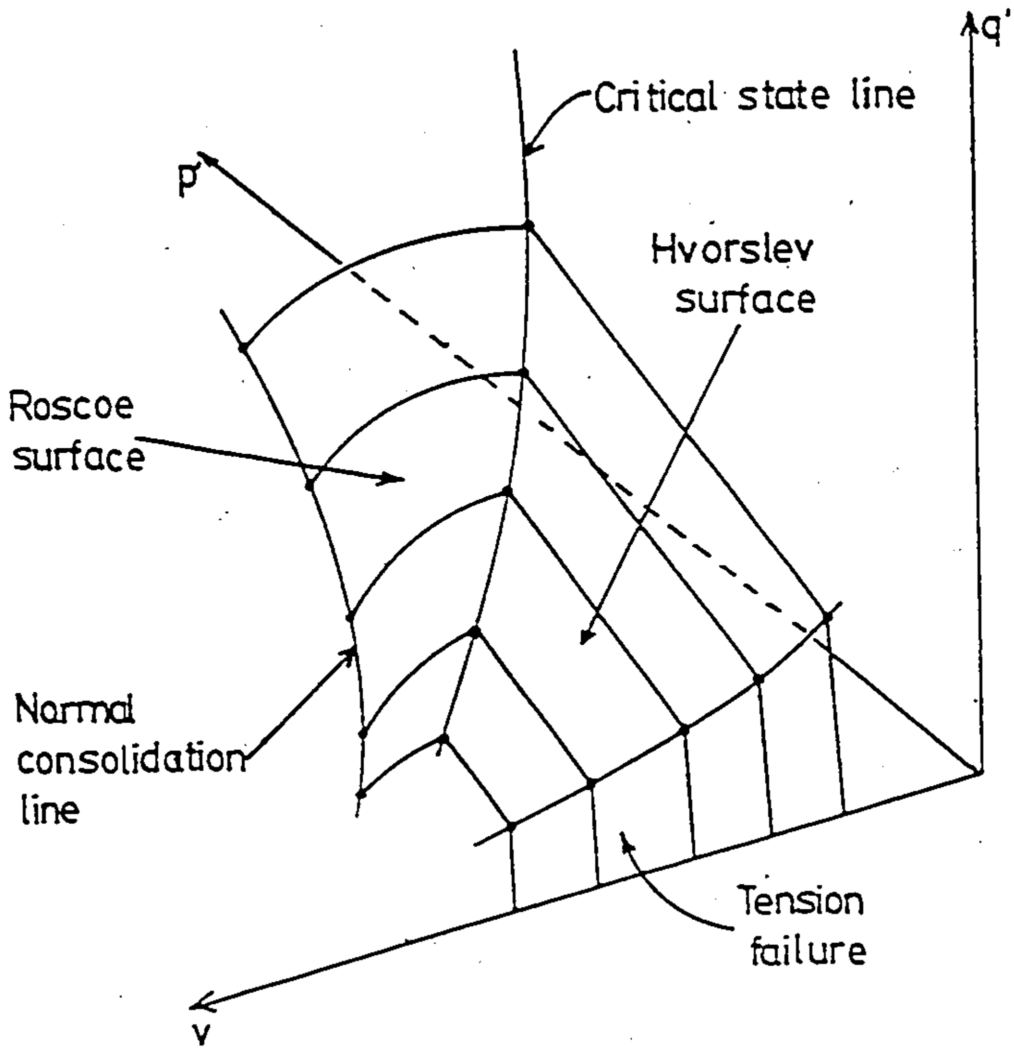

Figure 2.2 The complete boundary surface in q': p': v space.

(from Atkinson and Bransby 1978)

Chapter 3

Programme

3.1 Material Tested

The rockfill material tested in this study is a crushed, red sedimentary rock derived from a mechanical shale, known as Queenston Shale. The Queenston Formation is Upper Ordovician in age, and it occupies a position at the top of the Ordovician System in Ontario (Guillet 1977). The Queenston Shale outcrop belt is mainly situated in south-central Ontario, starting in Niagara Falls and running through Hamilton, Toronto, and Oshawa and extending North from that area to Georgian Bay. It also outcrops 26 km southeast of Ottawa, near the town of Russell, where it is quarried for the Ottawa brick plant of Domtar Construction Materials Limited. Since glacial erosion has removed most of the younger rock in the Ottawa region, Queenston Shale is the youngest sedimentary rock available in that area. As such, it is considered the least strong of all other remaining shale. This material was selected because it was believed that it would be easily weathered. Other reasons for the selection included its proximity and the lack of any other economical alternatives.

The thickness of the Queenston Formation is about 180 meters in the Hamilton area, decreasing to the north. Fossils are practically absent. The shale is predominantly brick-red, thin to thick-bedded, and moderately soft. The uniform red colour makes the formation a conspicuous lithologic unit in both boring samples and in field exposures. The colour is generally attributed to peculiar, and perhaps local, climatic conditions, which permitted extensive oxidation of the iron compounds present in the sediments while they were undergoing transportation or during and after deposition (Caley 1940). Thin green bands parallel to the bedding, and more rarely at right angles to it, have been formed by reducing action of acidic ground water. Queenston Shale is readily broken down by weathering, forming, ultimately, a red clay soil with superior ceramic properties (Guillet 1977).

For the testing program involved in this study, the material was procured in the fall of 1980 at the Russell quarry of Domtar Construction Materials Limited. About thirty boxes, made from 3/4 inch plywood, of approximate volume of 3 litres were constructed to store and transport the shale. The samples were obtained fresh from the bottom of the blasted walls of the pit by means of a loader (kindly provided by Domtar). The material was placed in plastic bags to prevent undue drying and fitted into the boxes.

In the laboratory, the boxes were placed in a permanent humid environment to preserve the natural moisture of the samples. The humidity cabinets used were fabricated from discarded household freezers. Each cabinet was connected to a small humidifier, to which water was fed from a central storage tank. The level in the humidifier was controlled by a float valve. Holes were drilled in the floor of the units to prevent the build up of water inside the cabinets.

3.1.1 Characteristics and Composition

According to Guillet (1967), the Queenston Shale is remarkably uniform in chemical and mineral composition from top to bottom of the formation. Lime content is most variable, ranging from 3 to 18 percent in brick quarries of the Toronto-Hamilton area, reflecting the proportion of green shale beds in sampled section. Green shale is harder, more limey and less easily broken down by weathering. The average mineral and chemical composition of Queenston Shale from nine quarries in the Toronto-Hamilton area is shown in Table 3.1. Clay minerals comprise 60% of the shale. Illite predominates, and chlorite is present in moderate amounts. Quartz and calcite are the major non-clay minerals. The resulting pattern of an X-ray diffraction analysis, performed by the Geology Department of the University of Ottawa, is presented in Appendix C.

Little calcareous materials were found within the shale. This was further substantiated by its neutral reaction to hydrochloric acid. In addition, it did not exhibit any tinkling or any significant high pitch sound when struck, indicating the absence of siliceous cementing. The rock did not indicate any preferred direction of cleaving. Most of the fragments were blocky, indicating similarities to mudstones. Large blocks of the material slaked readily when subjected to cycles of wetting and drying, breaking along roughly orthogonal planes. Slaking was less apparent in the lower size range, namely below particle size of 1 cm, thus, indicating that the slaking was more probably related to the propagation of Griffith's microcracks, than to volume expansion as a result of expansive minerals. The results of slaking tests performed on Queenston Shale, following the method of Morgenstern and Eigenbrod (1974), are presented in Appendix C. According to these investigators' classification, Queenston shale is a claystone, being a slow slaking material, whose loss of shear strength during saturation was about 20%. Using Underwood's (1967) classification, Queenston shale is between an active shale and an inactive one. The lack of any cementing material establishes the rock as a compaction shale. Geotechnical properties of samples of Queenston Shale have been determined in this study and are presented in Table 3.2 .

3.2 Triaxial Testing

Because of its versatility of application in terms of measureable pressures, both vertical and lateral, and the control of drainage conditions, triaxial testing was adopted as the means of establishing the strength and deformation characteristics of fragmented, Queenston Shale. A test specimen size of diameter 150 mm was chosen in order that the aggregates of the sample would be large enough to simulate rockfill conditions. Thus a large, high-capacity, triaxial cell, capable of accomodating specimens 150 mm by 300 mm, was selected for the testing programme. It was especially designed and built by Engineering Laboratory Equipment Limited, London, England. Apparatus for for volume change measurement and cell pressure application was also built for this study.

3.2.1 Triaxial Cell

The cell is constructed of a steel cylinder, welded to base and head rings, and has been treated to minimize corrosion. The base ring bolts to the cell base, which incorporates the necessary ducts for measurement of pore pressure, drainage, and application of lateral pressure. The head of the cell was designed to allow the piston to be accurately aligned with the upper platen. The diameter of the base is 370 mm, and the cell is 270 mm in diameter. The total height from the bottom of the base to the top of the piston collar is 680 mm. The piston has a stroke of 260 mm. Further details can be seen in Figs. 3.1, 3.2, and 3.3, which are drawings of the base, cell, and piston, respectively. The cell weighs approximately 75 kg including a specimen. Because of the weight, the head assembly incorporates lifting lugs and a detachable hanger to facilitate mounting onto the load frame. The cell has a capacity of 250 kN axial load and 5250 kPa maximum confining pressure.

3.2.2 Load Frame

The cell was mounted in a 450 kN capacity load frame, manufactured by ENERPAC, model number IPA-5021. The H-frame has two uprights, each consisting of two vertical steel members, welded together by three 15 cm spacers. Each upright is bolted at the bottom to a horizontal angle acting as a foot. At the top, the vertical members are welded to two outward facing channels, these also house the frame of the loading jack. The uprights were bored along the vertical in order that a hydraulically operated bed can be positioned at five different levels. The dimensions of the H-frame, seen in Plates 3.7 & 3.8, are approximately 1 m by 2 m. The bed consists of two outward facing channels welded to two 18.5 cm spacers. For this study, the bed was permanently bolted to the uprights at the second lowermost position in order to prevent any lateral movement. Vertical load was carried by a cam and saddle type arrangement, which provided the bearing for the bed. The arrangement, seen in Fig. 3.4, was also used to level the bed. It consists of an eccentrically bored steel cylinder bolted to the frame. A steel block, concave on the bottom, rests on the cylinder and has a matching curvature. The flat top of the block acts as the bearing surface for the bed. Four such devices, located in front and at the rear and on both sides of the frame, support the bed. Slightly rotating the cylinder below the corner of the bed changes the level at that point. A 40 cm square by 3 cm thick, steel plate acts as a seat for the triaxial cell. It incorporates a circular rotating pedestal, which matches the depression in the bottom of the cell. The plate is bolted to the bed of the frame. Two eccentrically bored steel cylinders are bolted at the rear of the plate and act as stoppers, permitting the cell to be aligned with the loading jack. The eccentricity provides a degree of adjustment of the level of the base, thereby facilitating the alignment of the cell.

3.2.3 Hydraulics

The strain controlled, hydraulic system, seen in Fig. 3.5, consists of five components: a jack, an electric oil pump, a shut off valve, a pressure relief valve, and a metering valve.

The jack, manufactured by ENERPAC, model number RC 506T, is housed at the top of the load frame. The single acting cylinder has a capacity of 450 kN and is equipped with a spring return. It has a stroke of 16 cm and an effective area of 72 cm^2. Fitted to the head of the cylinder, is a specially designed collar that incorporates a 5 cm diameter ball bearing, which transfers the load to the cell piston via a load cell. Thus, the cylinder can only impart vertical loads, and no moments can be transferred to the cell. The cylinder is driven by an oil pump, which is powered by a 60 Hz single phase, 115 volt motor of 1.5 horsepower. The oil capacity is 8 l and the maximum pressure available is 70000 kPa at a flow rate of 1000 cc/min. Included in the pump (ENERPAC, model no. PEM-3022A) is an air-cooled heat exchanger which keeps the oil temperature below 50 F. In addition, as seen in Fig. 3.6, the pump maintains an almost constant oil flow rate at a wide range of pressure, thus providing a smooth and steady operation of the cylinder. Immediately following the pump, the pressure relief or dump valve reroutes pressurized oil by allowing some oil to go on to the jack, while returning the remainder to the pump. A dial gauge, which has a pressure range of 0 to 1000 psi (7000 kPa), records the line pressure after the dump valve. The metering valve, which follows, is a screw-type needle valve. It controls the flow of oil to the cylinder. A second dial gauge, similar to the previous one, follows the metering valve and measures the pressure in the jack. The last valve, prior to the jack, is a shut-off valve. In order to maintain a constant rate of strain, a constant pressure difference must exist between the supplied flow after the dump valve and the flow delivered to the jack, following the metering valve. Since the the resistance of the specimen to the movement of the jack changes regularly, the constant pressure difference is maintained manually by adjusting the dump and metering valve during a test.

3.2.4 Cell Pressure and Volume Change

Pressurized water was used to apply the cell pressure for the confinement of the specimen. The water was pressurized by means of a compressed air supply fed through a system of regulators to a water-supply cylinder. Fig. 3.7 displays the system. The compressed air and the water were separated by a rubber membrane within the steel cylinder. Two regulators were used, the first reduced the line pressure of the compressed air (25000 kPa) to within a workable pressure range of 0 to 7000 kPa. The second regulator, which was operated by a control valve and an alternate pressure line fed to the water cylinder, reduced the line pressure to an accurate low pressure range (0 to 700 kPa). Since the first regulator was not sensitive enough in the low pressure range, the second regulator was utilized at the beginning of each test. The pressure supplied to the water cylinder, and hence, the cell pressure, was measured by a Bourdon pressure gauge (range: 0 to 7000 kPa).

Since the triaxial tests performed in this study were drained tests, volume changes occurred within the specimen. These changes were measured by monitoring the volume of air being expelled by or sucked into the specimen. The system is seen in Fig. 3.7. Basically, expelled air (for the case of specimen volume reduction) exiting the cell through duct No. 1 or 2, or both, travels through a gas-tight hose to valve No. 10 at the top of a cylinder. The cylinder is sealed from the atmosphere and filled to a known level with coloured water. The expelled air forces down the level of the water in the cylinder by an amount equivalent to its volume. The bottom of the cylinder is connected to a water tank and a glass manometer by a closed valve, No. 7. By matching the level in the cylinder with that of the manometer (accomplished by pumping water from the tank into the cylinder), a reading of the volume change is obtained. For the case of a saturated or partly saturated specimen, a second cylinder traps any water expelled from the specimen before the air reaches the former cylinder. The volume change is equal to the volume of water expelled plus the change in volume produced in the first cylinder as a result of any air expelled from the specimen.

3.2.5 Load Cell

The load, transmitted to the specimen in the triaxial cell is measured by a load cell, situated between the piston of the cell and the ball bearing attachment to the loading jack. It has a capacity of 180 kN, and is a flat compression load cell, model number FL 50C-2SP, manufactured by STRAINSERT Ltd. A multi-channel digital strain indicator, model S4-161 by B&F Instruments Inc, provided a digital readout of the force on the load cell. During a test, the load cell reading was printed on a paper roll by a chart recorder. The calibration of the cell, seen in Appendix C, was done against a certified-accurate Tinius-Olsen Universal Testing Machine with a capacity of 500,000 kN.

3.2.6 Specimen Preparation

The grain size distribution curve for the fragmented Queenston Shale was the same for each test and corresponded to the condition of the rock following crushing. The size of the triaxial cell restricted the diameter of the largest aggregate used to 19 mm. Since a high degree of granularity was desired in the specimen, no fines were included in the gradation. The smallest aggregate was retained on sieve number 40 (0.42 mm). The adopted grain size distribution curve, seen in Fig. 3.8, is uniform. Approximately 14 kg of material were needed to produce a specimen of 10 kg. The 14 kg, graded sample was prepared ahead of time and kept in the humidity cabinet in a large plastic bag until needed. Care was taken when preparing the graded sample to maintain the natural water content of the rock. This goal was accomplished by keeping the exposure time short and the amount of crushed material small. The rock was also covered with damp rags during this process. A weathered specimen of rock was obtained by drying a 14 kg, graded sample in an oven set at 50°C for 12 hours, and immersing it for one hour in a water bath at 50°C to prevent the occurrence of thermal stresses. Following the wetting, the rock was again dried at 50°C. One drying to another constituted one cycle of weathering. The shale specimens were submitted to 25 cycles of wetting and drying. The grain size distribution curve of the weathered material is seen in Fig. 3.8.

Prior to building the specimen, the base of the triaxial cell was prepared by verifying that all ducts were clean, permitting the free flow of air. The bottom aluminium platen was screwed into the base with a sealing O-ring, and a protective circular, steel plate was placed upon it. The hole, located in the centre of the plate, was covered with a fine-meshed screen to prevent clogging of the volume measuring passages. Following this procedure, the periphery of the platen was coated with a thin film of silicon grease, and a 150 mm diameter membrane was slipped on.

A rubber O-ring was stretched across the platen to seal the membrane. The membrane was then stretched across the inner surface and the top of the mold, which was placed around the lower platen. A small vacuum was applied to stretch the membrane flat against the surface of the mold by a venturi type suction arrangement.

The specimen was built up in ten to twelve lifts, each being rodded 25 times and tamped 25 times with a small 1 kg tamping weight. The material used for each lift was obtained by quartering the 14 kg, graded sample into 16 parts, with precautions taken to prevent the drying of the rock. The quartering, seen in Plate 3.2, prevented segregation of the fractions comprising the material in the specimen. Any compactive effort greater than that previously described tore the membrane and resulted in the collapse of the specimen when the mold was removed. The degree of compaction obtained varied from 65% to 75% of the optimum standard proctor density.

The material was packed to the top edge of the mold, resulting in a specimen height of 327 mm, which allowed for an extra 27 mm of travel for the piston. At this point, the top platen was placed on the surface of the specimen, the membrane was folded over its greased periphery, and an O-ring was slipped over, sealing the membrane. In the case of a saturated specimen, the procedure was the same except that, prior to fitting the platen, the specimen was flooded with water from the bottom, left standing for one hour, and then, drained before the top platen was fitted. Negative pressure was applied to the specimen, and the mold was removed. Because of the angularity of the rock, the low density of the specimen, and the lack of fines, membrane penetration occurred as seen in Plate 3.4. At high confining pressures, the membrane became susceptible to puncturing. The problem was resolved by covering the surface of the membrane with three coats of quick setting latex, as seen in Plate 3.5. Large cavities were filled with a mixture of latex and Polyfilla, which acted as a catalyst, causing the mixture to set within seconds. A second, sealing membrane was fitted over the specimen and sealed with two O-rings at the top and the bottom. As an added precaution, a 0.85 mm thick, neoprene membrane was placed over the specimen. Membrane correction factors were calculated for all membranes, including the latex covered one, and are presented in Appendix C.

Following the sealing of the specimen, the cell was bolted to the base, and the piston was lowered to the top of the platen. As seen in Plates 3.6 and 3.7, the assembled cell was installed in the load frame using a special hoist. Care was taken that the cell base was flush with the stoppers on the bed and that the top was aligned with the ball bearing of the jack.

The cell was filled with water, pressurized to 100 kPa, and the negative pressure in the specimen was released. The volume measurement hose was attached, and the corresponding reading represented zero change. The cell was pressurized in steps to the desired degree of confinement and the accompanying volume changes were recorded. With the attainment of equilibrium under the cell pressure, the axial load was applied. The test set up is seen in Plate 3.8. A more detailed laboratory procedure is presented in Appendix B.

The movement of the jack was maintained at a constant speed of 1 mm/min by manipulating the valves in the hydraulic system. Load was recorded every minute along with volume changes. A complete test lasted 100 minutes and resulted in a failed specimen of the type shown in Plate 3.9.

In the study, drained compression tests were performed for four different conditions of the rockfill. The shale was tested in a natural and saturated state, and the weathered material was tested dry and saturated. In order to get a good representation of the strength behaviour, the specimens were tested at three confining pressures: 1000 kPa, 2000 kPa, and 3000 kPa (150 psi, 275 psi, 400 psi)*. In addition, the effect of acid on the strength of the material was investigated. Specimens were tested in triaxial compression after treatment with a 0.2 N solution of EDTA (disodium salt of ethylene-diamine tetra acetic acid). The EDTA is a chemical which removes carbonates, gypsum, and iron compounds, all of which acts as particle cementing agents. Triaxial test were also performed on equivalent-sized specimens of powdered Queenston Shale, both saturated and dry.

---

* Regarding SI conversions see Notation.

CHEMICAL ANALYSIS

Chemical Compound	Percentage
SiO_2	56.28
Al_2O_3	16.00
Fe_2O_3	6.77
CaO	4.74
MgO	2.55
Na_2O	0.70
K_2O	3.93
TiO_2	0.85
CO_2	3.81
H_2O^+	3.21
H_2O^-	0.92
SO_3	0.33
MnO	-

MINERAL ANALYSIS

Mineral	Percentage
non-clay	
Quartz	26.0
Calcite	11.0
Dolomite	1.8
Soda-lime feldspar	1.3
Potash feldspar	trace
clay	
Illite	abundant
Chlorite	moderate
Vermiculite	trace

Table 3.1 Chemical and Mineral Composition of Queenston Shale (from Guillet 1967).

Properties	Average Value
Liquid Limit	20.2 %
Plastic Limit	18.4 %
Plasticity Index	1.8
Activity	3.0
Water Content	2 %
Density of the particles	2.77 Mg/m^3
Swell Potential	1 %
Proctor Density	2676 kg/m^3

Table 3.2 Geotechnical Properties of Queenston Shale.

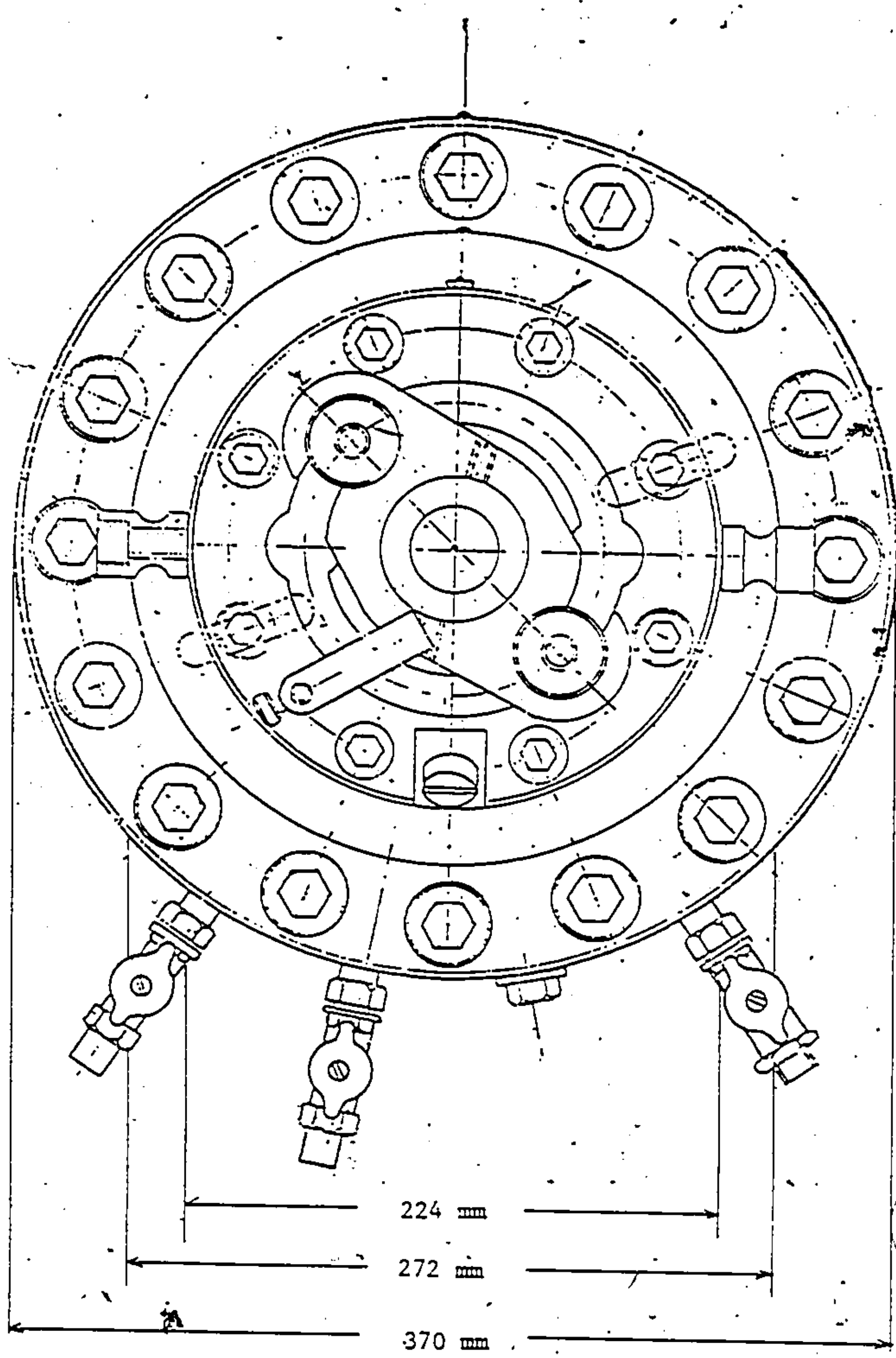

Figure 3.1 Top view of base.

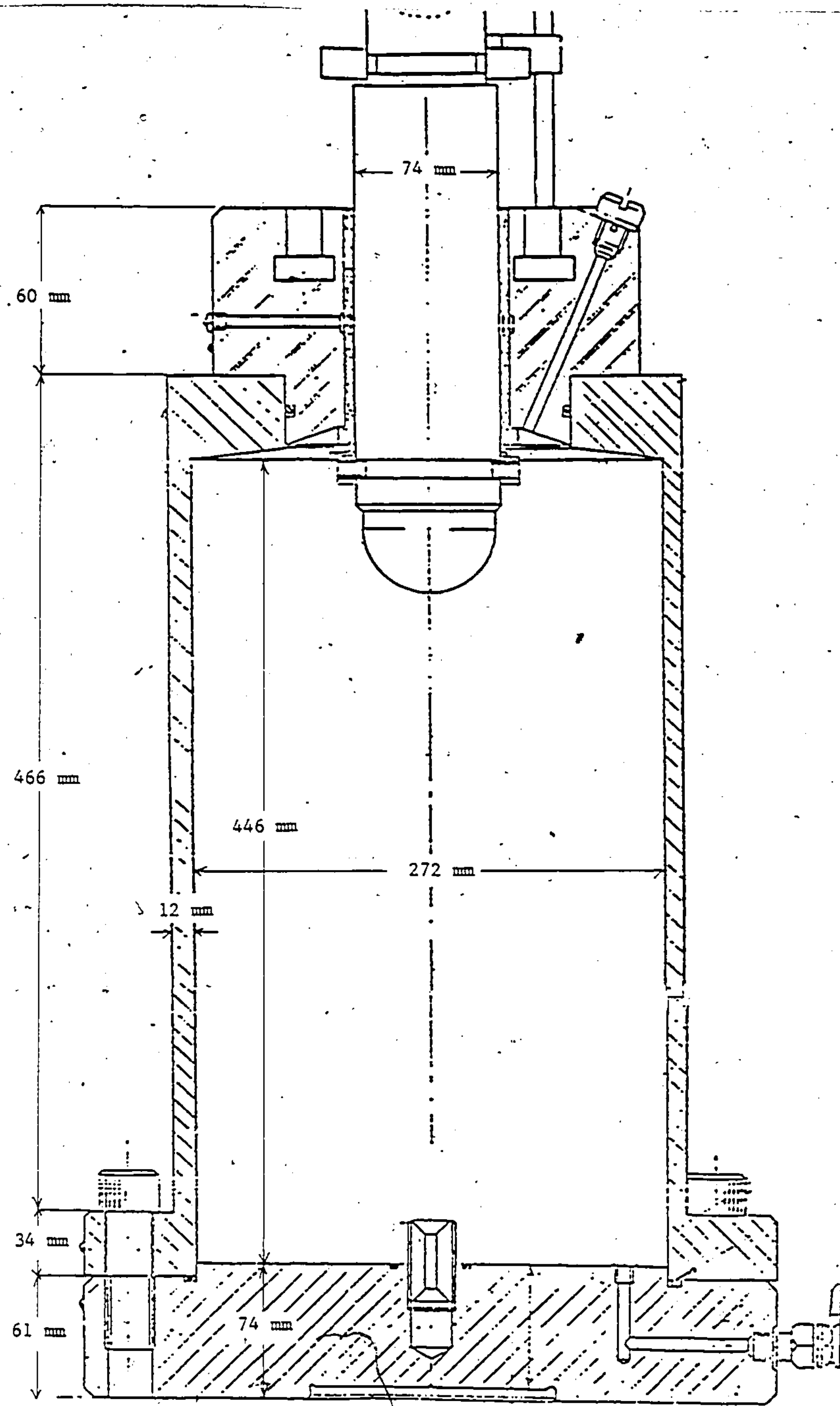

Figure 3.2 Side view of cell.

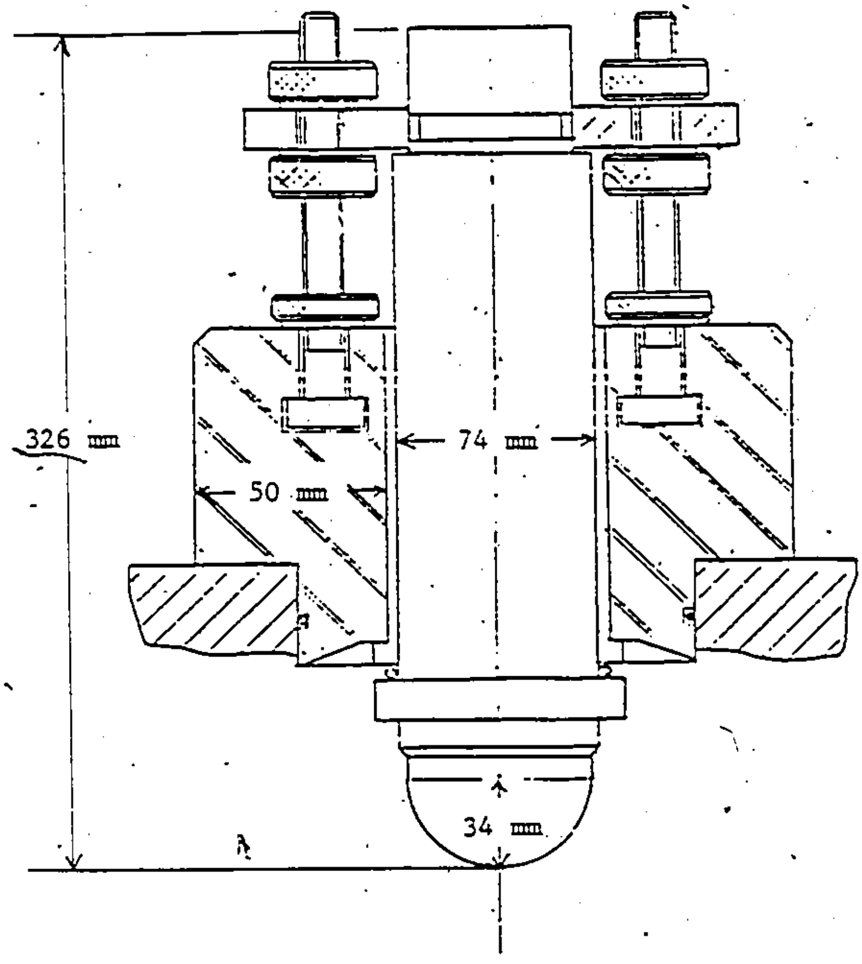

Figure 3.3 Side view of piston.

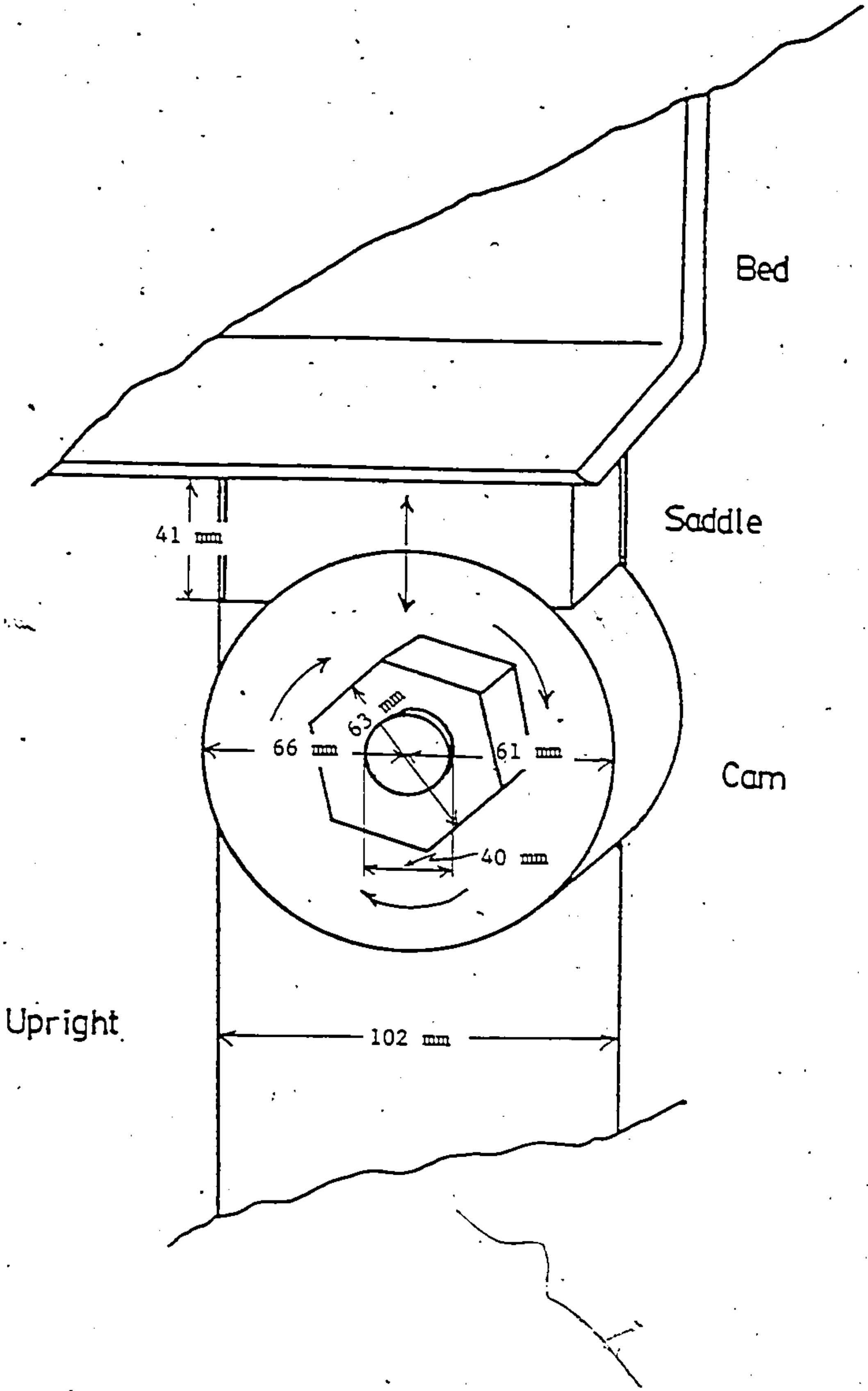

Figure 3.4 Cam and saddle arrangement.

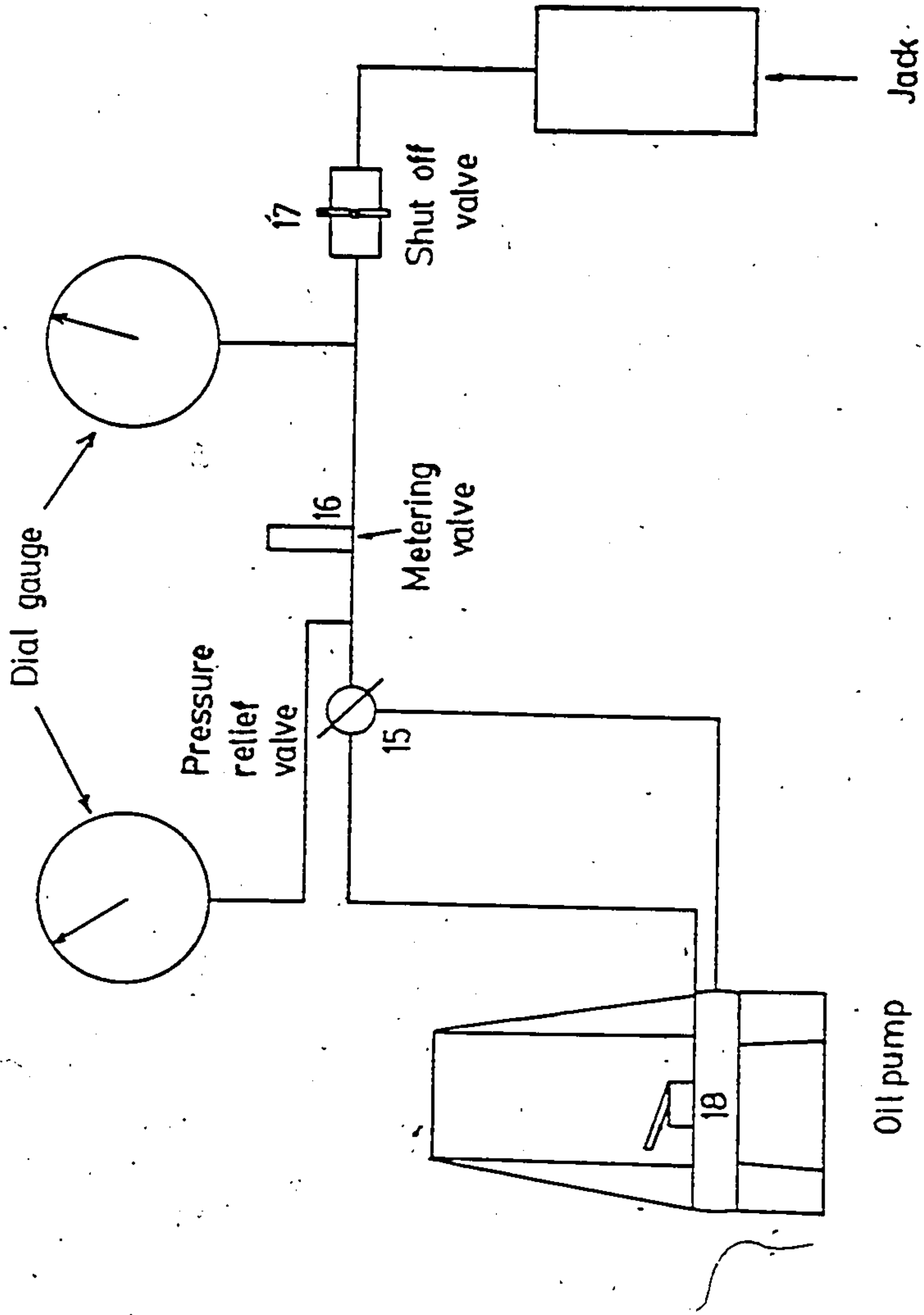

Figure 3.5 Strain controlled, hydraulic system.

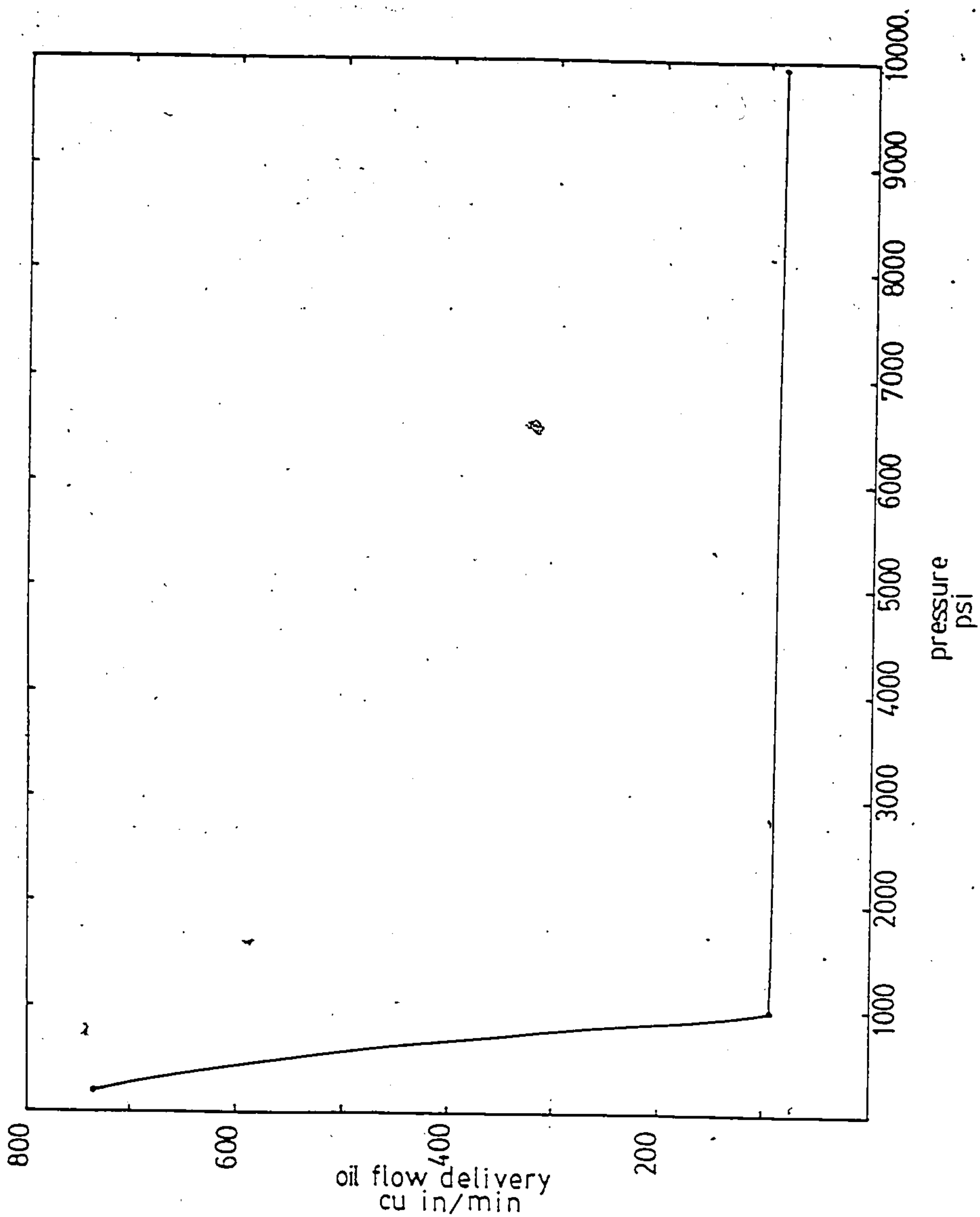

Figure 3.6 Pump specification.

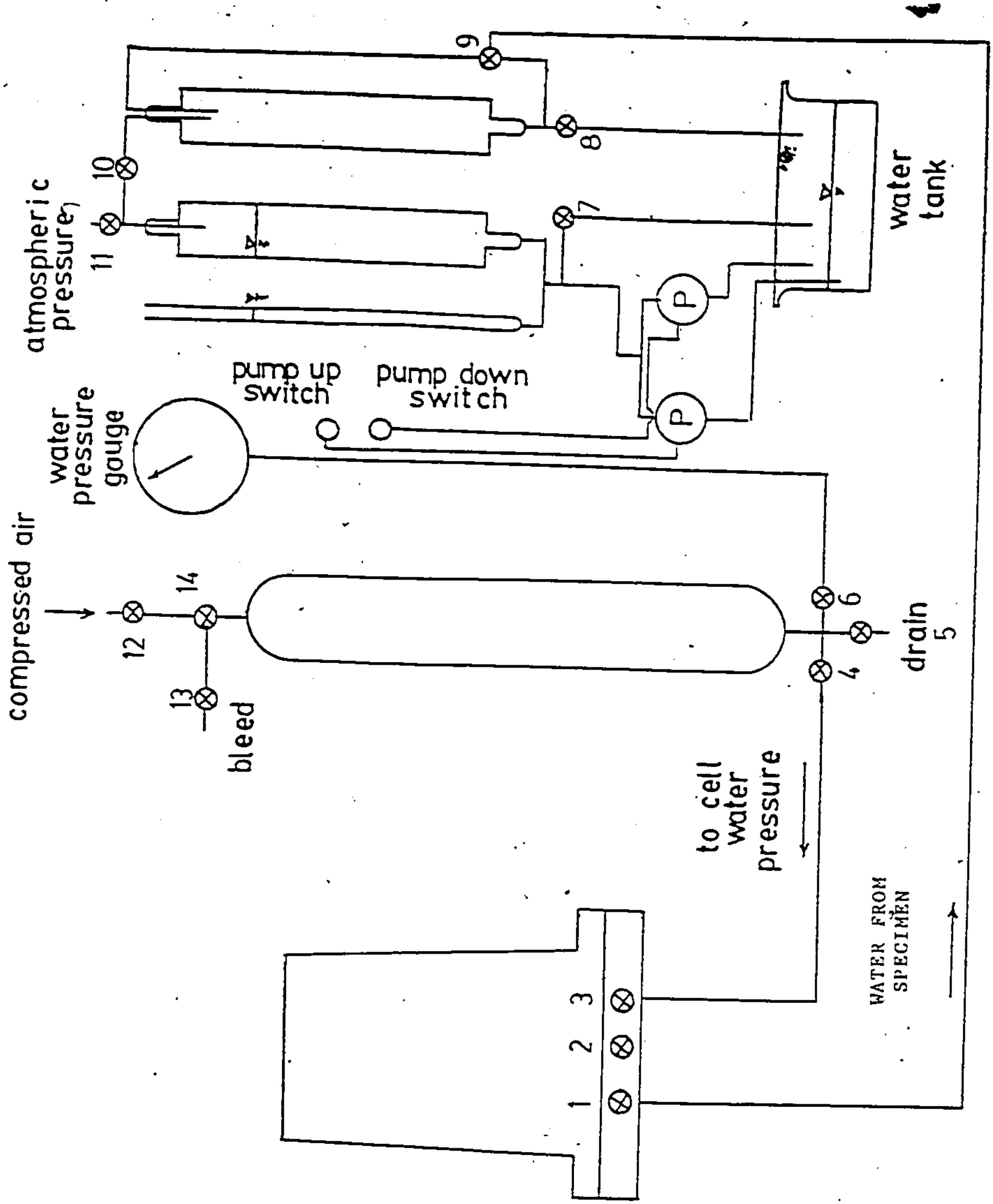

Figure 3.7 Cell pressure and volume change measurement.

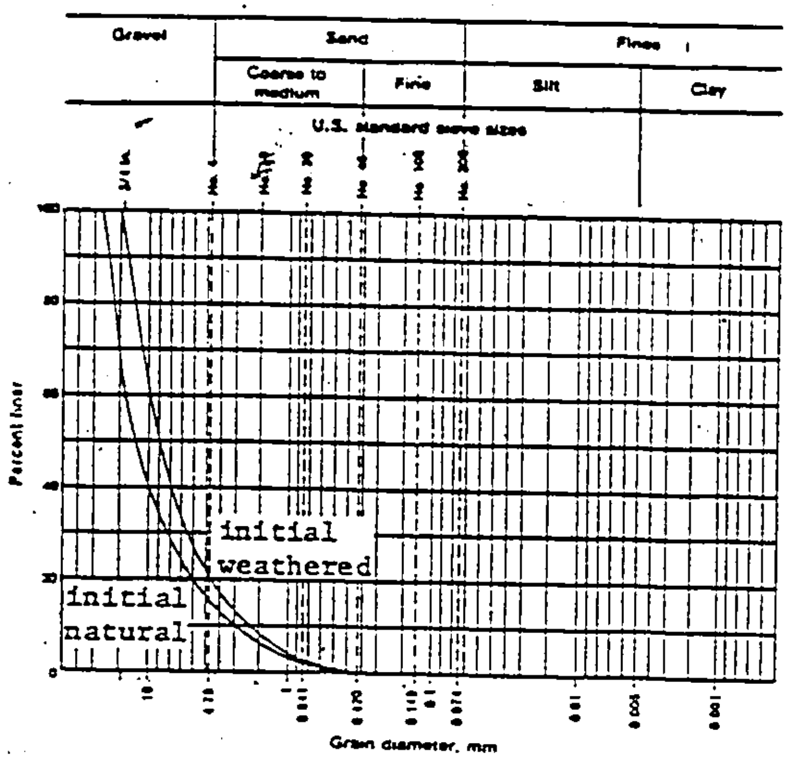

Figure 3.8 Gradation:initial and weathered.

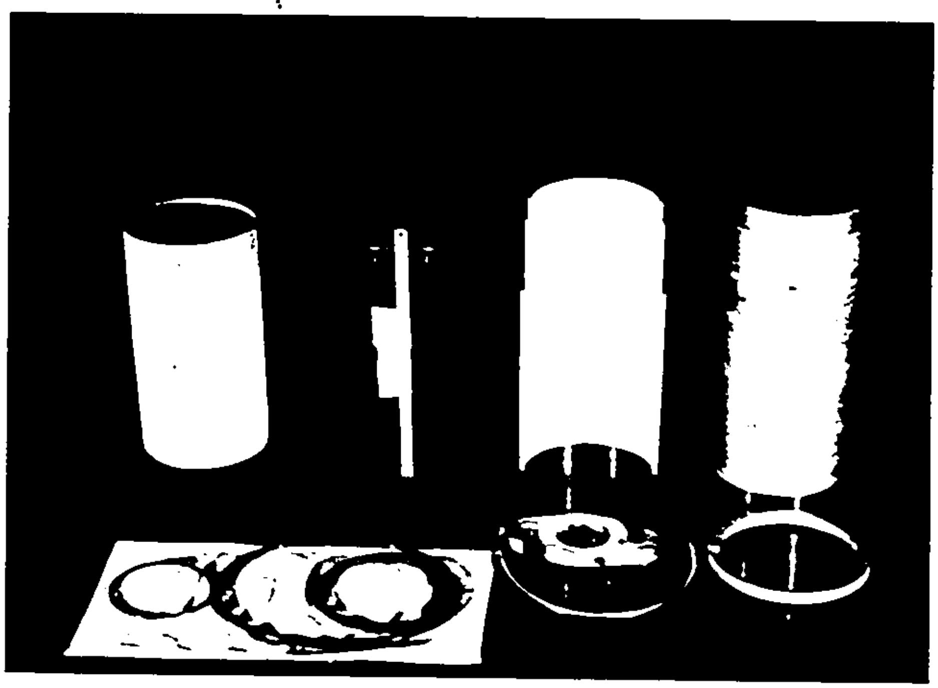

Plate 3.1 Specimen fabrication paraphernalia.

Plate 3.2 Sample quartering.

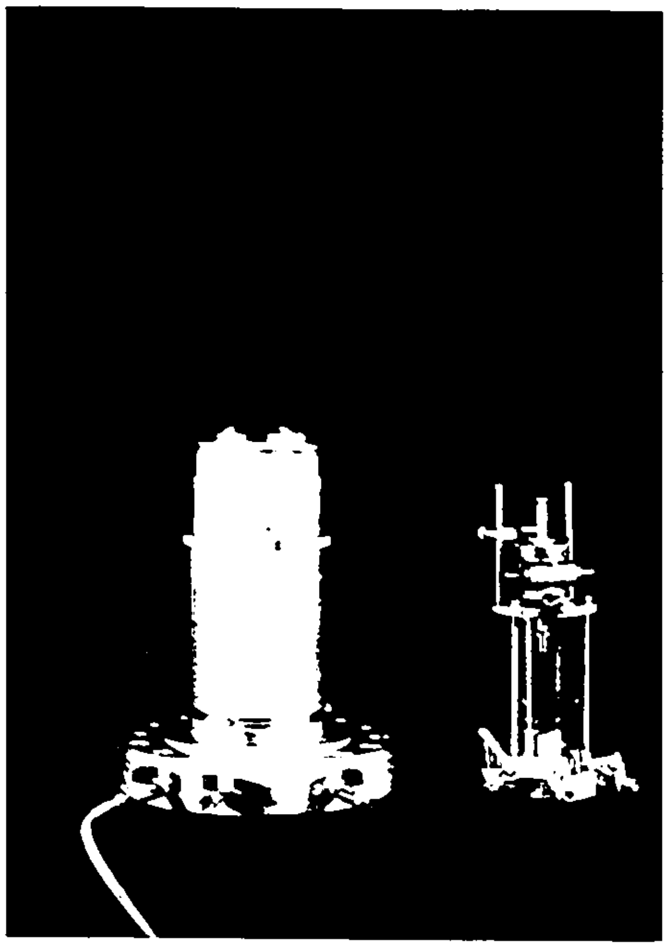

Plate 3.3 Test cell and standard cell size comparison.

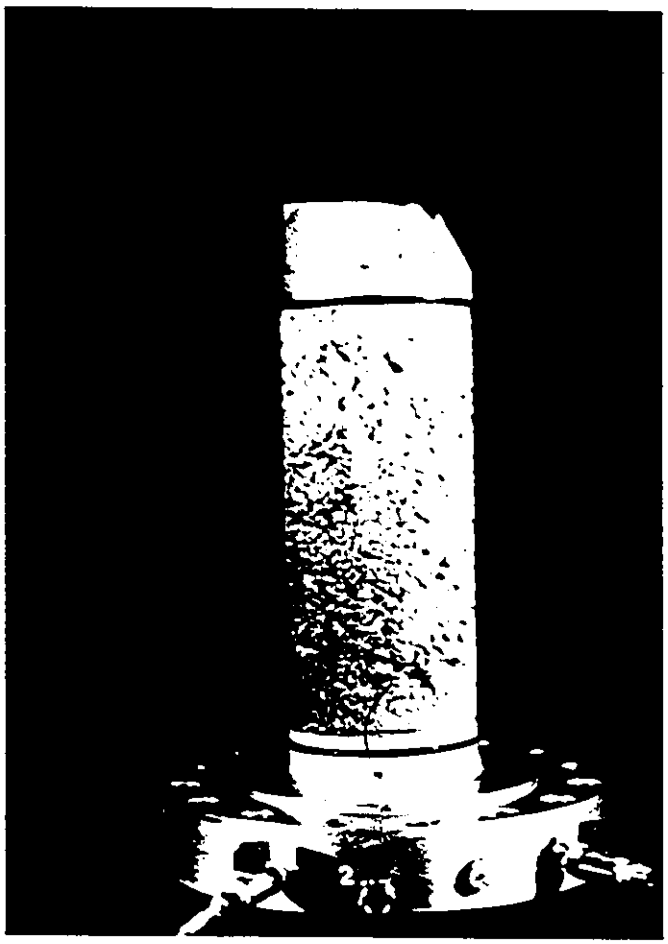

Plate 3.4 Membrane penetration.

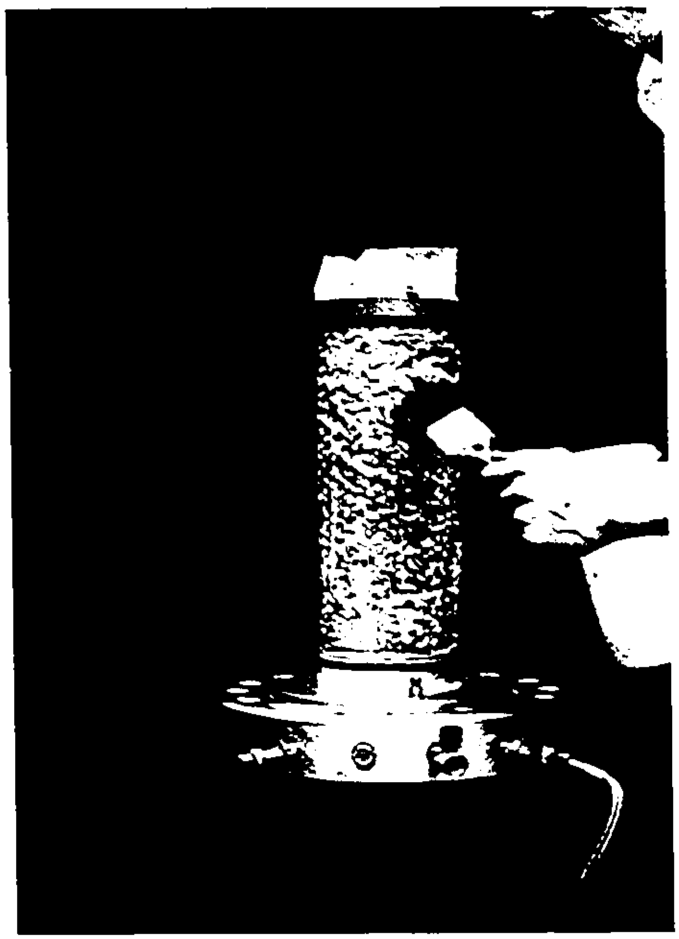

Plate 3.5 Latex application.

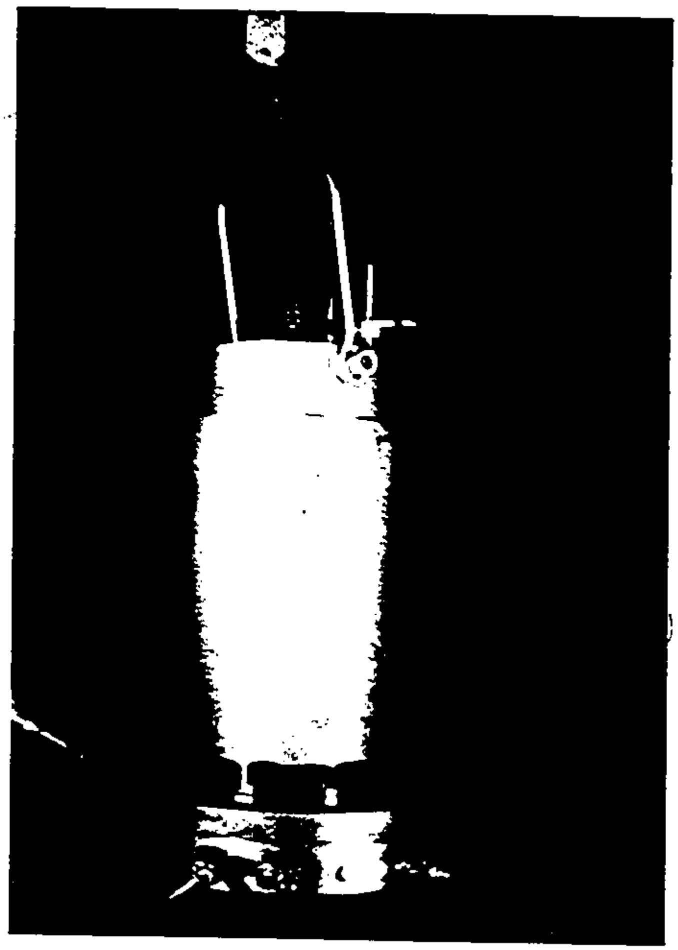

Plate 3.6 Hoisting of triaxial cell.

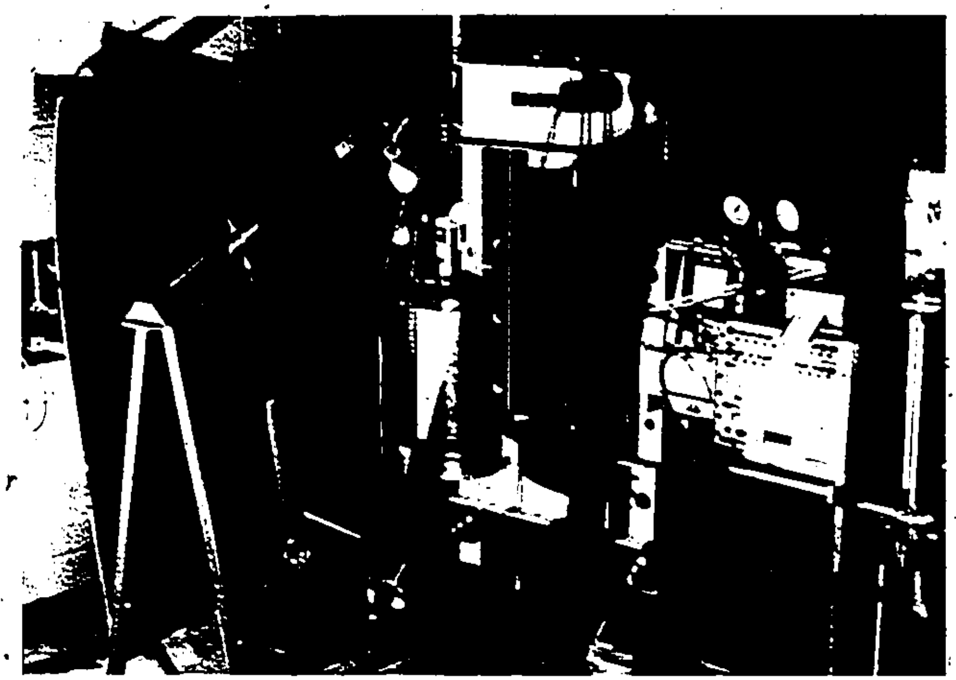

Plate 3.7 Installation of cell in load-frame.

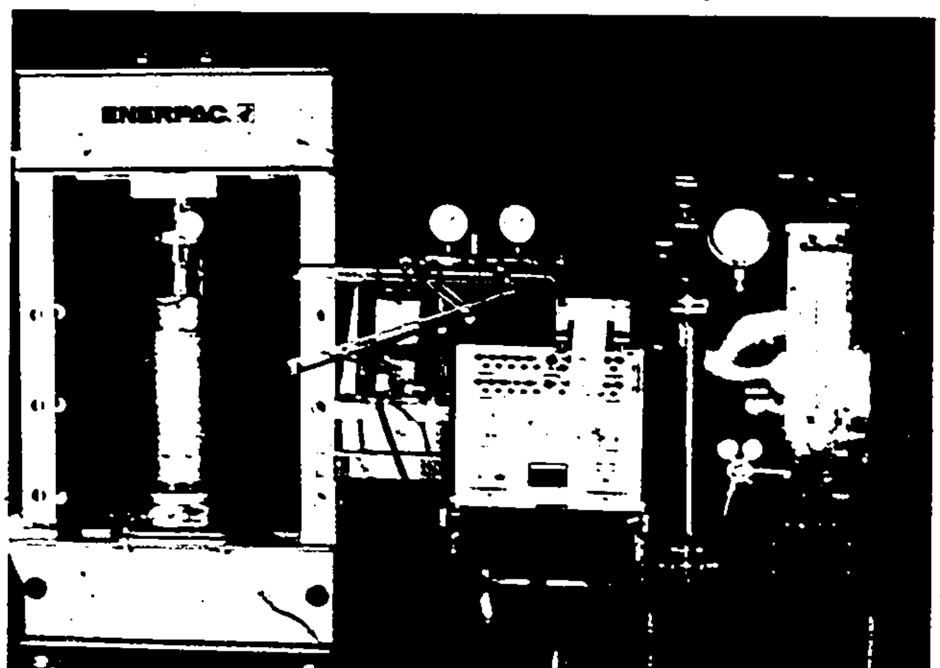

Plate 3.8 Test set up.

Plate 3.9 Tested specimen, barrel shape failure.

Chapter 4

Test Results

4.1 Observations

Four types of fragmented Queenston shale were tested under CID triaxial compression conditions. For each confining pressure of 1000, 2000, and 3000 kPa, the shale was tested dry natural, saturated natural, dry weathered, and saturated weathered. A specimen was also sheared under the same conditions after it had been treated with a 0.2 N EDTA solution.

An estimate of the ultimate weathered condition was established by powdering the shale. The powdered material was tested dry and saturated under CID triaxial compression conditions, with specimen sizes of the same order as that of the fragmented shale. Direct shear test were also conducted on the powder, dry and saturated. The results of the tests will be presented and analyzed in this chapter, while the raw data for the tests are tabulated in Appendix B.

All specimens exhibited barrel type or plastic flow failures and were assumed to deform as right cylinders. According to Bishop and Henkel (1962), the area of the specimen was continuously adjusted as calculations were made. All graphs were corrected for seating errors produced as result of test equipment. The sum of all correction factors, found in Appendix C, for the numerous membranes amounts to less than 0.2 % (5 kPa) of the deviator stress at 20 % strain. Consequently, and because of the order of stresses reached in all the tests, the effect of the membranes on the results was ignored. The data from triaxial tests were plotted according to standard methods as prescribed by Lambe (1951) and Bowles (1970).

All the specimens were within 65 % to 75 % of optimum standard proctor density before compression and 70 % to 80% following. Figs. 4.1 a,b, and c show plots of deviator stress versus axial strain for dry natural, saturated natural, dry weathered, and saturated weathered specimens at chamber pressures of 1000, 2000, and 3000 kPa. No distinct deviator stress peak was reached during shear for all specimens tested. Following an initial rapid rise, the stress increased slightly as the axial strain increased until a constant level was reached, usually at 24 % strain.

No appreciative contrast in deviator stress could be discerned between weathered specimens and natural specimens. The only difference at all, although not in shear behaviour, was in colour. Natural material was a deep lustrous red, while weathered material was a dull, reddish brown. The response to shear and the stress levels reached of weathered and natural specimens were the same or very nearly so in all cases, both in dry and saturated conditions. Weathered material behaved the same as natural material at this grain size level. There was a slight difference between the gradations of the weathered and natural specimens. The grain size distribution can be seen in Fig. 4.2a.

The stress level achieved for the saturated natural specimens was 10 % to 30 % lower than the corresponding dry natural specimens. The largest difference was found to be for specimens with the smallest confining pressure. As the chamber pressure increased, the difference decreased considerably, 10 % at high pressure.

The plots of volumetric strain versus axial strain corresponding to Figs. 4.1 a, b, and c are shown in Figs. 4.1 d, e, and f. The graphs are drawn illustrating compression as positive. All cases showed volume change as being compressive. In terms of the slope of the curves, natural and dry weathered specimens behaved the same, with compression increasing with increasing confinement, levelling off at medium and high confinement. Saturated natural and saturated weathered specimens also behaved the same, with compression higher than the dry cases and increasing as confinement increased to the medium level, and decreasing at the high stress to the same value as in the dry case.

Since the exact point of failure is difficult to establish in a plastic flow failure, two failure criteria were chosen. Both Lambe (1951) and Bowles (1970) consider the choice of failure strain as arbitrary in this type of failure. The first criterion adopted established failure at 10 % strain, the second at 24 % strain. The former was chosen because any earth structure is deemed failing if the strain exceeds 10 %, and the latter because it represented the maximum achievable strain with the test apparatus.

Figs. 4.3 a, b, c, and d represent the Mohr-Coulomb failure envelope at 10 % axial strain for dry natural, dry weathered, saturated natural, and saturated weathered specimens, respectively. The failure envelope was straight through the origin for saturated specimens and curved for dry specimens. The angle of internal friction obtained from the relationship

$$\phi = \sin^{-1} \frac{(\sigma_1/\sigma_3-1)}{(\sigma_1/\sigma_3+1)} \qquad -(4.1)$$

for the four types of the material at 10 % strain with the values in order of increasing confining pressure was as follows:

dry weathered specimens ϕ = 33.5°, 32.8°, and 28.9°,

saturated weathered specimens ϕ = 33.4°, 28.8°, and 28.2°,

dry natural specimens ϕ = 34.0°, 33.1°, and 29.2°,

and saturated natural specimens ϕ = 28.6°, 29.5°, and 28.2°.

In terms of deviator stess level reached, the shear strength of dry weathered material was within 5 % of the strength of dry natural material, with no trend with regards to confinement. Saturated weathered material was slightly lower (less than 10 %) in shear strength at low confinement than saturated natural material. This difference disappeared at high confining pressure. Dry natural material was stronger in shear than saturated normal material by 25 % at low confining pressure. This difference reduced to 2 % at high confining pressure. Similar observations were noted about dry weathered material and saturated weathered material. The former had higher shear strength than the latter. The largest difference was 25 % at 1000 kPa confining pressure; beyond that stress, the difference decreased substantially. At 3000 kPa , it was less than 3 %. Application of Rowe's (1962) correction of the deviator stress for volume change for all four types of the material at 10 % strain brought the Mohr-Coulomb envelopes approximately together, although there were some irregularities with the data.

Figs. 4.4 a,b,c, and d represent the Mohr-Coulomb plots at 24 % strain for dry natural, dry weathered, saturated natural, and saturated weathered specimens respectively. Saturated specimens had failure envelopes that were straight or nearly so, while dry specimens had curved envelopes, but less so than the corresponding curved envelopes of the 10 % dry specimens.

The shear stress of dry weathered material, as measured by the deviator stress level, was the same as the strength of the dry natural material. Similarly, saturated weathered material had the same shear strength as saturated natural material. Dry natural material reached higher shear stresses than saturated natural material. At low confining stress the difference was 25 % and decreased to 10 % at high confining stess. There existed some ambiguity in interpreting the comparable situation between dry weathered and saturated weathered material. The largest difference in shear stress was 15 % at a moderate confinement in favour of the dry material. For lower and higher confinement the saturated weathered material was 10 % weaker than the dry weathered material. The trend of the results indicated that, similarly to the 10 % failure observations, saturation decreased the shear strength, and this drop was a function of the confinement. Since the shear characteristics of 10 % and 24 % failure were the same, further plots utilized the 10 % strain failure criterion.

Fig. 4.2 a shows the grain size distribution curve of the natural material and the weathered material. The slaking process produced only a small change in gradation, increasing the coefficient of uniformity, C_u, from 3.6 to 4.2.

Fig. 4.5 a shows the grain size curves of dry natural material after shear testing at confinements of 1000 kPa, 2000 kPa, and 3000 kPa. C_u changed from an initial value of 3.7 to 7.9, 11.7, and 12.7 for the respective confining pressures. Similarly, Fig. 4.5 b shows the grain size curve for dry weathered material after shearing. C_u changed from 4.3 to 6.6, 10.1, and 11.4 at 1000, 2000, and 3000 kPa respectively.

Fig. 4.5 c shows the grain size distribution curve for saturated natural material after shearing. The coefficient of uniformity changed from 3.6 to 9.1, 19.4, and 13.6. Fig. 4.5 d shows the grain size distribution of saturated weathered material after shear testing. The coefficient changed from 4.4 to 21.6, 35, and 16.3. The grain size distributions of the saturated material (natural and weathered), after shearing at high confinement, showed a distinctive change in behaviour of the degradation of the fragments. This change was noticeable primarily in the shape of the distribution curve. For the specimens sheared at high confining stress, the curve changed from concave to convex.

Plots of void ratio versus mean normal stress are presented in Figs. 4.6 a, b, and c for the four types of the material at 1000 kPa, 2000 kPa, and 3000 kPa confining pressure. The graphs show the compression and the shear test divided by a line indicating the confining pressure. The void ratios at 10 % failure are indicated on the plots.

At the same confinement, dry specimens, natural and weathered, reached the approximate same void ratio after compression even though initial void ratios were different. Similar observations were noted about saturated specimens except that the void ratio reached was smaller than in the dry cases.

Assuming that the Cam-clay model could be applicable to these materials, all materials behaved as overconsolidated soils and failed on a line that may be said to be parallel to the critical state line and the normal consolidation line of the material (see Figs. 4.6 a, b, & c and Fig. 4.9 c). This failure line had a constant slope, λ equal to 8.75×10^{-5}, for all four types of the material, whether saturated or dry. At a confinement of 3000 kPa and using the 10 % failure criteria, all specimens, saturated and dry, reached failure at an approximate mean normal stress of 4500 kPa. At 2000 kPa confining pressure, all specimens failed at an approximate mean normal stress of 3000 kPa. At 1000 kPa confining stress, all specimens failed at approximately 2000 kPa mean normal stress.

A general view of the behaviour of the material during shear was obtained through normalization. This method involved plotting the quotient of the deviator stress divided by the confining pressure against the deviator strain. Normalization produced excellent results for saturated specimens, both natural and weathered, as seen in Figs. 4.7 c and d. Both curves were identical. For the case of dry natural and dry weathered materials, normalization produced less unification, but, nevertheless, reasonable results were otained as seen in Figs. 4.7 a and b. Since there was no difference between natural and weathered materials, these two curves were considered the same.

The two normalized curves obtained for the dry and saturated conditions were unique and were hyperbolic in shape. Kondner's (1963) hyperbolic transformation was applied to them, resulting in the following expressions for the shear modulus, G :

$$G = \frac{\sigma_{conf}}{2} \left[\frac{1}{[1 + 11.9(\varepsilon_1-\varepsilon_3)]^2}\right] \qquad -(4.2)$$

for the saturated case, where σ_{conf} is the confining pressure and $(\epsilon_1-\epsilon_3)$ is the deviator strain. For the dry case the expression was

$$G = \frac{\sigma_{conf}}{2} \left[\frac{1}{[1 + 7.6(\varepsilon_1-\varepsilon_3)]^2}\right] \qquad -(4.3)$$

A second normalization technique was attempted in order to obtain a more general representation of the material in any state. Normalization involved dividing the deviator stress by the mean normal stress. The results of this normalization are presented in Fig. 4.8. This process produced one unique curve for all four types of materials: dry natural, dry weathered, saturated natural, and saturated weathered. Kondner's (1963) hyperbolic transformation was applied to the curve, resulting in the following equation for the shear modulus:

$$G = \frac{\sigma_m}{2} \left[\frac{1}{[1 + 21.5(\varepsilon_1-\varepsilon_3)]^2}\right] \qquad -(4.4)$$

Plots of volumetric strain versus mean normal stress for dry natural, saturated natural, dry weathered, and saturated weathered material after hydrostatic compression are shown in Figs. 4.9 a, b, c, and d, respectively. The bulk modulus, K (see Appendix A), was obtained from these plots. The results of the tests at three confining pressures is represented on each of these graphs. At each pressure, the tests plotted as straight, parallel lines. The slopes of the lines were equal for all four types of the material. One value of K, independent of the confinement, was obtained for the material natural and weathered, either saturated or dry. That value was found to be 18.3 MPa. This value of K is valid for the shearing phase of loading only.

Analysis of the compression data in terms of Janbu's (1967) tangent modulus concept is found in Table 4.1, while the graphs, from which the values were obtained, are presented in Appendix C. An examination of these curves shows an approximately linear relationship between stress and strain at strains of 10 % and lower. The stress exponent, β, was found to vary between 0.001 to 0.003. The data indicated that the exponent decreased to 0.001 at high confinement. The modulus number, m, was 10^6 for the dry material and 10^5 for the saturated material.

Comparable graphs to the plots of the four types of the material are presented in Figs. 4.10 and 4.11 for a specimen treated with EDTA and tested at a confining pressure of 2000 kPa. The plot of deviator stress versus axial strain, Fig. 4.10 a, was identical to the plot of saturated materials at the same confinement (Fig. 4.1 b). The plot of volumetric strain versus axial strain, Fig. 4.10 b, was identical to the plot of saturated natural material (Fig. 4.1 e) at 2000 kPa confining stress. The Mohr diagram at 10 % strain, Fig. 4.12 a, seemed to have a similar trend as the saturated material at the same confinement (Figs. 4.3 c & d). In Fig. 4.10 c, the void ratio after compression of the chemically treated material reached a 10 % lower value than the corresponding void ratios of saturated specimens (Fig. 4.6 b). In Fig. 4.11 a, the equation of the shear modulus using the confining stress for normalization was the same as equation 4.2. The equation the shear modulus curve using the mean normal stress, was the same as equation 4.4. The slope of the line in Fig. 4.11 c yielded the same constant value of the bulk modulus. The grain size distribution of the treated material after shearing (Fig. 4.2 b) was similar to the other saturated specimens.

For the case of the powdered Queenston Shale, dry and saturated conditions (at dry densities of 1.85 Mg/m^3 and 1.99 Mg/m^3, respectively), are presented together in Figs. 4.10 and 4.11. In Fig. 4.10 a, the dry powder reached a deviator stress maximum of 6750 kPa at approximately 10 % axial strain and levelled out at 24 % to 6000 kPa, equivalent to the value reached by dry natural and dry weathered specimens at 24 % at the same confinement. The saturated powder had no pronounced peak, but gradually rose to a maximum of 2150 kPa at 24 % strain. This value was 65 % lower than the dry powder value. At 10 % strain, the saturated powder reached a value of 1489 kPa, 80 % lower than the dry powder. These two saturated values were 60 % lower than corresponding values for saturated natural and saturated weathered material. In Fig. 4.10 b, the volumetric strain reached after 10 % axial strain was 1.5 % for dry powder and 2.5 % for saturated powder. The volumetric strain reached for dry fragmented specimens, both natural and weathered, was 7 %. For the dry powder, the slope, λ, of the failure line (see p. 71) in Fig. 4.10 c was 4.5×10^{-5}; while, for the saturated powder the slope was 8.75×10^{-5}, the same as all other plots of the fragmented materials (Figs. 4.6 a,b, & c). In Fig. 4.11 a, the equation of the shear modulus (using confining stress) for the dry powder is as follows:

$$G = \frac{\sigma_{conf}}{2} \left[\frac{1}{[1 + 9.6(\varepsilon_1 - \varepsilon_3)]^2}\right] \qquad -(4.5)$$

and for the saturated case

$$G = \frac{\sigma_{conf}}{2} \left[\frac{1}{[1 + 56.9(\varepsilon_1 - \varepsilon_3)]^2}\right] \qquad -(4.6)$$

Using Fig. 4.11 b (mean normal stress for normalization), the equation of the shear modulus for the dry powder is

$$G = \frac{\sigma_m}{2} \left[\frac{1}{[1 + 12.3\ (\varepsilon_1 - \varepsilon_3)]^2}\right] \qquad -(4.7)$$

while for the saturated powder the equation is

$$G = \frac{\sigma_m}{2} \left[\frac{1}{[1 + 15.8(\varepsilon_1 - \varepsilon_3)]^2}\right] \qquad -(4.8)$$

The bulk modulus, found in Fig. 4.11 c, had a dry value of 44.4 MPa, while for the saturated case, K was 18.3 MPa.

In Fig. 4.12 a, the ϕ_{dry} value, both observed from the plot and calculated using equation 4.1, was 39.8°, while for equivalent dry fragmented material ϕ was ~33°. The powder ϕ_{sat}

value was 16.3°, while the value of the comparable saturated material was 29°. The results of direct shear tests on 5 cm^2, powdered specimens of Queenston Shale, performed by Thompson (1981), indicated that ϕ_{sat} was approximately equal to ϕ_{dry}. The results have been plotted and are presented in Fig. 4.12 b. The value of ϕ were 36° at a normal stress of 700 kPa, 22° at 2000 kPa and 18° at 3000 kPa.

4.2 Discussion

The fact that there were no pronounced peaks in the stress-strain plots of the specimens tested, and that all volume change was compressive was most probably due to the low relative density of the specimens (Terzaghi and Peck 1948). However, a second reason could exist as described by the De Beer (1965) and Lee and Seed (1967a). These investigators found that dense specimens, under conditions of high confinement behaved as loose specimens (similar to the behaviour of specimens tested in this study), intead of dilating and showing peaks in their stress-strain curves. Since the confining pressure of 3000 kPa, the upper limit of the testing programme, can be considered to be on the verge of the of the high pressure range (Vesic and Clough 1968), it seems necessary to investigate if this pressure had any effect on the stress-strain behaviour of the specimens. From an examination of Fig. 4.1, it is evident that the overall stress-strain behaviour is more or less the same at all confining pressures and that at low confinement (Fig. 4.1 a) the specimens definitely behaved as loose specimens. Therefore, with a relative density of 70 % to 80 %, specimens in this study can be considered as loose. Furthermore, the confining pressure did not seem to change the basic stress-strain behaviour of these loose specimens. This behaviour was due to the relative density of the specimens.

The curved failure envelopes of the dry natural and weathered materials (Figs. 4.3 a & b and Figs. 4.4 a & b) appear to be a normal condition for rockfill materials. The straigthness of the envelopes of the saturated materials, both natural and weaththered (Figs. 4.3 c & d and Figs. 4.4 c & d), appears to be an oddity. Such behaviour was not encountered in any of the investigations found in the literature review.

Three factors affect the shear strength and deformation behaviour of a rockfill material: grain size distribution, shape of the grains, and crushing strength of the grains. As these factors seemed to be similar, it is not surprising that the shear strength and the deformation behaviour of the weathered and natural materials were similar , as seen in Fig. 4.1. It appears that at that particle-size level of testing (19 mm or less) fragments of Queenston Shale are very resistant to weathering. However, this conclusion does not imply that larger fragments were equally resistant, as evidenced from visual observations in the field.

The difference in colour of the natural and weathered materials is most likely attributed to the presence of water in the natural material and the absence of it in the other, as a result of the drying process.

The difference in shear strength of the dry specimens and the saturated ones could have been due to water acting as a lubricant, thus lowering the coefficient of friction and allowing particles to re-orient themselves more easily. This hypothesis was discounted by Taylor (1948), Terzaghi and Peck (1948), and Lee and Seed (1967b). It was proven untrue by Marsal (1973). The more reasonable cause of the drop in shear strength is the fracture and degradation of highly stressed particles as a result of external forces and internal forces caused by saturation. As presented by Van Eeckhout (1976), these forces are due to capillary tension decrease and fracture energy reduction. The result is a change in volumetric strain. Since the Mohr-Coulomb, corrected by using Rowe's (1962) equation, were the same, it appears that saturation produces a volumetric effect and not a pure frictional one.

The fact that the saturation effect diminished as the confinement increased can best be looked at from the point of view of grain breakage. Saturation increased grain breakage, as demonstrated by the grain size distribution (Fig. 4.5). But at high confinement both dry specimens and saturated specimens experienced less relative grain breakage. From a fundamental view point, the particles were getting so small at high stresses that degradation, through saturation, was no longer important phenomenon at that scale level. The decrease in the coefficient of uniformity of the saturated specimens (natural and weathered), at confining stress of 3000 kPa, is due to the convex nature of these curves (Figs. 4.5 c & d). The convexity is most likely due to at least two separate concentrations of mass in the distribution, as opposed to one in the normal concave curves.

The question remains why particle breakage for dry and saturated specimens reach a constant lower relative value at high confinement. According to Marsal (1973), particle breakage is a function of the contact forces on the particles. These forces are directly proportional to the number of contacts per particle, a relatively constant value, and to the principal stresses, and inversely proportional to the surface concentration, n_s, which increases with particle breakage. Therefore, the average contact force tends to remain constant because the increment of principal stresses is compensated by the increase of n_s. In addition, since fragmented Queenston Shale showed fundamentally different shear behaviour at medium and high confinement, and since Leps (1970) demonstrated that rockfill had a unique behaviour at low confinement, Vesic and Clough's (1968) breakdown stress concept may be applicable to this rockfill. This concept would indicate that the fragmented shale would behave as a linear elastic solid at conditions of high confinements.

The uniqueness of the bulk modulus, during the shearing phase, confirms Clough and Woodward's (1967) assumption regarding its constancy.

If the Cam-clay model is valid for this material, the parameter, λ, which is the same for all types of the material, is a unique soil constant which describes the behaviour of the material (Atkinson and Bransby 1978). Even if this model is not applicable for fragmented Queenston Shale, an empirical relationship can be established to determine the void ratio during shear, at a certain mean normal stress. The relationship is of the form:

$$e = e_o - \lambda \log \sigma_m \qquad -4.9$$

where e_o is the initial void ratio prior to shear, λ is the slope of the failure line (Fig. 4.6), and σ_m is the mean normal stress.

The observation, that all types of specimens (saturated and dry), under the same confinement, fail (10 % axial strain) at the same mean normal stress is too general a statement to make. The observation implies that the volumetric strain is also the same at this stress, since the bulk modulus was found to be constant. This implication is not correct because the plots of volumetric strain-axial strain (Figs. 4.1 a,b, & c) indicated that $d\epsilon_v/d\epsilon_a$ was different for saturated and dry materials at the same confinement. Thus, when ϵ_a is 10 %, ϵ_v is different for saturated and dry materials. Since the void ratio-mean normal stress plots indicated that specimens failed at approximately the same mean normal stress value, the generalization that they fail at the same value cannot be made.

Since the mean normal stress takes into account the intermediate stress, σ_2, it seems more reasonable that normalization of the deviator stress using mean normal stress (Fig. 4.8) produces better results with less scattering than with confining stress (Fig. 4.7). The fact that one unique curve for the shear modulus is obtained for both the saturated and dry cases, using mean normal stress for normalization, points to the conclusion that saturation affects the compressibility of the material and not its pure frictional behaviour. Saturation affects the volumetric strain (Fig. 4.1 d, e, & f), which affects the mean normal stress through the bulk modulus. But the mean normal stress affects the shear modulus (eq. 4.4), which relates deviator stress with deviator strain. Thus saturation indirectly affects the deviator stress. But saturation does not seem to affect the pure frictional part of the shear strength. This conclusion is supported by the fact that the corrected deviator stress-strain curves (using Rowe's (1962) equation) of all types of the material become one curve. This fact indicates that the difference in shear strength between saturated and dry specimens at the same confinement is due to the difference in volumetric strain, which saturation produces.

The similarity of all the plots of the acid treated specimen (Figs. 4.10 & 4.11 a, b, & c) to the saturated plots confirms that Queenston Shale is not affected by acid and is not a cemented shale.

The results of the test on the dry powder are obviously in error because the deviator stress level reached is 50 % higher than the dry fragmented shale at the same confinement, even though the density of the dry powder after compression (1.99 Mg/m^3) was less than the rockfill specimens (2.14 Mg/m^3). Thus, the dry powder had no reason to have higher shear strength. As the shear shear strength (measured by the Mohr-Coulomb envelope, Fig. 4.12) of the saturated powdered specimen was more or less the same as that obtained from direct shear test on the saturated powder, more attention should be given to Thompson's (1981) conclusion that $\varnothing_{sat}$ was the same as $\varnothing_{dry}$. This statement further supports the conclusion that saturation produces a change in compressibility of fragmented Queenston Shale by facilitating grain breakage. At the size level of the powder (below 74 µm), saturation does not cause significant grain breakage, because the grains are too small. Thus, the uniqueness of the angle of internal friction for the powdered shale in saturated and dry conditions is not surprising. Saturation does not seem to affect the coefficient of friction of Queenston Shale in fragmented and powdered conditions, but does reduce the shear strength indirectly by affecting the mean normal stress.

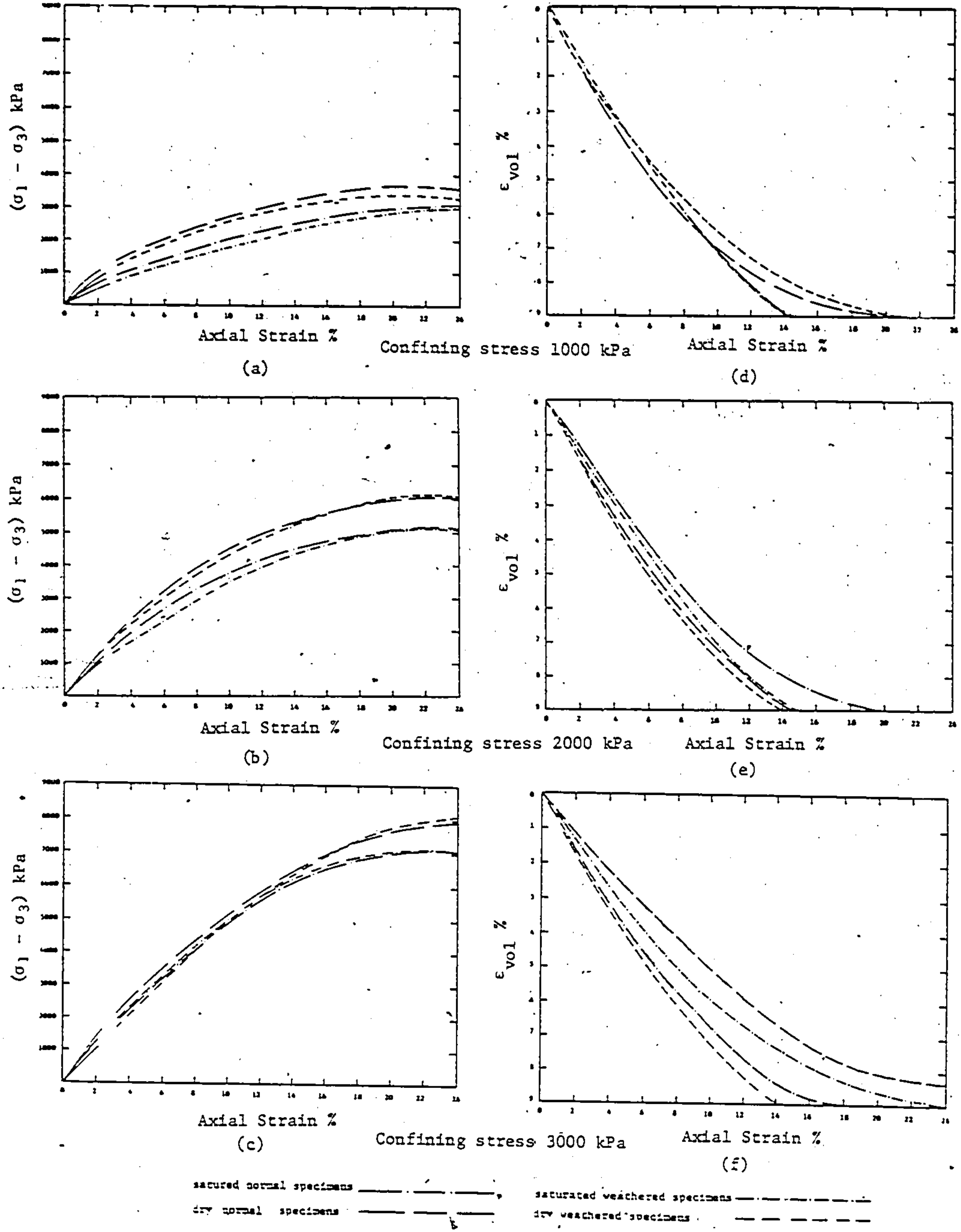

Figure 4.1 Deviatoric stress and volumetric strain versus axial strain.

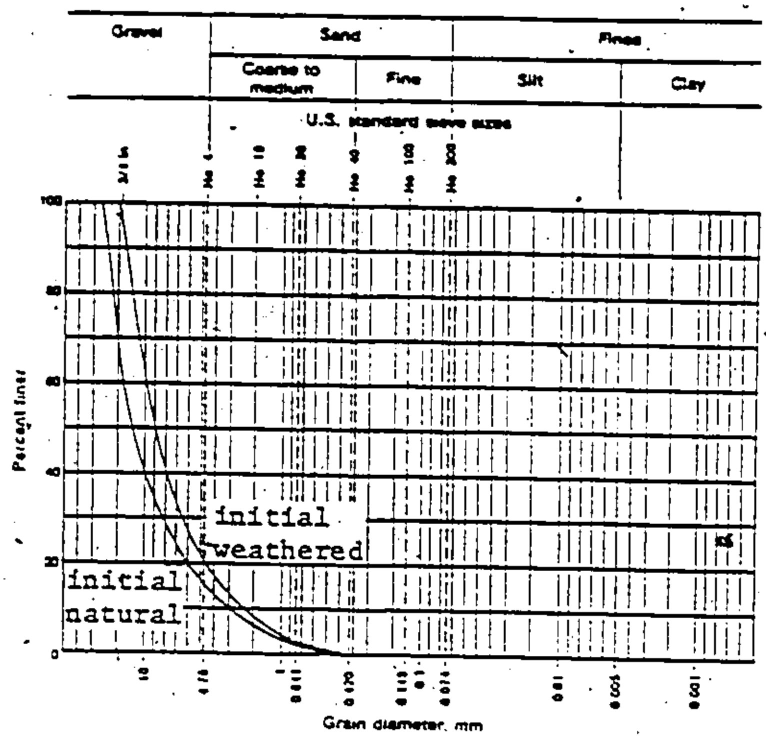

(a)

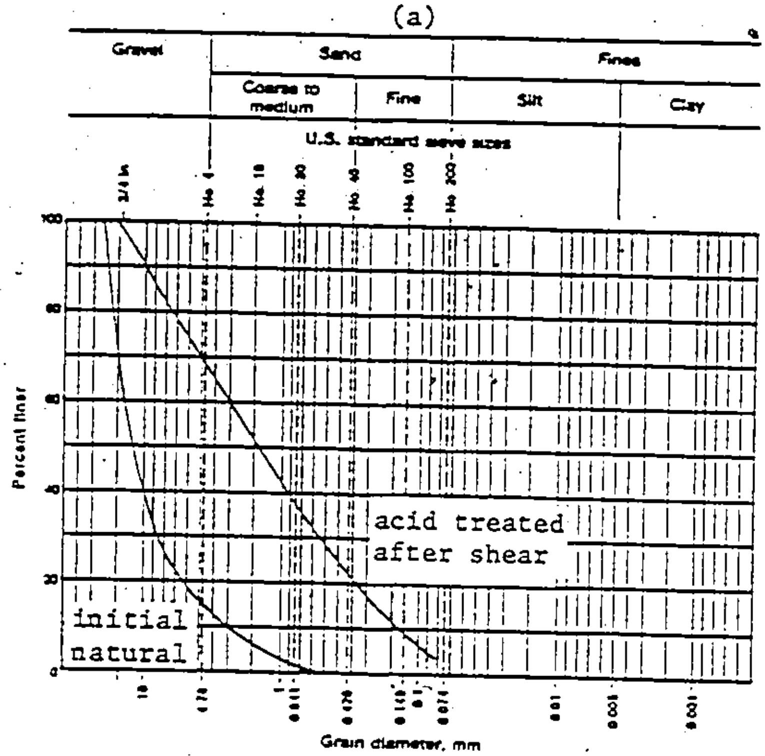

(b)

Figure 4.2 Gradation: initial, weathered, and acid treated after shear.

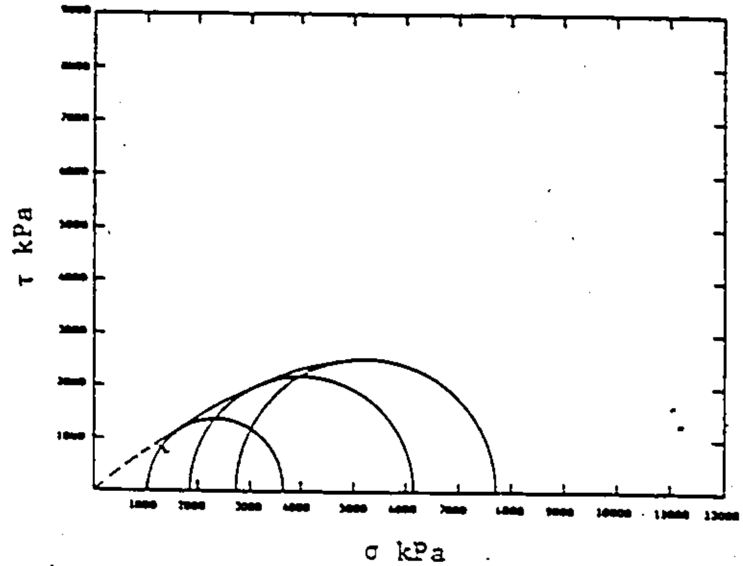

Dry natural specimens

(a)

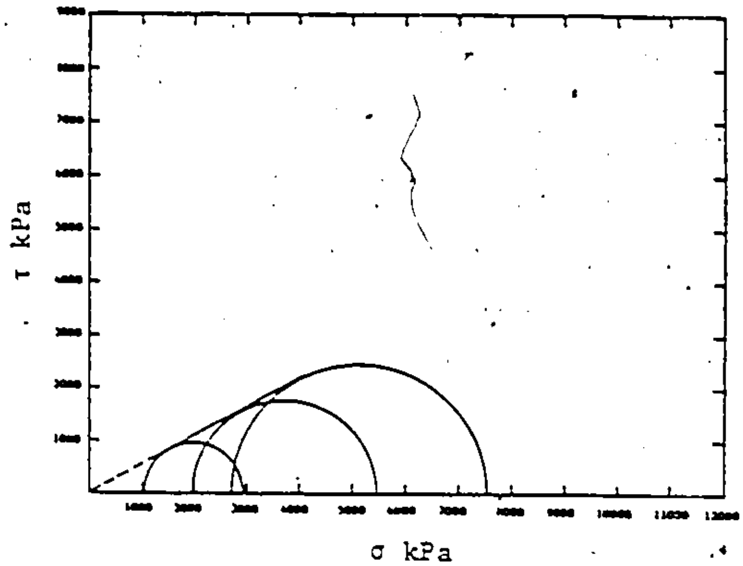

Saturated natural specimens

(c)

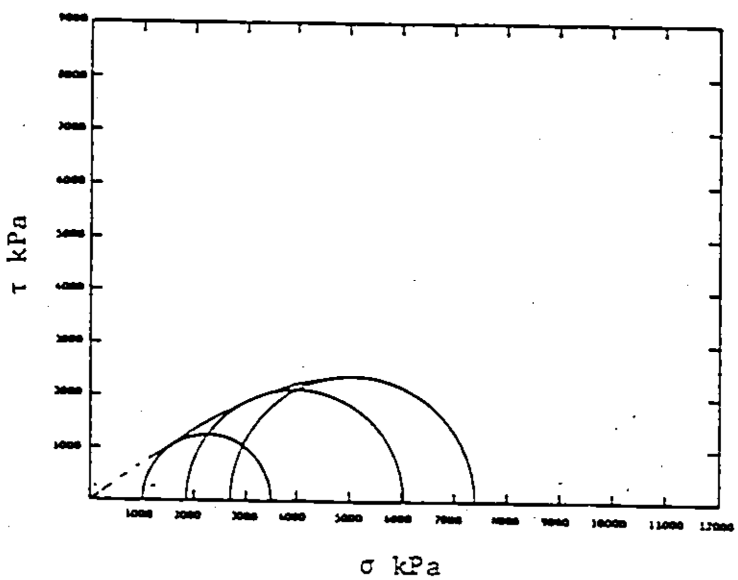

Dry weathered specimens

(b)

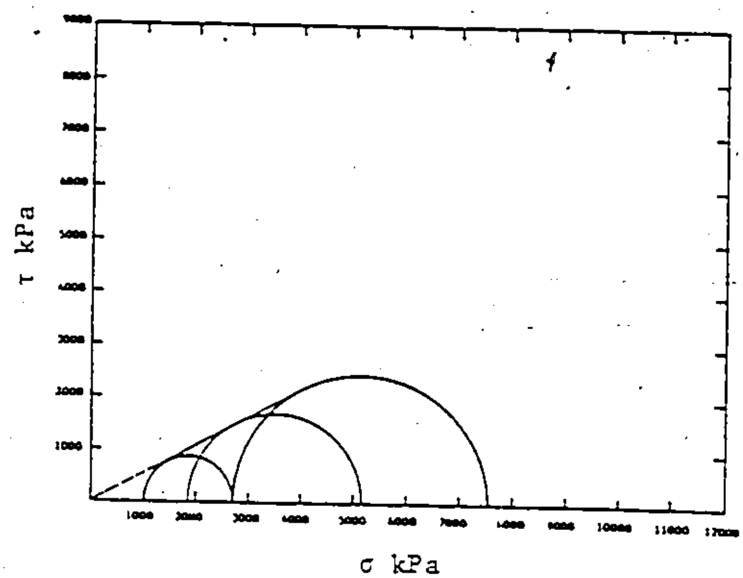

Saturated weathered specimens

(d)

Figure 4.3 Mohr-Coulomb failure envelope at 10 % strain.

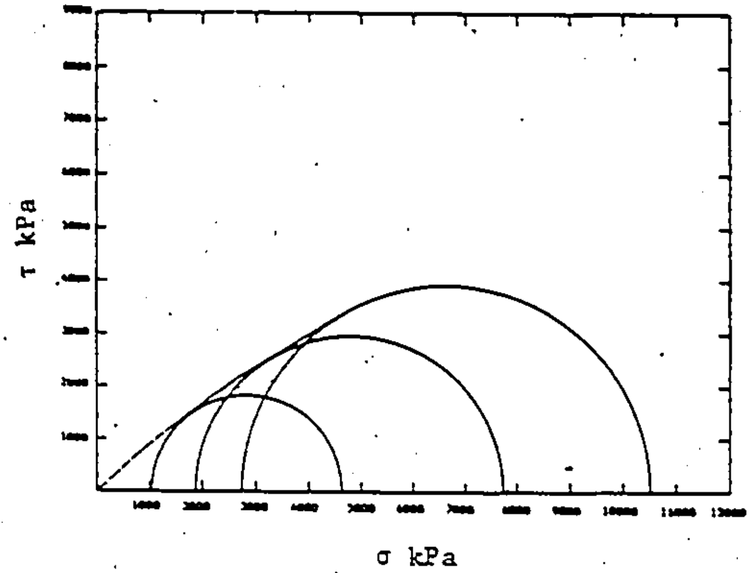

Dry natural specimens

(a)

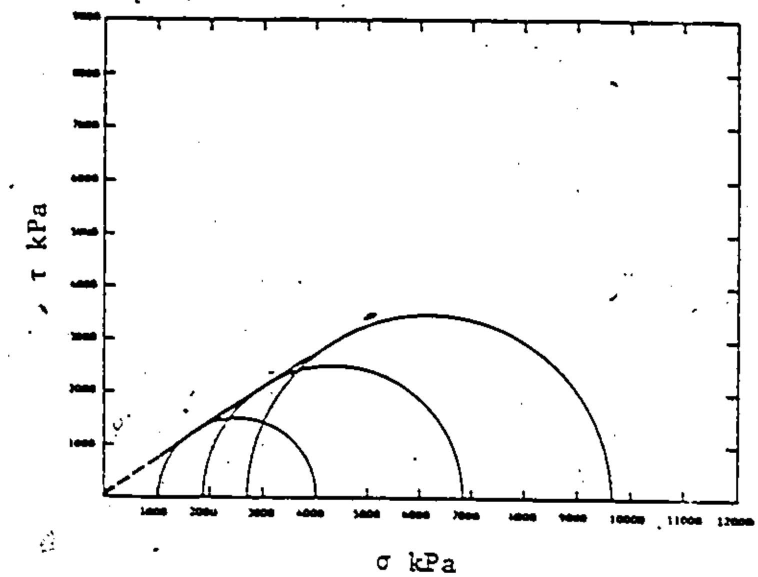

Saturated natural specimens

(c)

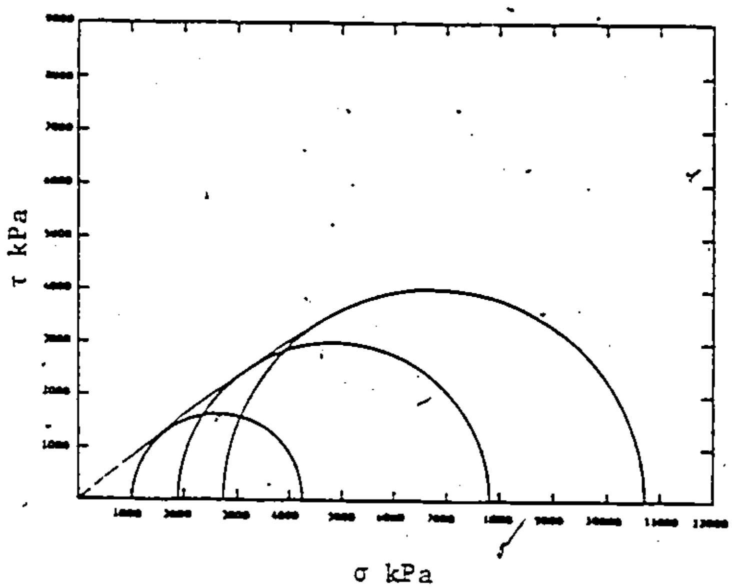

Dry weathered specimens

(b)

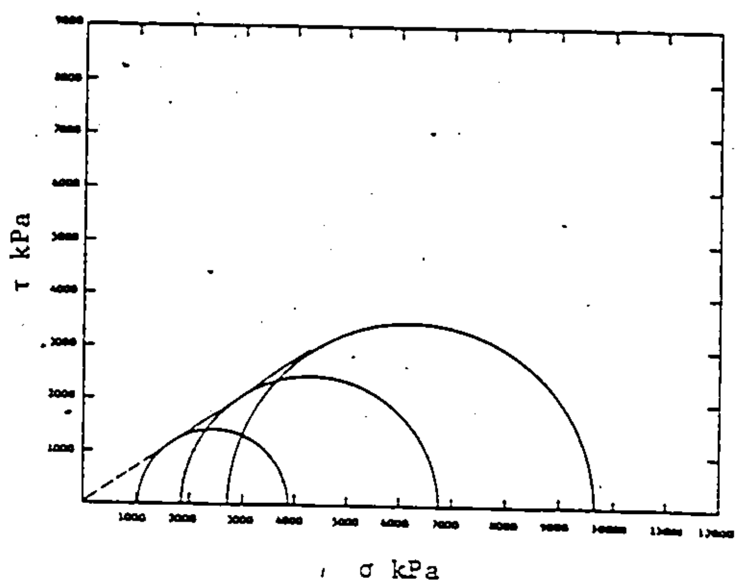

Saturated weathered specimens

(d)

Figure 4.4 Mohr-Coulomb failure envelope at 24 % strain.

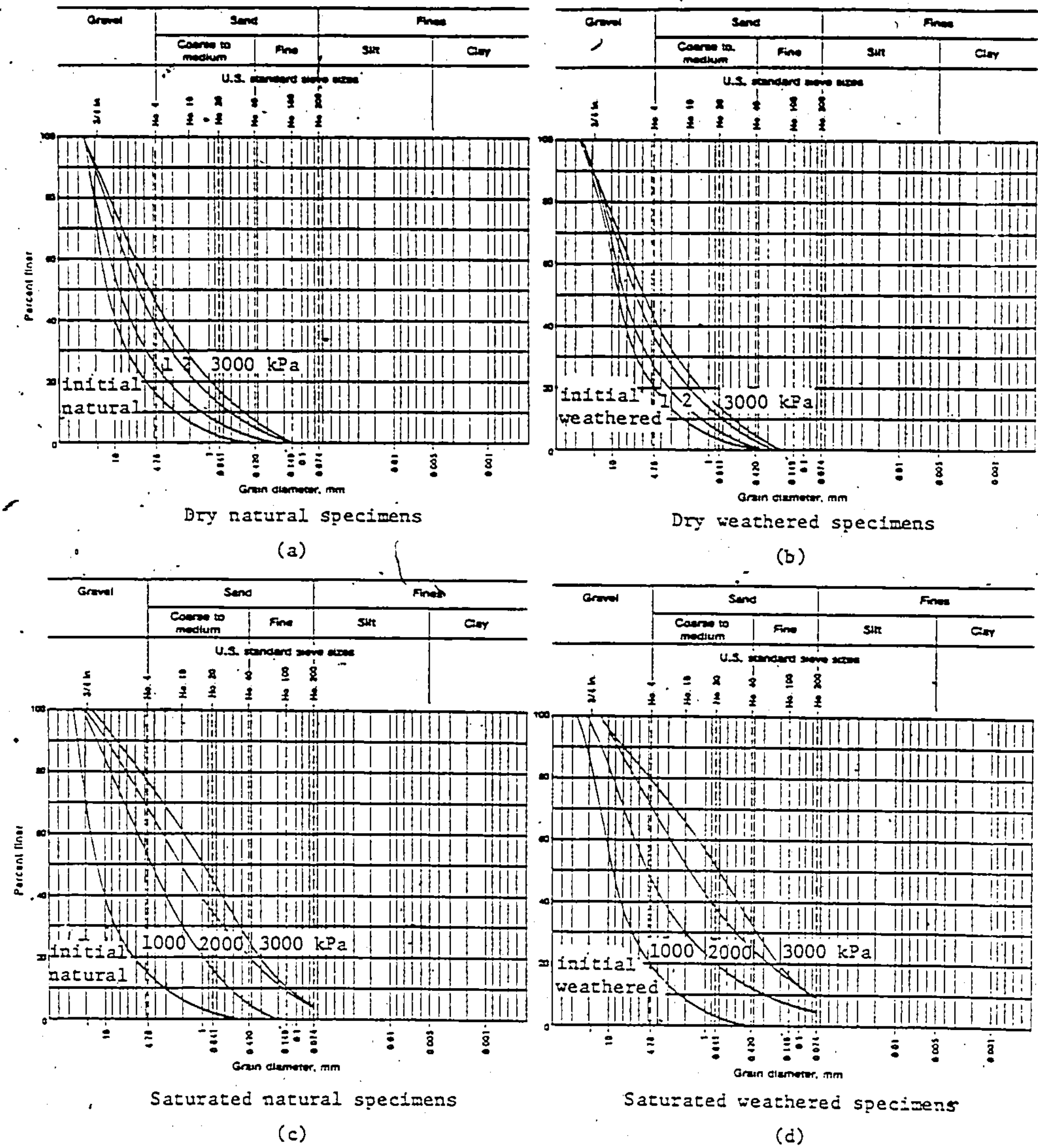

Figure 4.5 Gradation before and after shear for the four types.

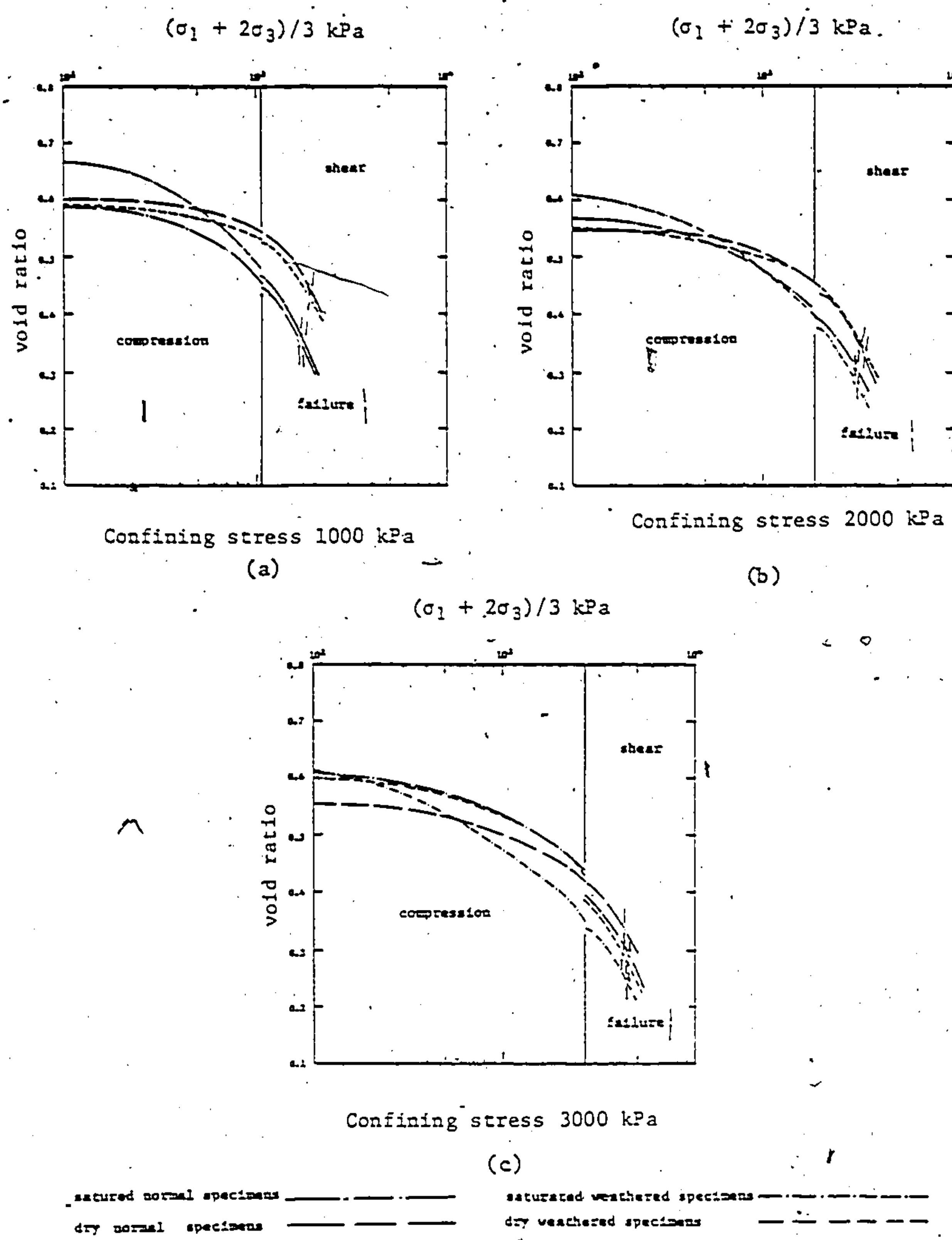

Figure 4.6 Void ratio versus mean normal stress.

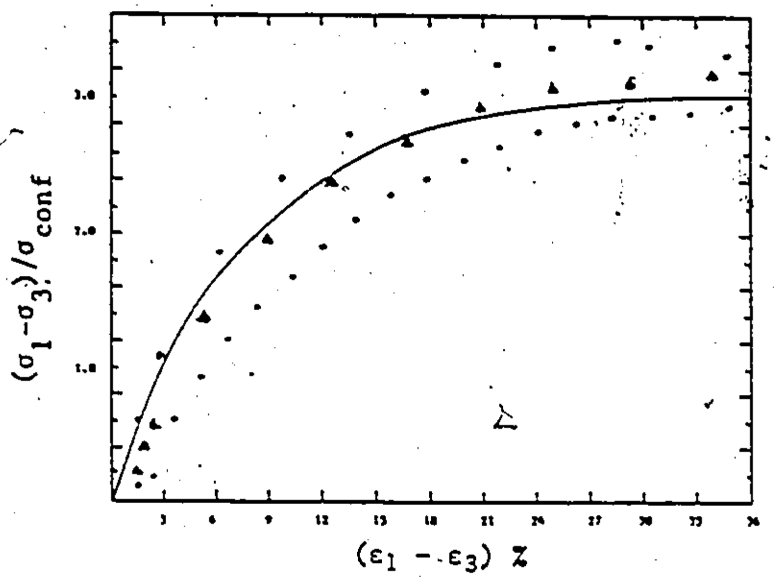

Dry natural specimens

(a)

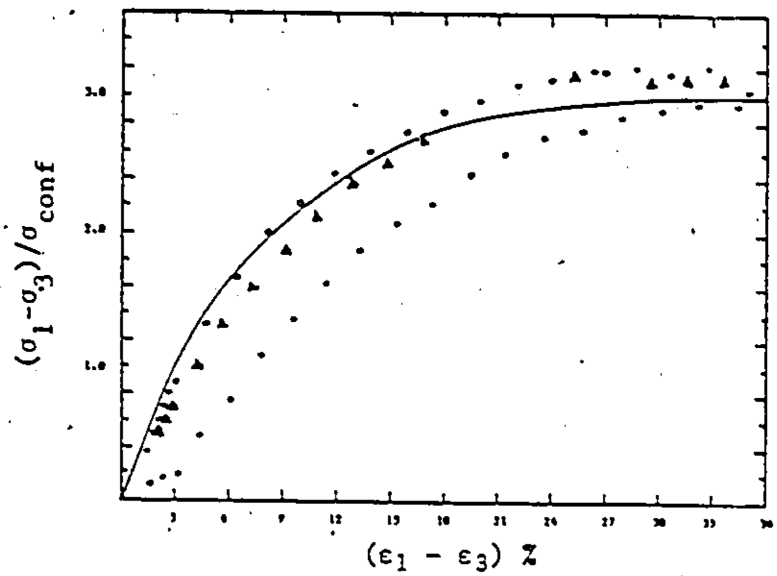

Dry weathered specimens

(b)

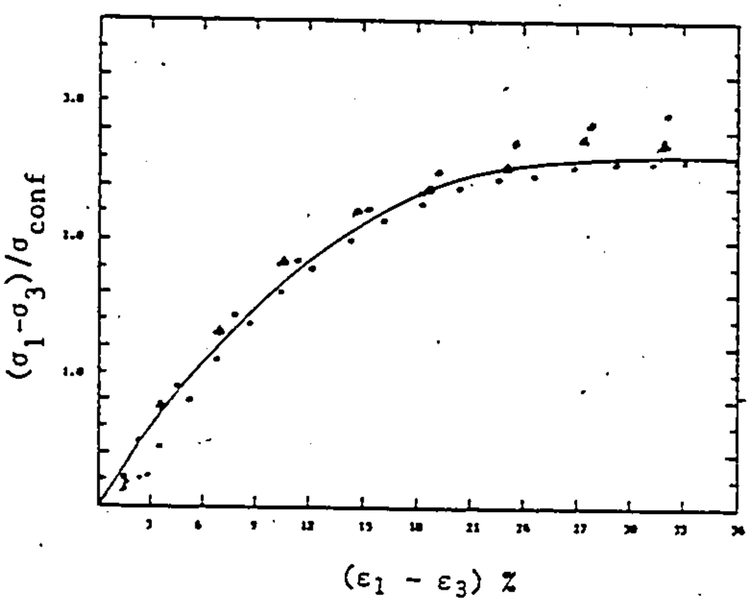

Saturated natural specimens

(c)

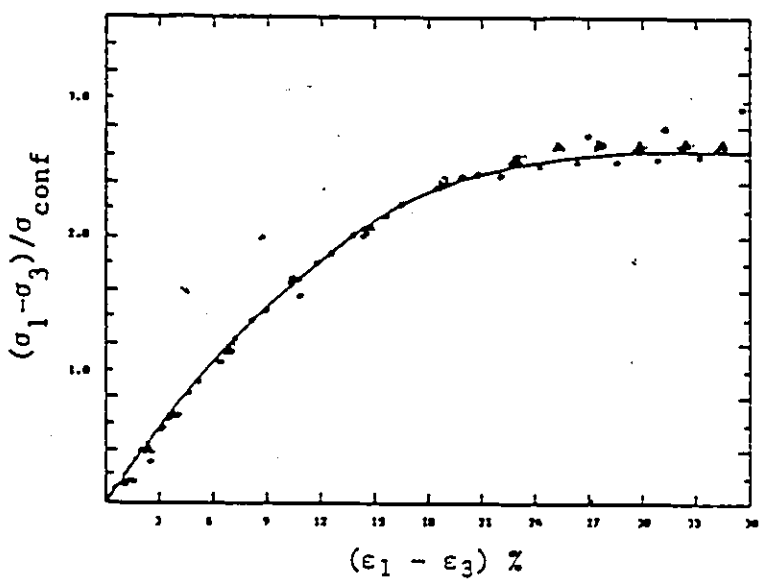

Saturated weathered specimens

(d)

1000 kPa ○ 2000 kPa ▲ 3000 kPa ●

Normalized Deviator Stress vs Deviatoric Strain

Figure 4.7 Shear Modulus curves using σ_{conf} for normalization.

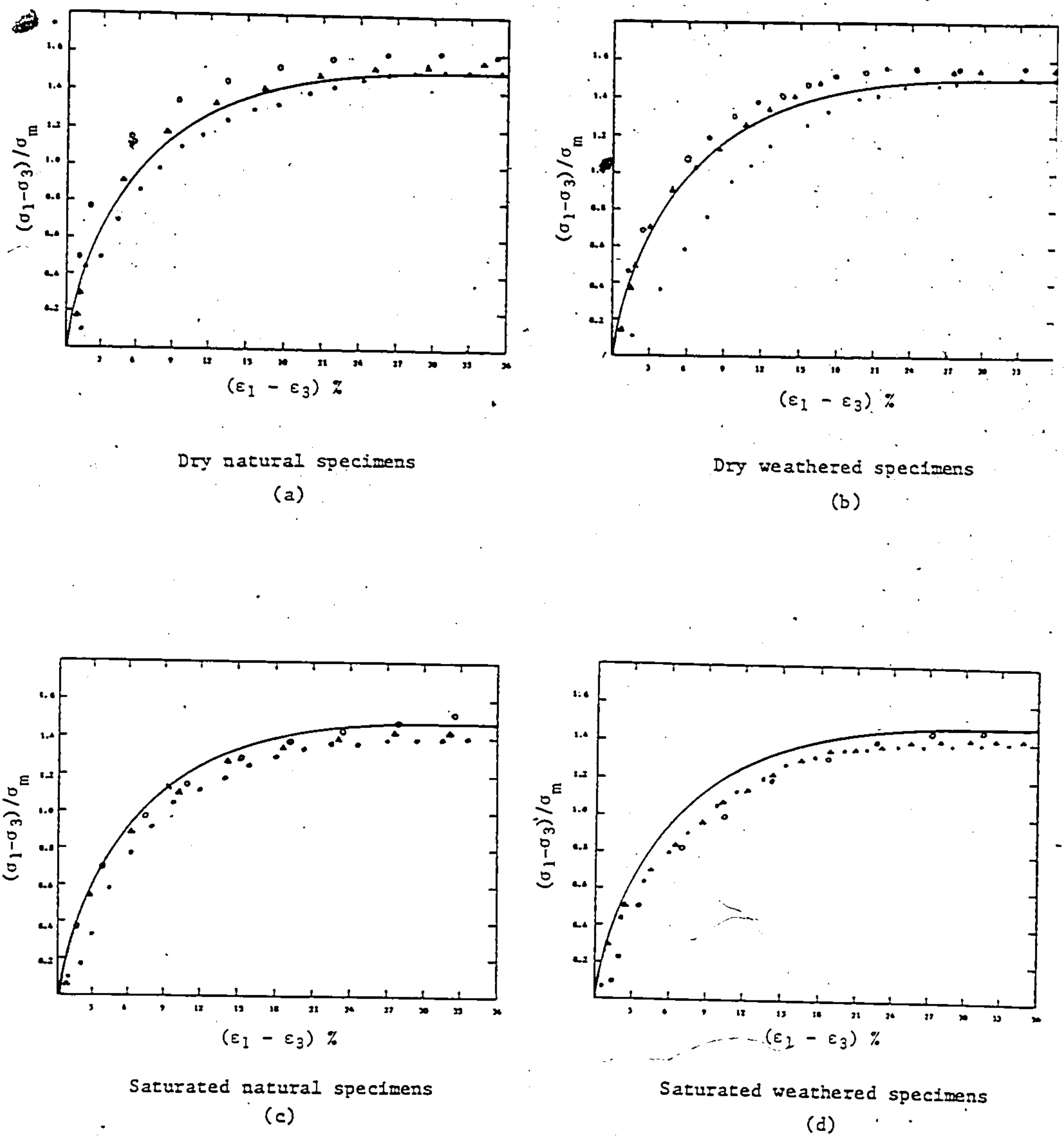

1000 kPa ∘ 2000 kPa ▲ 3000 kPa •

Normalized Deviator Stress vs Deviatoric Strain

Figure 4.8 Shear Modulus curves using σ_m for normalization.

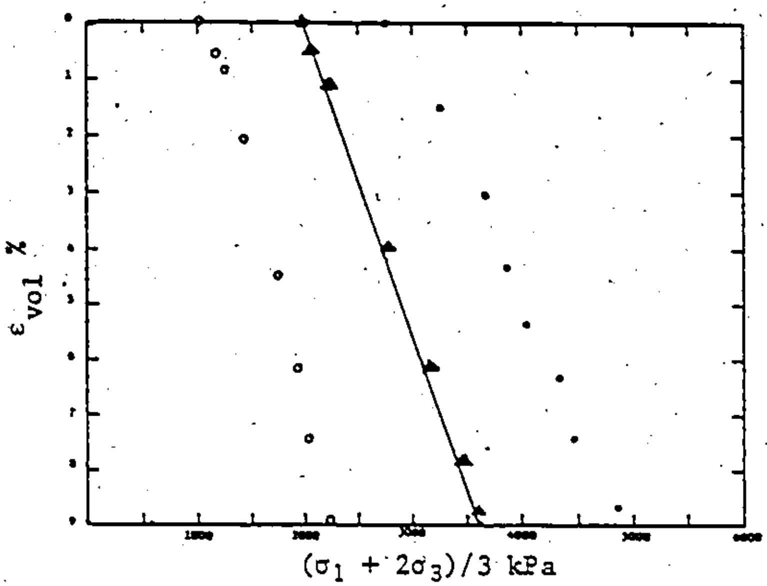

Dry natural specimens

(a)

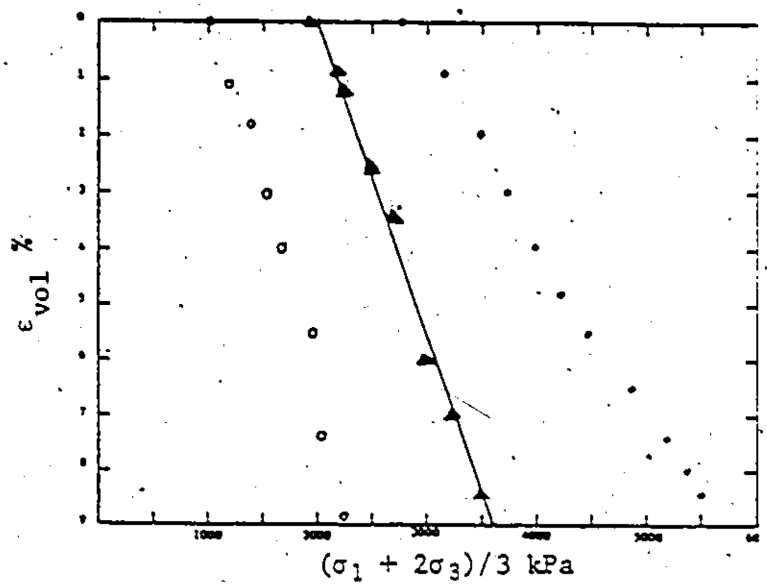

Dry weathered specimens

(c)

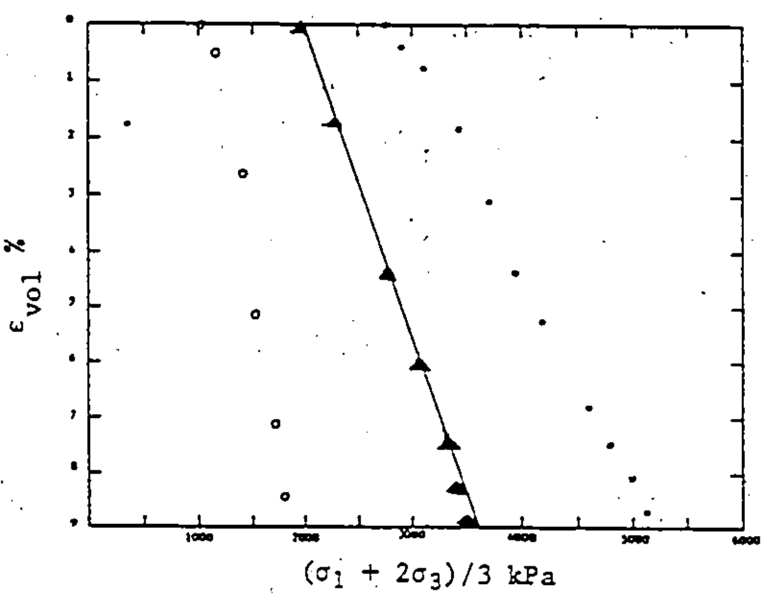

Saturated natural specimens

(b)

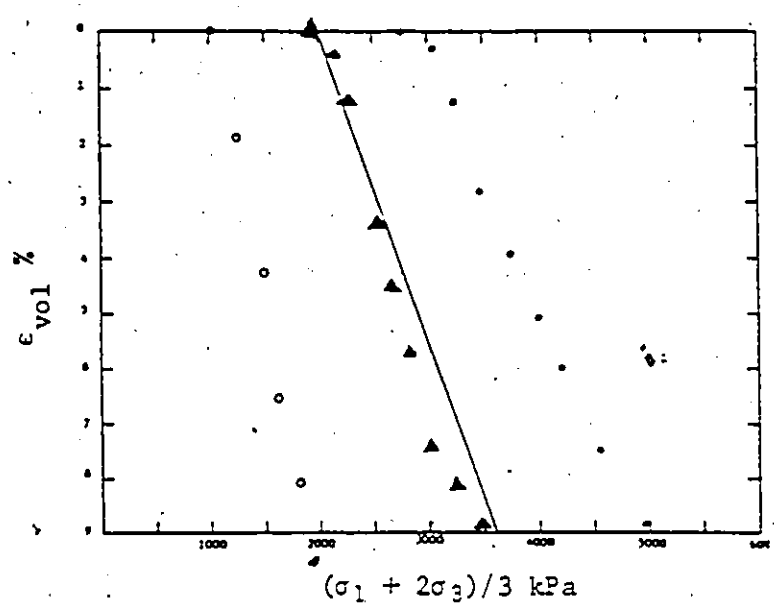

Saturated weathered specimens

(d)

1000 kPa ○ 2000 kPa ▲ 3000 kPa ●

Volumetric Strain vs Mean Normal Stress

Figure 4.9 Bulk Modulus curves.

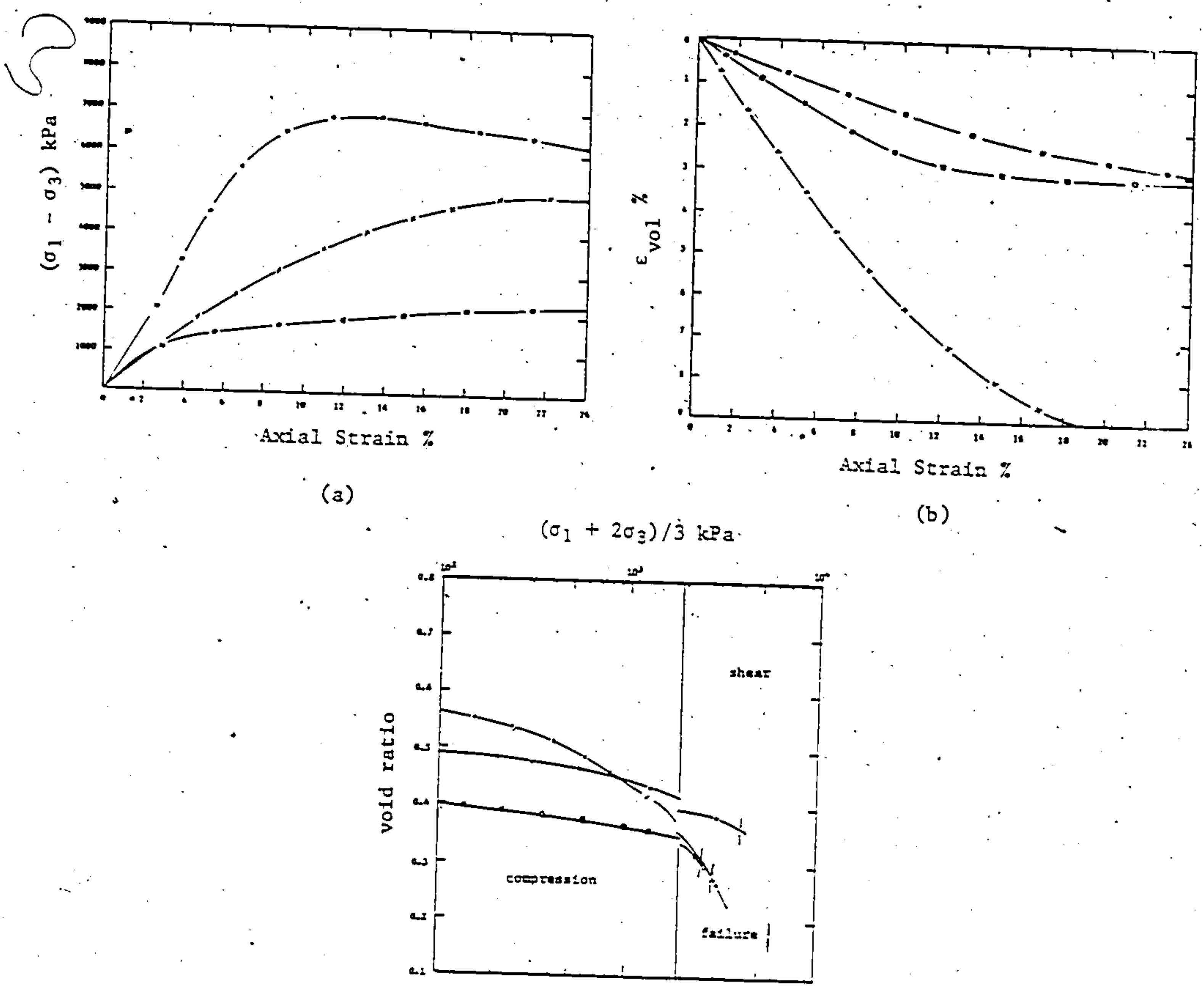

(c)

acid-treated —x— dry powder —■— saturated powder—□—

Confining stress 2000 kPa

Figure 4.10 Deviator stress and volumetric strain versus axial strain, void ratio versus mean normal stress.

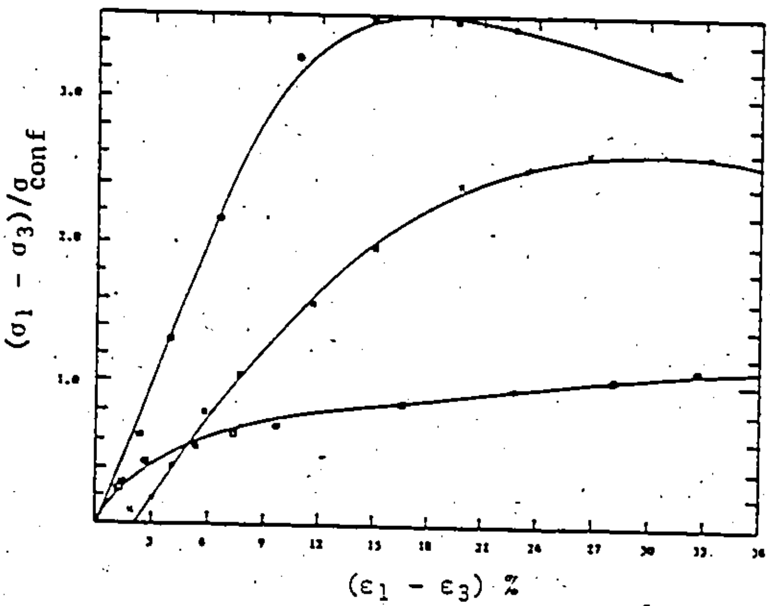

a)

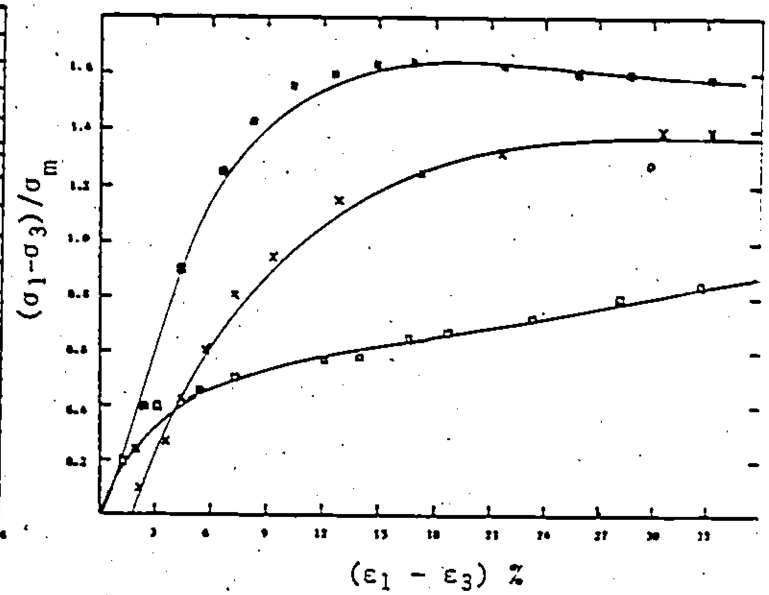

b)

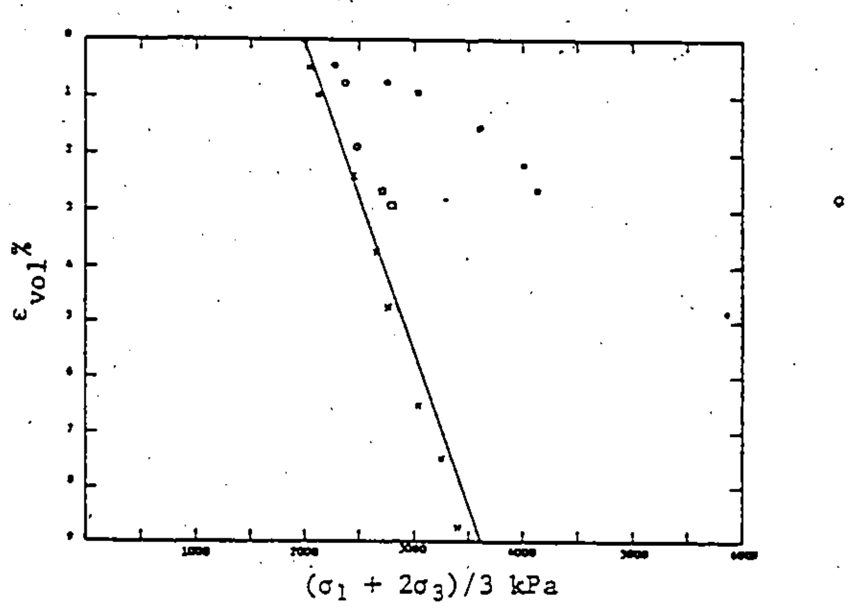

c)

acid-treated —x— dry powder —■— saturated powder—□—

Figure 4.11 Shear and bulk modulus curves.

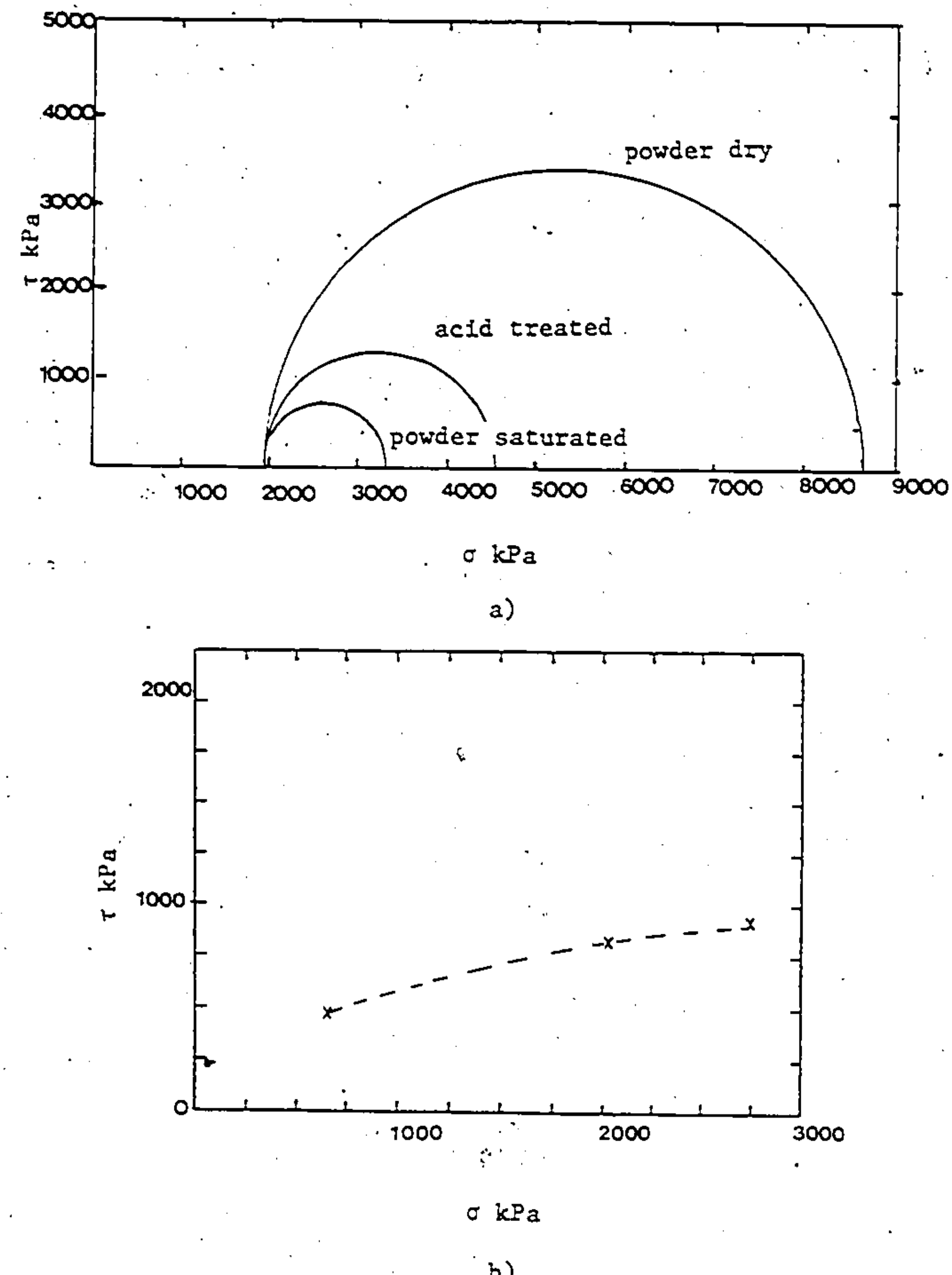

Figure 4.12 Mohr circle and direct shear test results.

State of material		Confinement		
		1000 kPa	2000 kPa	3000 kPa
dry natural	β =	0.002	0.001	0.001
	m =	10^6	10^6	10^6
sat. natural	β =	0.003	0.002	0.001
	m =	10^5	10^5	10^5
dry weathered	β =	0.002	0.002	0.001
	m =	10^5	10^5	10^5
sat. weathered	β =	0.003	0.002	0.001
	m =	10^5	10^5	10^5

table 4.1 Tangent Modulus parameters of Queenston Shale

CHAPTER 5

CONCLUSIONS

5.1 Specific

1. The lack of any definite peaks in the stress-strain curves, and the compression characteristics of the fragmented, Queenston Shale specimens tested in this study was due to their loose relative density.

2. Membrane correction was unnecessary for triaxial compression tests at such high pressures as those used in this study.

3. Under the same test conditions, natural and weathered materials had the same behaviour in shear and compression.

4. Dry specimens of fragmented Queenston Shale, at 70 to 80 % relative density, had an expectantly normal curved, Mohr-Coulomb failure envelope.

5. Surprisingly, saturated specimens, at the same relative densities, had straight envelopes, and, when projected back, intersected the origin.

6. As expected, dry material was stronger than saturated material.

7. At low confinement, there was a 25 % difference in shear strength, as measured by deviator stress, between dry and saturated specimens. At high confinement, this difference reduced to 10 % or less.

8. Rowe 's (1962) volume change correction brought all deviator stress-strain curves to one approximately unique curve.

9. The failure characteristics of fragmented Queenston Shale, at 70 to 80 % relative density, using the 24 % and 10 % failure strain criteria were more or less the same.

10. Slaking, below a particle size of 20 mm, did not affect the material very much.

11. Shear testing and compression of dry specimens changed the grain size distibution of the material more than slaking did under no stress conditions (except gravitational).

12. Shear testing and compression of saturated specimens affected grain size distribution more than they did dry specimens under the same conditions.

13. Shear testing and compression of saturated specimens at high confinement appeared to alter, slightly, the degradation process.

14. Specimens compressed to the same stress and the same saturation conditions reached the same void ratio, even though initial void ratios were different.

15. The parameter λ was constant for all types of the material, including saturated powdered material.

16. Normalization of the deviator stress using the mean normal stress produced excellent results, and is a much better normalization technique than one using confining stress.

17. The shear modulus of both saturated and dry fragmented Queenston Shale at 70 to 80 % relative density was dependent, not only on deviator stress and strain, but also on mean normal stress (Parameters determined by monotonic loading).

18. For all conditions tested in this study, the bulk modulus

for the shearing phase was approximately constant.

19. Janbu's (1967) tangent modulus parameter, β, is approximately zero, while the modulus number, m is 1×10^6 for dry material and 1×10^5 for saturated material.

20. EDTA, a cementing bond dissolver, did not seem to have any affect on the stress-strain characteritics of fragmented Queenston Shale.

21. Saturated powdered Queenston Shale, at a density of 1990 kg/m^3, had a 60 % lower shear strength (measured by deviator stress) than saturated fragmented shale at 2000 kPa confining stress.

22. The expression for the shear modulus of the saturated powder is non-linear, and the normalization version of it using σ_m has a different constant than the one for the fragmented shale.

23. Since the tests on the powdered shale were at one confining pressure, it was impossible to determine if the shear modulus of this type of material was dependent on the mean normal stress.

24. The shear strength of powdered Queenston Shale (saturated and dry), as determined from direct shear tests (Thompson 1981) indicated that the failure envelope was curved, as expected.

25. The angle of internal friction of dry and saturated powdered specimens at the same normal stress is the same.

5.2 General

Queenston Shale is a mechanical compaction shale. It has a neutral reaction to, at least, two acids, indicating that it is non-cemented. As a mechanical shale, Queenston Shale should slake easily. Indeed, large blocks of it readily break down by weathering, ultimately, forming a red clay soil. But, such behaviour was not the case at a particle size of 20 mm or less. At this scale level, the material proved to be quite resistant to weathering. In addition, Queenston Shale does not contain any expansive clay minerals. Any weathering which occurs is probably as a result of the propagation of Griffith's cracks. This propagation, most likely, occurs because of capillary tension decrease, fracture energy reduction, and, in a stress environment, local pore pressure increase.

The shear and compressibility behaviour of fragmented Queenston Shale at 70 to 80 % relative density is similar to that of a loose sand. It experiences only compression in triaxial compression, and has no definite peak behaviour in its stress-strain curve. The Mohr-Coulomb failure envelope is curved, at least for dry specimens. Surprisingly, the envelope is straight for saturated specimens.

Saturation of fragmented Queenston Shale in conditions of stress, such as in triaxial compression, increases the compressibility of the material by facilitating grain breakage. Increased compressibility affects the mean normal stress, which influences the deviator stress through the shear modulus. Thus, saturation indirectly reduces the shear strength of the material, by increasing the occurrence of grain breakage, but it does not seem to affect the pure frictional part of the shear strength, as defined by Taylor (1948).

5.3 Recommendations

In order to obtain a more thorough investigation of the behaviour of fragmented Queenston Shale, undrained triaxial compression test along with extension tests should be performed.

A better method of measuring volume changes in the specimens than monitoring the air expelled would be to measure the volume of fluid entering or leaving the triaxial cell.

A correlation should be made between the slaking characteristics of large fragments of Queenston Shale and the ones investigated in this study. The deterioration effects of freezing and thawing should also be examined.

Since the literature review has established that the shear strength of granular materials decreases with the increase in size of the particles, the values of the angle of internal friction determined in this study should be reduced in any design of structures using fragmented Queenston Shale as a building material.

All parameters determined in this study need to be verified with field data from actual case studies.

Since slaking affects large blocks of Queenston Shale, eventually reducing them to fine soil consistency, a conservative design could utilize the shear strength of the powdered shale to design structures which are meant to have a long life span.

In order to make this study more relevant, a correlation could be made between the strength and slaking charateristics of Queenston Shale and the slaking behaviour of other mechanical shales.

Bibliography

Atkinson, J.H., and Bransby, P.L., (1978). The Mechanics of Soils, An Introduction to Critical State Soil Mechanics. McGraw-Hill Co, London, 1978, pp. 235-244.

Bishop, A.W., (1954). Correspondence on "Shear Characteristics of a Saturated Silt, Measured in Triaxial Compression". Géotechnique, Vol. 4, pp. 43-45.

Bishop, A.W., and Henkel, D.J., (1962). The Measurement of Soil Properties in the Triaxial Test. 2nd ed., Edward Arnold Ltd., London.

Bjerrum, L., (1967). "Engineering Geology of Normally Consolidated Marine Clays as Related to the Settlements of Buildings". Seventh Rankine Lecture, Geotechnique, Vol. 17, No. 2, pp. 82-118.

Boussinesq, J., (1885). Applications des Potentielles à l'Etude de l'Equilibre et du Movement des Solides Elastiques, Paris, Gauthier-Villars.

Bowles, J.E., (1970). Engineering Properties of Soils and their Measurement, McGraw-Hill Book Co., New York, p. 135.

Caley, J.F., (1940). "Palaeozoic Geology of the Toronto-Hamilton Area, Ontario". Geological Survey of Canada, Memoir 224.

Casagrande, A., (1936a). "Characteristics of Cohesionless Soils Affecting the Stability of Slopes and Earth Fills". J. Boston Soc. Civil Engrs., 23, No. 1, pp. 13-32.

Casagrande, A., (1936b). "Notes on the Shearing Resistance and the Stability of Cohesionless Soils and their Relation to the

Design of Earth Dams". Proceedings, First Int. Conf. Soil Mech. Found. Eng., Cambridge, Mass., Vol. 3, pp. 56-60.

Charles, J.A. and Watts, K.S., (1980). "The Influence of Confining Pressure on the Strength of Compacted Rockfill". Geotechnique, 30, No. 4, pp. 353-367.

Christian, J.T. and Desai, C.S., (1977). "Constitutive Laws for Geological Media". Numerical Methods in Geotechnical Engineering, Desai and Christian, ed., McGraw-Hill Book Co., New York, pp. 65-115.

Clough, R.W. and Woodward, R.J., (1967). "Analysis of Embankment Stresses and Deformations". J. of Soil Mech. and Found. Div., ASCE, Vol. 93, No. SM4, pp. 529-549.

Coste, J.F. and Parayre, J.P., (1962). "Influence de la Pression Moyenne et du Deviateur sur le Module de Déformation d'un Sable". Annales des Ponts et Chaussées, Vol. 132, No. 6, Paris, pp. 707-724.

De Beer, E.E., (1965). "The Scale Effect on the Phenomenon of Progressive Rupture in Cohesionless Soils". Proceedings, 6th Int. Conf. Soil Mech. Found. Eng., Montreal, Vol. 2, pp. 13-17.

Griffith, A.A., (1921). "The Phenomena of Rupture and Flow in Solids". Philosophical Transactions, Royal Society of London, Series A, 221, pp. 163-198.

Guillet, G.R., (1967). "The Clay Products Industry of Ontario". Ontario Dept. Mines, IMR 22, p. 68.

Guillet, G.R., (1977). "Clay and Shale Deposits of Ontario". Ontario Geological Survey, Mineral Deposits Circular MDC 15, p. 24.

Hall, E.B. and Gordon, B.B., (1963). "Triaxial Testing with Large Scale High Pressure Equipment". Laboratory Shear Testing of Soils, Special Technical Publication No. 361, ASTM, pp. 315-328.

Hirschfeld, R.C. and Poulos, S.J., (1963). "High Pressure Triaxial Tests on a Compacted Sand and an Undisturbed Silt". Laboratory Shear Testing of Soils, Special Technical Publication No. 361, ASTM, pp. 329-341.

Holtz, W.G. and Gibbs, H.J., (1956). "Triaxial Shear Tests on Pervious Gravelly Soils". J. Soil Mech. Found. Div., ASCE, Vol. 82, No. SM 1, pp. 1-22.

Jaeger, J.C., (1972). Rock Mechanics and Engineering, Cambridge University Press, London, p. 69.

Jaeger, J.C., (1978). Elasticity, Fracture, and Flow with Engineering and Geological Applications, Chapman and Hall, London, p. 55.

Janbu, N., (1967). "Settlement Calculations Based on the Tangent Modulus Concept". Bulletin 2, Norwegian Institute of Technology, Trondheim, pp. 1-51.

Jumikis, A.R. and Jumikis, A.A. (1975). "Red Brunswick Shale and Its Engineering Aspects". Engineering Research Bulletin No. 55, Rutgers, State University of New Jersey.

Jurgenson, Leo, (1934). "The Shearing Resistance of Soils". J. Boston Society of Civil Eng., No.3, reprinted in Contributions to Soil Mechanics 1925-1940, Boston Soc. Civil Eng., 1940, pp. 184-217.

Kavazanjian, E. and Mitchell, J.K., (1980). "Time-Dependent Deformation Behavior of Clays". J. of the Geotech. Eng. Div., ASCE, Vol. 106, No. GT9, pp. 611-630.

Kondner, R.L., (1963). "Hyperbolic Stress-Strain Response: Cohesive Soils". J. of Soil Mech. Found. Div., ASCE, Vol. 89, No. SM1, pp. 115-144.

Ladanyi, B., (1960). "Etude des Relations Entre les Contraintes et les Déformations lors du Cisaillement des Sols Pulvérulents". Annales des Travaux Publics de Belgique, 3: pp. 241-274.

Ladanyi, B., (1967). "Discussion". Can. Geotech. J., Vol. 4, pp. 87-88.

Lambe, T.W., (1951). Soil Testing for Engineers, John Wiley and Sons, Inc., New York, p. 118.

Lee, K.L. and Farhoomand, I., (1967). "Compressibility and Crushing of Granular Soil in Anisotropic Triaxial Compression". Can. Geotech. J., Vol. 4, pp. 68-86.

Lee, K.L. and Seed, H.B., (1967a). "Drained Strength Characteristics of Sands". J. Soil Mech. Found. Div., ASCE, SM 6, pp. 117-141.

Lee, K.L. and Seed, H.B., (1967b). "Effect of Moisture on the Strength of a Clean Sand". J. Soil Mech. Found. Div., ASCE, SM 6, pp. 17-41.

Leps, T.M., (1970). "Review of Shearing Strength of Rockfill". J. Soil Mech. Found. Div., ASCE, SM 4, pp.1159-1170.

Lo, K.Y. and Hori, M., (1979). "Deformation and Strength Properties of Some Rocks in Southern Ontario". Can. Geotech. J., Vol. 16, pp. 108-120.

Marachi, N.D., Chan, C.K., and Seed, H.B., (1972). "Evaluation of Properties of Rockfill Materials". J. Soil Mech. Found. Div., ASCE, SM 1,pp. 95-114.

Marsal, R.J., (1965). "El Infernillo Dam, Observations During the Construction Period and First Filling of the Reservoir". CFE Publication, Mexico.

Marsal, R.J., (1967). "Large-Scale Testing of Rockfill Materials". J. Soil Mech. Foud. Div., ASCE, SM 2, pp. 27-43.

Marsal, R.J., (1973). "Mechanical Properties of Rockfill". Embankment-Dam Engineering; John Wiley and Sons, Inc., New YorK, 1973, pp. 109-199.

Morgenstern, N.R. and Eigenbrod, K.D., 1974. "Classification for Argillaceous Soils and Rocks". J. Geotech. Eng. Div., ASCE, GT 10, pp. 1137-1156.

Penman, A.D.M., Burland, J.B., and Charles, J.A., (1971). "Observed and Predicted Deformations in a Large Embankment Dam During Construction". Proceeding of the Institution of Civil Engneers, (Britain), Vol. 49, pp. 1-21.

Perloff, W.H., (1975). "Pressure Distributions and Settlements". Foundation Engineering Handbook, Winterkorn and Fang, ed., Van Nostrand Reinhold Co., New York, pp. 148-196.

Pettijohn, E.J. (1975). Sedimentary Rocks, 3rd ed., Harper and Row, New York, P. 17.

Pit Slope Manual (1977). "Waste Embankments", chap. 9, CANMET; Energy, Mines, and Resources, Canada, p. 36.

Roscoe, K.H., Schofield, A.N., and Wroth, C.P., (1958). "On the Yielding of Soils". Géotechnique, Vol. 8, pp. 22-53.

Rowe, P.W., (1962). "The Stress-Dilatancy Relation for Static Equilibrium of an Assembly of Particles in Contact". Proceedings, Royal Society, Series A, London, Vol. 269, No. 1339, pp. 500-527.

Steele, I.C., (1951). Handbook of Applied Hydraulics, McGraw-Hill Book Co., New York.

Tavenas, F. and Leroueil, S., (1977). "Effects of Stresses and Time on Yielding of Clays". 9th ICSMFE, Vol. 1, Tokyo, pp. 319-326.

Taylor, D.W., (1948). Fundamentals of Soil Mechanics, John Wiley and Sons, Inc., New York, pp. 346-350.

Terzaghi, K., (1925). "Modern Conceptions Concerning Foundation Engineering". Boston Soc. Civil Eng., Vol. XIII, No. 10, reprinted in Contributions to Soil Mechanics 1925-1940, Boston Soc. Civil Eng., 1940, pp. 1-43.

Terzaghi, K. and Peck, R.B., (1948). Soil Mechanics in Engineering Practice, John Wiley and Sons., Inc., New York.

Thompson, W.J., (1981). Unpublished results, personal communication.

Underwood, L.B., (1967). "Classification and Identification of Shales". J. Soil Mech. Found. Div., ASCE, Vol. 93, SM 6, pp. 97-116.

Van Eeckhout, E.M., (1976). "The Mechanisms of Strength Reduction Due to Moisture in Coal Mine Shales". Int. J. Rock Mech. Min. Sci. and Geomech. Abst., Vol. 13, pp. 61-67.

Vesic, A.S. and Clough, G.W., (1968). "Behavior of Granular Materials under High Stresses". J. Soil Mech. Found. Div., ASCE, SM 3, pp. 661-688.

Windisch, S.J. and Soulie, M., (1970). "Technique for the Study of Granular Materials". J. Soil Mech. and Found. Div., ASCE, SM 4, pp. 1113-112.

Appendix A

REVIEW OF ELASTICITY THEORY

The theory of elasticity is well documented and for this reason, with a special application to soil mechanics will only be briefly discussed in the following section. Most of the interpretation is attributed to Christian and Desai (1977).

A1 Stress

The stress tensor that represents the stress state in space can be described by the matrix

$$\sigma_{ij} = \begin{bmatrix} \sigma_{xx} & \sigma_{xy} & \sigma_{xz} \\ \sigma_{xy} & \sigma_{yy} & \sigma_{yz} \\ \sigma_{xz} & \sigma_{yz} & \sigma_{zz} \end{bmatrix}$$

Each component of the stress represents a force acting in a specific coordinate direction on a unit area oriented in a particular way. Thus, σ_{xy} is the force in the positive x direction acting on a unit area, whose normal is in the y direction. The terms σ_{xx}, σ_{yy}, and σ_{zz} are normal stresses and the rest are shear stresses. Because compression is more common than tension in geotechnical problems, the usual geotechnical convention is to make compression positive.

If two coordinate systems are represented by x, y, z, and a, b, c and the direction cosines are the cosines of the angles between pairs of coordinate directions, then they can be denoted by the coordinate labels enclosed in parentheses. For instance (y,a) is the cosine between direction y and direction a. A point with coordinates (x, y, z) in one system will have coordinates (a, b, c) in the other system defined by:

$$\begin{Bmatrix} a \\ b \\ c \end{Bmatrix} = \begin{bmatrix} (x,a) & (y,a) & (z,a) \\ (x,b) & (y,b) & (z,b) \\ (x,c) & (y,c) & (z,c) \end{bmatrix} \begin{Bmatrix} x \\ y \\ z \end{Bmatrix}$$

This 3 x 3 matrix is called the transformation matrix T . Any vector v written in the x, y, z system can be transformed into v^* in the a, b, c system by

$$\{v^*\} = [T]\{v\}$$

The stress σ in the x, y, x system can be transformed into σ^* in the a, b, c system by

$$[\sigma^*] = [T][\sigma][T]^T$$

By using the theory of matrices a set of rotations of coordinates can be found that will give a stress σ^* that has only diagonal or normal terms:

$$[\sigma^*] = \begin{bmatrix} \sigma_1 & 0 & 0 \\ 0 & \sigma_2 & 0 \\ 0 & 0 & \sigma_3 \end{bmatrix}$$

The diagonal terms are called the principal stresses and they are the solutions of the equation

$$\sigma^3 - I_1\sigma^2 + I_2\sigma - I_3 = 0$$

where

$$I_1 = \sigma_{xx} + \sigma_{yy} + \sigma_{zz}$$

$$I_2 = \begin{vmatrix} \sigma_{xx} & \sigma_{xy} \\ \sigma_{xy} & \sigma_{yy} \end{vmatrix} + \begin{vmatrix} \sigma_{yy} & \sigma_{yz} \\ \sigma_{yz} & \sigma_{zz} \end{vmatrix} + \begin{vmatrix} \sigma_{xx} & \sigma_{xz} \\ \sigma_{xz} & \sigma_{zz} \end{vmatrix}$$

$$I_3 = \begin{bmatrix} \sigma_{xx} & \sigma_{xy} & \sigma_{xz} \\ \sigma_{xy} & \sigma_{yy} & \sigma_{yz} \\ \sigma_{xz} & \sigma_{yz} & \sigma_{zz} \end{bmatrix}$$

These are called, respectively, the first, second, and third invariant of the stress. Since the principal stresses are physical quantities, independent of the choice of coordinate axes, the invariants must also be independent of the choice of axes and are, therefore, invariant under the rotations of coordinates.

The average normal stress is called the octahedral normal stress, σ_{oct}, and it is also invariant:

$$\sigma_{oct} = I_1 / 3$$

$$\begin{bmatrix} \sigma_{oct} \end{bmatrix} = \begin{bmatrix} \sigma_{oct} & 0 & 0 \\ 0 & \sigma_{oct} & 0 \\ 0 & 0 & \sigma_{oct} \end{bmatrix}$$

The deviator stress is then defined as

$$\begin{bmatrix} s \end{bmatrix} = \begin{bmatrix} \sigma_{xx} - \sigma_{oct} & \sigma_{xy} & \sigma_{xz} \\ \sigma_{xy} & \sigma_{yy} - \sigma_{oct} & \sigma_{yz} \\ \sigma_{xz} & \sigma_{yz} & \sigma_{zz} - \sigma_{oct} \end{bmatrix}$$

and also has principal values and invariants, which are identified by J_1, J_2, and J_3. By analogy to the preceding discussion on invariants, the principal stresses are solutions to the equation

$$s^3 - J_2 s - J_3 = 0$$

where

$$J_1 = 0$$

$$J_2 = \frac{1}{2} \sum_{i=1}^{3} \sum_{j=1}^{3} s_{ij} s_{ij} =$$

$$J_3 = \frac{1}{3}\sum_{i=1}^{3}\sum_{j=1}^{3}\sum_{k=1}^{3} s_{ij}s_{jk}s_{ki}$$

When the directions of the three principal stresses are taken as coordinates, it is easy to determine that planes which have outward normals, forming equal angles with these three axes, must have the octahedral normal stress σ_{oct} acting on them as the normal stress. The resultant shearing stress acting on an octahedral plane is called the octahedral shearing stress τ_{oct}

$$\tau_{oct} = 1/9\left[(\sigma_1 - \sigma_2)^2 + (\sigma_1 - \sigma_3)^2 + (\sigma_2 - \sigma_3)^2\right] = 2/3\, J_2$$

A2 Strain

The deformation of a body is described by the strain. If the displacements are u, v, and w in the x, y, z directions, respectively, the components of strain are:

$$\epsilon_{xx} = \frac{\partial u}{\partial x} \qquad \epsilon_{yy} = \frac{\partial v}{\partial y} \qquad \epsilon_{zz} = \frac{\partial w}{\partial z}$$

$$\gamma_{xy} = \frac{\partial u}{\partial y} + \frac{\partial v}{\partial x} \qquad \gamma_{xz} = \frac{\partial u}{\partial z} + \frac{\partial v}{\partial x} \qquad \gamma_{yz} = \frac{\partial v}{\partial z} + \frac{\partial w}{\partial y}$$

The first three components are normal strains and the last three are shear strains. The same equations can be expressed more compactly by using a subscript notation, in which u_1, u_2, and u_3 are the displacements in the x_1, x_2, and x_3 directions respectively. The strain is then

$$\epsilon_{ij} = \frac{1}{2}\left(\frac{\partial u_i}{\partial x_j} + \frac{\partial u_j}{\partial x_i}\right) \qquad \gamma_{ij} = 2\epsilon_{ij}$$

The tensor representation of strain is

$$\epsilon_{ij} = \begin{bmatrix} \epsilon_{xx} & \epsilon_{xy} & \epsilon_{xz} \\ \epsilon_{xy} & \epsilon_{yy} & \epsilon_{yz} \\ \epsilon_{xz} & \epsilon_{yz} & \epsilon_{zz} \end{bmatrix}$$

This tensor obeys all the transformation laws described in the previous section for stress. It has invariants, principal values and so on.

The strain can be separated into an octahedral normal component

$$\epsilon_{oct} = \frac{\epsilon_{xx} + \epsilon_{yy} + \epsilon_{zz}}{3}$$

$$[\epsilon_{oct}] = \begin{bmatrix} \epsilon_{oct} & 0 & 0 \\ 0 & \epsilon_{oct} & 0 \\ 0 & 0 & \epsilon_{oct} \end{bmatrix}$$

and a deviatoric one.

$$[e] = \begin{bmatrix} \epsilon_{xx} - \epsilon_{oct} & \epsilon_{xy} & \epsilon_{xz} \\ \epsilon_{xy} & \epsilon_{yy} - \epsilon_{oct} & \epsilon_{yz} \\ \epsilon_{xz} & \epsilon_{yz} & \epsilon_{zz} - \epsilon_{oct} \end{bmatrix}$$

If the volume of a small element is V, the volumetric strain ϵ_{oct} is defined by

$$\epsilon_{vol} = \frac{\Delta V}{V} = \frac{\partial u}{\partial x} + \frac{\partial v}{\partial y} + \frac{\partial w}{\partial z} = \epsilon_{xx} + \epsilon_{yy} + \epsilon_{zz} = 3\epsilon_{oct}$$

Since there are 6 independent components of stress and 6 of strain , 36 coefficients are needed to relate them linearly in the most general way. However, by considering the energy stored in a strained linearly elastic body, it can be shown that the coefficients must form a symmetric array. This symmetry of the stress-strain relation reduces the number of independent terms to 21.

The number of independent terms is reduced considerably by considering the planes or axes of isotropy in the material. In geotechnical engineering the two most commonly used types are complete isotropy and cross anisotropy. Cross anisotropy applies when there is some plane (usually horizontal) in which all stress-strain relations are isotropic. The elastic constants for stresses and strains outside the plane are different. The result is five independent constants. Total isotropy exist when the axes can be chosen arbitrarily with no effect on the elastic constants, which are then reduced to two.

The constants can be expressed in terms of several different parameters. The most common ones are as follows:

1. Young's modulus, E, relates axial strain to axial stress in a simple tension or compression test

$$\sigma_{xx} = E\epsilon_{xx} \qquad \text{all other } \sigma\text{'s} = 0$$

2. Poisson's ratio, ν, relates axial strain to transverse normal strain in a simple tension or compression test

$$\epsilon_{yy} = \epsilon_{zz} = -\nu\epsilon_{xx} \qquad \text{all other } \sigma\text{'s except } \sigma_{xx} = 0$$

3. Shear modulus , G, relates shear stress to shear strain

$$\sigma_{xy} = 2G\epsilon_{xy} = G\gamma_{xy}$$

4. Bulk modulus, K, relates volumetric strain to average or octahedral stress

$$\sigma_{oct} = K\epsilon_{vol}$$

5. Lame's constant, λ, μ, relate the stresses and strains as follows:

$$\sigma_{xx} = \lambda\epsilon_{vol} + 2\mu\epsilon_{xx}$$

$$\sigma_{xy} = 2\mu\epsilon_{xy}$$

If the equations connecting a number of variables contain all the variables to the first power only, they are said to be linear. The importance of linearity is twofold: firstly, the equations are easy to solve, and secondly, the principle of superposition holds. If E_1 is the effect of a cause C_1, and E_2 that of a cause C_2, then $E_1 + E_2$ is the effect of the combined causes $C_1 + C_2$ (Jaeger 1978).

APPENDIX B

LABORATORY PROCEDURE

B1 Detailed Test Procedure

The following is the procedure adopted after the cell is placed in the load-frame to the end of the test. It includes, pressurization, operation of hydraulics, volume measurement and recording of data. Figures 3.5 & 3.7 show the complete system, including the valve numbering notation.

1) Zero dial gauge for measuring axial deformation.

2) Fill cell with water through valve no. 3, until water exits from the outlet valve at the top of the cell. Close valve no. 3 and outlet valve. Connect the high pressure tube from valve no. 4, (closed) on the water tank, to valve no. 3.

3) Fill water tank cylinder, by sucking water in from the bottom of the tank at valve no. 5. Shut valve No. 5.

4) Set valve no.12 to low pressure, opening valve no. 14 and no. 6. Apply a pressure of 100 kPa on the Bourdon gauge, using the low pressure regulator, and close valve no. 13.

5) Open valve no. 4 and no. 3 to pressurize the cell. Verify the pressure, by opening the outlet valve, and notice if the water is pressurized.

6) Pressure being confirmed, open valve no. 2, the duct from the specimen, to release the vacuum.

7) Fill volume measuring cylinder to the top and record the reading. Close valve no. 11 and no. 7. Set valve no. 10 and no.

8 to test. Set valve no. 9 to dry.

8) Connect volume measuring tube from valve no. 9 to valve no. 1, or to a combination of valve no. 1 and no. 2, otherwise keep valve no. 2 closed.

9) Connect load cell to digital reader and zero the value.

10) Raise the pressure in the cell in small increments, at a steady rate, until the desired confining pressure is reached. Record the corresponding volume change reading for each increment, after matching the level with the standpipe.

11) Let stand for one and a half hours and record any further volume change.

12) Turn off valve no. 17. Switch on fuel pump. Turn on valve no. 18. Set valve no. 16 to 1/2 division and slowly open valve no. 17.

13) Adjust valve no. 15 and no. 16 so that a constant pressure differential exist between the two gauges in the hydraulic system.

14) Switch on recorder, when dial gauge is at zero. Continually adjust valve no. 15 and no. 16, so that the dial gauge reads a steady speed of 1 mm / min, by matching the speed of the needle to the second hand of a clock.

15) Continuously adjust the level in the volume measuring cylinder to the standpipe. Note down the reading at the same time as the force in the load cell is recorded (every minute).

16) After 100 readings (100 minutes) close valve no. 18 on the pump and depressurize cell.

B2 Raw Data

The experimental data and calculations for dry weathered (25D), saturated weathered (25W), dry natural (N), saturated natural (NW), dry powdered (PD), saturated powdered (PW), and acid treated (AW) specimens are presented in the following pages.

Test no. 20

COMPRESSION DATA

		Pressure kPa	Time interval	Volume change reading	Volume change cc	corr. Volume cc	Void Ratio e
State of specimen	25D	103	5 min	75.5	0.0	5894.0	0.606
Date tested	29/5/81	345	5 min	72.8	66.8	5827.2	0.588
Confining pressure	2758 kPa	690	5 min	68.8	165.8	5728.2	0.561
Initial volume	5894 cc	1034	5 min	65.1	257.4	5636.6	0.536
Initial height	327 mm	1379	5 min	62.5	321.8	5572.3	0.518
Weight of specimen	10.2 kg	1723	5 min	59.5	396.0	5498.0	0.498
Water content	0.2 %	2068	5 min	56.6	467.8	5426.2	0.478
Volume of solids	3771 cc	2413	5 min	53.9	534.6	5359.4	0.460
		2758	5 min	50.1	628.7	5265.4	0.435
		2758	1.5 h	43.0	804.4	5089.6	0.387

SHEAR DATA

No.	Load cell reading	Force N	Volume change read.	Volume change cc	corr. Volume cc	Axial read.	Height change mm	corr. Height mm	corr. Area cm^2
6	238	0	42.8	809.3	5084.7	600	6.0	321.0	158.0
7	242	200	42.7	811.8	5082.2	700	7.0	320.0	159.0
8	272	1700	42.6	814.3	5079.7	800	8.0	319.0	159.0
9	293	2750	42.3	821.7	5072.3	900	9.0	318.0	160.0
10	315	3850	42.1	826.7	5067.4	1000	10.0	317.0	160.0
12	346	5400	41.7	836.6	5057.5	1200	12.0	315.0	161.0
15	608	18500	40.2	873.7	5020.3	1500	15.0	312.0	161.0
20	894	32800	37.0	952.9	4941.1	2000	20.0	307.0	161.0
25	1172	46700	34.1	1024.7	4869.4	2500	25.0	302.0	161.0
30	1427	59450	31.4	1091.5	4802.5	3000	30.0	297.0	162.0
35	1680	72100	29.1	1148.4	4745.6	3500	35.0	292.0	163.0
40	1922	84200	27.0	1200.4	4693.6	4000	40.0	287.0	164.0
45	2126	94400	25.4	1240.0	4654.0	4500	45.0	282.0	165.0
50	2308	103500	24.0	1274.6	4619.4	5000	50.0	277.0	167.0
55	2532	114700	22.7	1306.8	4587.2	5500	55.0	272.0	169.0
60	2698	123000	21.6	1334.0	4560.0	6000	60.0	267.0	171.0
65	2874	131800	20.8	1353.8	4540.2	6500	65.0	262.0	173.0
70	2950	135600	20.0	1373.6	4520.4	7000	70.0	257.0	176.0
75	3108	143500	19.6	1383.5	4510.5	7500	75.0	252.0	179.0
80	3202	148200	19.2	1393.4	4500.6	8000	80.0	247.0	182.0
85	3306	153400	18.9	1400.9	4493.1	8500	85.0	242.0	186.0
90	3352	155700	18.6	1408.3	4485.7	9000	90.0	237.0	189.0
95	3424	159300	18.4	1413.2	4480.8	9500	95.0	232.0	193.0
99	3522	164200	18.3	1415.7	4478.3	9900	99.0	228.0	196.0

Test no. 20 (cont.)

SHEAR DATA (cont.)

No.	Deviatoric stress kPa	Volumetric stress kPa	Void ratio e	Axial strain %	Volumetric strain %	Deviatoric strain %	$(\sigma_1-\sigma_3)/\sigma_{conf}$	$(\sigma_1-\sigma_3)/\sigma_m$
6	0.0	2757.9	0.385	0.0	0.0	0.0	0.000	0.000
7	12.6	2762.1	0.385	0.3	0.0	0.6	0.005	0.005
8	106.8	2793.5	0.384	0.6	0.1	0.9	0.039	0.038
9	172.4	2815.4	0.382	0.9	0.2	1.3	0.063	0.061
10	240.9	2838.2	0.381	1.3	0.3	1.8	0.087	0.085
12	336.3	2870.0	0.378	1.9	0.4	2.7	0.122	0.117
15	1149.7	3141.1	0.368	2.8	0.9	3.8	0.417	0.366
20	2037.9	3437.2	0.346	4.4	2.0	5.6	0.739	0.593
25	2896.4	3723.4	0.327	5.9	3.1	7.3	1.050	0.778
30	3676.5	3983.4	0.308	7.5	4.0	9.3	1.323	0.923
35	4436.4	4236.7	0.293	9.0	4.8	11.1	1.609	1.047
40	5148.6	4474.1	0.279	10.6	5.6	13.1	1.867	1.151
45	5720.0	4664.6	0.268	12.2	6.1	15.3	2.074	1.226
50	6206.4	4826.7	0.259	13.7	6.6	17.3	2.250	1.286
55	6801.2	5025.0	0.250	15.3	7.1	19.4	2.466	1.354
60	7202.0	5158.6	0.242	16.8	7.5	21.5	2.612	1.396
65	7605.8	5293.2	0.237	18.4	7.7	23.8	2.758	1.437
70	7709.4	5327.7	0.232	20.0	8.0	26.0	2.795	1.447
75	8017.3	5430.3	0.229	21.5	8.2	28.2	2.907	1.476
80	8133.5	5469.1	0.226	23.1	8.3	23.1	2.949	1.487
85	8262.1	5511.9	0.224	24.6	8.4	32.7	2.996	1.499
90	8226.3	5500.0	0.222	26.2	8.5	35.1	2.983	1.496
95	8248.0	5507.2	0.221	27.7	8.6	37.3	2.991	1.445
99	8359.8	5544.5	0.220	29.0	8.6	39.2	3.031	1.508

Test no. 15

State of specimen	25D
Date tested	8/5/81
Confining pressure	1896 kPa
Initial volume	5894 cc
Initial height	327 mm
Weight of specimen	10.5 kg
Water content	0.5 %
Volume of solids	3787 cc

COMPRESSION DATA

Pressure kPa	Time interval	Volume change reading	Volume change cc	corr. Volume cc	Void Ratio e
103	5 min	59.1	0.0	5894.0	0.557
414	5 min	56.1	74.3	5819.7	0.537
690	5 min	53.4	141.1	5752.9	0.519
1034	5 min	50.2	220.3	5673.7	0.498
1379	5 min	47.2	294.5	5599.5	0.479
1793	5 min	44.7	356.4	5537.6	0.462
1896	5 min	43.7	381.2	5512.8	0.456
1896	5 min	43.0	398.5	5495.5	0.451

SHEAR DATA

No.	Load cell reading	Force N	Volume change read.	Volume change cc	corr. Volume cc	Axial read.	Height change mm	corr. Height mm	corr. Area cm^2
5	162	~0	42.7	405.9	5488.1	497	5.0	322.0	170.0
6	199	1850	42.6	408.4	5485.6	597	6.0	321.0	171.0
7	265	5150	42.4	413.3	5480.7	696	7.0	320.0	171.0
8	386	11200	41.0	448.0	5446.8	795	8.0	319.0	171.0
9	453	14550	40.7	455.4	5438.6	895	9.0	318.0	171.0
10	519	17850	40.1	470.3	5423.8	996	10.0	317.0	171.0
11	572	20500	39.5	485.1	5408.9	1095	11.0	316.0	171.0
15	768	30300	36.9	549.5	5344.6	1495	15.0	312.0	171.0
20	998	41800	34.0	621.2	5272.8	1995	20.0	307.0	172.0
25	1203	52050	31.4	685.6	5208.4	2495	25.0	302.0	173.0
30	1399	61850	29.1	742.5	5151.5	2995	30.0	297.0	174.0
35	1580	70900	27.1	792.0	5102.0	3496	35.0	292.0	175.0
40	1746	79200	25.3	836.6	5057.5	3997	40.0	287.0	176.0
45	1875	85650	23.8	873.7	5020.3	4497	45.0	282.0	178.0
50	2020	92900	22.6	903.4	4990.6	4996	50.0	277.0	180.0
51	2500	172000	19.6	977.6	4916.4	7096	71.0	256.0	192.0
55	2552	119500	19.1	990.0	4904.0	7495	75.0	252.0	195.0
60	2524	118100	18.8	997.4	4896.6	7996	80.0	247.0	198.0
65	2610	122400	18.7	999.9	4894.1	8497	85.0	242.0	202.0
70	2662	125000	18.5	1004.9	4889.1	8996	90.0	237.0	206.0
75	2700	126900	18.3	1009.8	4884.2	9496	95.0	232.0	211.0
79	2750	129400	18.2	1012.3	4881.7	9895	99.0	228.0	214.0

Test no. 15 (cont.)

SHEAR DATA (cont.)

No.	Deviatoric stress kPa	Volumetric stress kPa	Void ratio e	Axial strain %	Volumetric strain %	Deviatoric strain %	$(\sigma_1-\sigma_3)/\sigma_{conf}$	$(\sigma_1-\sigma_3)/\sigma_m$
5	0.0	1896.1	0.449	0.0	0.0	0.0	0.000	0.000
6	108.3	1932.2	0.449	0.3	0.1	0.4	0.057	0.056
7	300.7	1996.3	0.447	0.6	0.1	0.9	0.159	0.151
8	656.0	2114.8	0.438	0.9	0.8	1.0	0.346	0.310
9	850.8	2179.7	0.436	1.2	0.9	1.4	0.449	0.390
10	1043.3	2243.9	0.432	1.6	1.2	1.8	0.550	0.465
11	1197.7	2295.3	0.428	1.9	1.4	2.2	0.632	0.522
15	1768.8	2485.7	0.411	3.1	2.6	3.4	0.933	0.712
20	2433.8	2707.4	0.392	4.7	3.9	5.1	1.284	0.899
25	3018.0	2902.1	0.375	6.2	5.1	6.8	1.592	1.040
30	3565.9	3084.7	0.360	7.8	6.1	8.7	1.881	1.156
35	4057.8	3248.7	0.347	9.3	7.0	10.5	2.140	1.249
40	4494.4	3394.2	0.336	10.9	7.9	12.4	2.370	1.324
45	4811.1	3499.8	0.326	12.4	8.5	14.4	2.537	1.375
50	5156.3	3614.9	0.318	14.0	9.1	16.5	2.719	1.426
51	6092.3	3926.9	0.298	20.5	10.4	25.6	3.213	1.551
55	6140.7	3943.0	0.295	21.7	10.6	27.3	3.239	1.557
60	5957.4	3881.9	0.293	23.3	10.8	29.6	3.142	1.535
65	6052.3	3913.5	0.292	24.9	10.8	32.0	3.192	1.547
70	6059.3	3915.9	0.291	26.4	10.9	34.2	3.196	1.547
75	6027.8	3905.4	0.290	28.0	11.0	36.5	3.179	1.544
79	6043.6	3910.6	0.289	29.2	11.1	38.3	3.187	1.545

Test no. 16		Pressure kPa	Time interval	Volume change reading	Volume change cc	corr. Volume cc	Void Ratio e
State of specimen	25D	103	5 min	52.9	0.0	5894.0	0.597
Date tested	12/5/81	345	5 min	50.6	56.9	5837.1	0.581
Confining pressure	1034 kPa	690	5 min	47.2	141.1	5752.9	0.558
Initial volume	5894 cc	896	5 min	45.4	185.6	5708.4	0.546
Initial height	327 mm	1034	5 min	44.3	212.9	5681.1	0.539
Weight of specimen	10.2 kg	1034	1.5 h	43.0	245.0	5649.0	0.530
Water content	1.0 %						
Volume of solids	3692 cc						

COMPRESSION DATA

SHEAR DATA

No.	Load cell reading	Force N	Volume change read.	Volume change cc	corr. Volume cc	Axial read.	Height change mm	corr. Height mm	corr. Area cm^2
3	92	0	43.0	245.0	5649.0	300	3.0	324.0	174.0
4	102	500	42.8	250.0	5644.0	400	4.0	323.0	175.0
5	197	5250	42.3	262.4	5631.6	500	5.0	322.0	175.0
6	249	7850	41.6	279.7	5614.3	600	6.0	321.0	175.0
7	285	9650	40.8	299.5	5594.5	700	7.0	320.0	175.0
8	329	11850	40.3	311.9	5582.1	800	8.0	319.0	175.0
10	396	15200	39.1	341.6	5552.4	1000	10.0	317.0	175.0
15	560	23400	36.2	413.3	5480.7	1500	15.0	312.0	176.0
20	693	30050	33.8	472.7	5421.3	2000	20.0	307.0	177.0
25	808	35800	31.8	522.2	5371.8	2500	25.0	302.0	178.0
30	912	41000	30.0	566.8	5327.2	3000	30.0	297.0	179.0
35	1012	46000	28.4	606.4	5287.6	3500	35.0	292.0	181.0
40	1089	49850	27.1	638.6	5255.4	4000	40.0	287.0	183.0
45	1161	53450	26.0	665.8	5228.2	4500	45.0	282.0	185.0
50	1239	57350	24.9	693.0	5201.0	5000	50.0	277.0	188.0
55	1300	60400	24.1	712.8	5181.2	5500	55.0	272.0	191.0
60	1352	63000	23.4	730.1	5163.9	6000	60.0	267.0	193.0
65	1387	64750	22.9	742.5	5151.5	6500	65.0	262.0	197.0
70	1435	67150	22.5	752.4	5141.6	7000	70.0	257.0	200.0
75	1468	68800	22.1	762.3	5131.7	7500	75.0	252.0	204.0
80	1474	69100	21.9	767.3	5126.8	8000	80.0	247.0	208.0
85	1522	71500	21.7	772.2	5121.8	8500	85.0	242.0	212.0
90	1472	69000	21.5	777.2	5116.8	9000	90.0	237.0	216.0
95	1545	72650	21.4	779.6	5114.4	9500	95.0	232.0	221.0
100	1546	72700	21.2	784.6	5109.4	10000	100.0	227.0	225.0

Test no. 16

SHEAR DATA (cont.)

No.	Deviatoric stress kPa	Volumetric stress kPa	Void ratio e	Axial strain %	Volumetric strain %	Deviatoric strain %	$\frac{(\sigma_1-\sigma_3)}{\sigma_{conf}}$	$\frac{(\sigma_1-\sigma_3)}{\sigma_m}$
3	0.0	1034.2	0.530	0.0	0.0	0.0	0.000	0.000
4	28.6	1043.7	0.529	0.3	0.1	0.4	0.028	0.027
5	300.2	1134.3	0.526	0.6	0.3	0.8	0.290	0.265
6	448.8	1183.8	0.521	0.9	0.6	1.1	0.434	0.379
7	552.0	1218.2	0.515	1.2	1.0	1.3	0.534	0.453
8	677.2	1259.9	0.512	1.5	1.2	1.7	0.655	0.538
10	867.8	1323.5	0.504	2.2	1.7	2.5	0.655	0.656
15	1332.1	1478.2	0.485	3.7	3.0	4.1	1.288	0.901
20	1701.7	1601.4	0.469	5.3	4.0	6.0	1.646	1.063
25	2012.7	1705.1	0.455	6.8	4.9	7.8	2.043	1.180
30	2285.8	1796.1	0.443	8.3	5.7	9.6	2.211	1.273
35	2540.3	1881.0	0.432	9.9	6.4	11.7	2.457	1.351
40	2722.3	1941.6	0.424	11.4	7.0	13.6	2.633	1.402
45	2883.0	1995.2	0.416	13.0	7.5	15.8	2.788	1.445
50	3054.4	2052.3	0.409	14.5	7.9	17.8	2.954	1.488
55	3170.9	2091.2	0.403	16.1	8.3	20.0	3.067	1.516
60	3257.4	2120.0	0.399	17.6	8.6	22.1	3.150	1.537
65	3293.1	2131.9	0.395	19.1	8.8	24.3	3.185	1.155
70	3356.5	2153.0	0.393	20.7	9.0	26.6	3.246	1.559
75	3378.5	2160.4	0.390	22.2	9.2	28.7	3.261	1.564
80	3329.2	2143.9	0.389	23.8	9.3	31.1	3.220	1.553
85	3378.3	2160.3	0.387	25.3	9.3	33.3	3.267	1.564
90	3195.9	2099.5	0.386	26.9	9.4	35.7	3.091	1.522
95	3295.6	2132.7	0.385	28.4	9.5	37.9	3.187	1.545
100	3229.9	2110.8	0.384	29.9	9.6	40.1	3.124	1.530

Test no. 12

State of specimen	25W							
Date tested	27/4/81							
Confining pressure	2758 kPa							
Initial volume	5894 cc							
Initial height	327 mm							
Weight of specimen	10.1 kg							
Water content	3.0 %							
Volume of solids	3641 cc							

COMPRESSION DATA

Pressure kPa	Time interval	Volume change reading	Volume change cc	corr. Volume cc	Void Ratio e
103	5 min	84.3	0.0	5894.0	0.619
345	5 min	76.8	185.6	5708.4	0.568
758	5 min	68.1	401.0	5493.0	0.509
1034	5 min	61.6	561.8	5332.2	0.465
1379	5 min	56.6	685.6	5208.4	0.431
1724	5 min	54.1	747.5	5146.6	0.414
2068	5 min	51.4	814.3	5079.7	0.395
2413	5 min	48.8	878.6	5015.4	0.378
2758	5 min	44.8	977.6	4916.4	0.350
2758	1.5 h	43.0	1022.2	4871.8	0.338

SHEAR DATA

No.	Load cell reading	Force N	Volume change read.	Volume change cc	corr. Volume cc	Axial read.	Height change mm	corr. Height mm	corr. Area cm^2
18	251	0	42.7	1029.6	4864.4	1800	18.0	309.0	157.0
19	287	1800	42.6	1032.1	4861.9	1900	19.0	308.0	158.0
20	295	2200	42.5	1034.6	4859.4	2000	20.0	307.0	158.0
21	312	3050	42.5	1034.6	4859.4	2100	21.0	306.0	158.0
22	528	13850	41.9	1049.4	4844.6	2203	22.0	305.0	159.0
25	692	22050	40.0	1096.4	4797.6	2500	25.0	302.0	159.0
30	938	34350	37.3	1163.3	4730.8	3000	30.0	297.0	159.0
35	1199	47400	34.8	1225.1	4668.9	3498	35.0	292.0	160.0
40	1451	60000	32.6	1279.6	4614.4	4000	40.0	287.0	161.0
45	1682	71550	30.8	1324.1	4569.9	4501	45.0	282.0	162.0
50	1869	80900	29.2	1363.7	4530.3	5998	50.0	277.0	164.0
55	2094	92150	27.8	1398.4	4495.6	5500	55.0	272.0	165.0
60	2246	99750	26.8	1423.1	4470.9	6004	60.0	267.0	168.0
65	2408	107850	26.0	1442.9	4451.1	6495	65.0	262.0	170.0
70	2586	116750	25.3	1460.3	4433.8	7002	70.0	257.0	173.0
75	2634	119150	25.0	1467.7	4426.3	7499	75.0	252.0	176.0
80	2754	125150	24.6	1477.6	4416.4	7996	80.0	247.0	179.0
85	2834	129150	24.4	1482.5	4411.5	8499	85.0	242.0	182.0
90	2892	132050	24.2	1487.5	4406.5	9000	90.0	237.0	186.0
95	2970	135950	24.1	1490.0	4404.0	9500	95.0	232.0	190.0
100	3044	139650	24.1	1490.0	4404.0	9996	100.0	227.0	194.0

Test no. 12 (cont.)

SHEAR DATA (cont.)

No.	Deviatoric stress kPa	Volumetric stress kPa	Void ratio e	Axial strain %	Volumetric strain %	Deviatoric strain %	$\frac{(\sigma_1 - \sigma_3)}{\sigma_{conf}}$	$\frac{(\sigma_1 - \sigma_3)}{\sigma_m}$
18	0.0	2757.9	0.336	0.0	0.0	0.0	0.000	0.000
19	114.0	2795.9	0.335	0.3	0.1	0.4	0.041	0.041
20	139.0	2804.2	0.335	0.6	0.1	0.9	0.050	0.050
21	192.1	2821.9	0.335	0.9	0.1	1.3	0.070	0.068
22	872.0	3048.6	0.331	1.3	0.4	1.8	0.316	0.286
25	1388.0	3220.6	0.318	2.2	1.4	2.6	0.503	0.431
30	2156.5	3476.7	0.299	3.8	2.8	4.3	0.782	0.620
35	2964.5	3746.1	0.282	5.3	4.0	6.0	1.075	0.791
40	3731.8	4001.8	0.267	6.9	5.1	7.8	1.353	0.933
45	4415.2	4229.6	0.255	8.4	6.1	10.0	1.601	1.044
50	4946.6	4406.8	0.244	10.0	6.9	11.6	1.794	1.123
55	5575.4	4616.4	0.235	11.6	7.6	13.6	2.022	1.208
60	5957.1	4743.6	0.228	13.1	8.1	15.6	2.160	1.256
65	6348.3	4874.0	0.223	14.7	8.5	17.8	2.302	1.303
70	6767.4	5013.7	0.218	16.3	8.9	20.0	2.454	1.350
75	6783.5	5019.1	0.216	17.8	9.0	22.2	2.460	1.352
80	6999.9	5091.0	0.213	19.4	9.2	24.5	2.538	1.375
85	7084.8	5119.5	0.212	20.9	9.3	26.7	2.569	1.384
90	7102.2	5125.3	0.210	22.5	9.4	29.1	2.575	1.386
95	7161.7	5145.1	0.210	24.1	9.5	31.4	2.597	1.392
100	7198.1	5157.3	0.210	25.6	9.5	33.7	2.610	1.396

Test no. 14

State of specimen	25W
Date tested	5/5/81
Confining pressure	1896 kPa
Initial volume	5894 cc
Initial height	327 mm
Weight of specimen	10.1 kg
Water content	4.2 %
Volume of solids	3647 cc

COMPRESSION DATA

Pressure kPa	Time interval	Volume change reading	Volume change cc	corr. Volume cc	Void Ratio e
103	5 min	78.1	0.0	5894.0	0.616
345	5 min	71.1	173.3	5720.7	0.569
690	5 min	63.3	366.3	5527.7	0.516
1034	5 min	55.8	551.9	5342.1	0.465
1379	5 min	50.9	673.2	5220.8	0.432
1724	5 min	47.2	767.3	5126.7	0.406
1896	5 min	45.6	804.4	5089.6	0.396
1896	1.5 h	43.0	868.7	5025.3	0.378

SHEAR DATA

No.	Load cell reading	Force N	Volume change read.	Volume change cc	corr. Volume cc	Axial read.	Height change mm	corr. Height mm	corr. Area cm^2
17	173	0	42.7	876.2	5017.9	1704	17.0	310.0	162.0
18	207	1700	42.6	876.6	5015.4	1809	18.1	308.9	162.0
19	222	2450	42.4	883.6	5050.4	1907	19.1	307.9	163.0
20	375	10100	42.0	893.5	5000.5	2008	20.1	306.9	163.0
23	476	15150	40.1	940.5	4953.5	2306	23.1	303.9	163.0
25	536	18150	38.9	970.2	4923.8	2506	25.1	301.9	163.0
30	725	27600	36.0	1042.0	4852.0	3008	30.1	296.9	163.0
35	881	35400	33.5	1103.9	4790.2	3505	35.1	291.9	164.0
40	1056	44150	31.2	1160.8	4733.2	4006	40.1	286.9	165.0
45	1219	52300	29.2	1210.3	4683.7	4506	45.1	281.9	166.0
50	1356	59150	27.6	1249.9	4644.1	5008	50.1	276.9	168.0
55	1499	66300	26.1	1287.0	4607.0	5508	55.1	271.9	169.0
60	1628	72750	24.9	1316.7	4577.3	6005	60.1	266.9	172.0
65	1747	78700	24.0	1339.0	4755.0	6505	65.1	261.9	174.0
70	1824	82550	23.3	1356.3	4577.7	7008	70.1	256.9	177.0
75	1936	87650	22.8	1368.7	4525.3	7508	75.1	251.9	180.0
80	2016	92150	22.3	1381.1	4512.9	8006	80.1	246.9	183.0
85	2072	94950	22.1	1386.0	4508.0	8505	85.1	241.9	186.0
90	2096	96150	21.9	1391.0	4503.0	9007	90.1	236.9	190.0
95	2162	99450	21.8	1393.4	4500.6	9507	95.1	231.9	194.0
100	2198	101250	21.7	1395.9	4498.1	10007	100.1	226.9	198.0

Test no. 14

SHEAR DATA (cont.)

No.	Deviatoric stress kPa	Volumetric stress kPa	Void ratio e	Axial strain %	Volumetric strain %	Deviatoric strain %	$(\sigma_1-\sigma_3)/\sigma_{conf}$	$(\sigma_1-\sigma_3)/\sigma_m$
17	0.0	1896.1	0.376	0.0	0.0	0.0	0.000	0.000
18	104.7	1931.0	0.375	0.4	0.0	0.6	0.055	0.054
19	150.6	1946.3	0.374	0.7	0.2	1.0	0.079	0.077
20	619.9	2102.7	0.371	1.0	0.4	1.3	0.327	0.295
23	929.5	2205.9	0.358	2.0	1.3	2.4	0.490	0.421
25	1112.9	2267.1	0.350	2.6	1.9	3.0	0.587	0.490
30	1688.9	2459.1	0.331	4.2	3.3	4.7	0.891	0.687
35	2157.2	2615.2	0.314	5.8	4.5	6.5	1.138	0.825
40	2676.1	2788.1	0.298	7.7	5.7	8.7	1.411	0.960
45	3147.8	2945.4	0.284	9.1	6.7	10.3	1.660	1.069
50	3526.7	3071.7	0.274	10.7	7.5	12.3	1.860	1.148
55	3913.0	3200.4	0.263	12.3	8.2	14.4	2.064	1.223
60	4242.0	3310.1	0.255	13.9	8.8	16.5	2.237	1.282
65	4525.0	3404.4	0.249	15.5	9.2	18.7	2.385	1.329
70	4673.5	3453.9	0.244	17.1	9.6	20.9	2.465	1.353
75	4879.0	3522.4	0.241	18.7	9.8	23.2	2.573	1.385
80	5041.5	3576.6	0.238	20.4	10.1	25.5	2.659	1.410
85	5095.0	3594.4	0.236	22.0	10.2	27.9	2.687	1.418
90	5058.3	3582.2	0.235	23.6	10.3	30.3	2.668	1.412
95	5124.3	3604.2	0.234	25.2	10.3	32.7	2.703	1.422
100	5107.4	3598.6	0.234	26.8	10.4	35.0	2.694	1.419

Test no. 10	
State of specimen	25W
Date tested	13/4/81
Confining pressure	1034 kPa
Initial volume	5894 cc
Initial height	327 mm
Weight of specimen	9.8 kg
Water content	3.5 %
Volume of solids	3528 cc

COMPRESSION DATA

Pressure kPa	Time interval	Volume change reading	Volume change cc	corr. Volume cc	Void Ratio e
103	5 min	71.5	0.0	5894.0	0.670
206	5 min	69.9	39.6	5854.4	0.660
344	5 min	63.6	195.5	5698.5	0.615
483	5 min	58.9	311.9	5582.1	0.582
690	5 min	52.5	470.3	5423.7	0.537
896	5 min	48.3	574.2	5319.8	0.508
1034	5 min	45.3	648.5	5245.6	0.487
1034	1.5 h	43.0	705.4	5188.6	0.471

SHEAR DATA

No.	Load cell reading	Force N	Volume change read.	Volume change cc	corr. Volume cc	Axial read.	Height change mm	corr. Height mm	corr. Area cm^2
11	92	0	42.9	707.9	5186.1	1100	11.0	316.0	164.0
12	108	800	42.7	712.8	5181.2	1200	12.0	315.0	165.0
13	117	1250	42.7	712.8	5181.2	1298	13.0	314.0	165.0
14	121	1450	42.6	715.3	5178.7	1395	14.0	313.0	166.0
15	176	4200	42.4	720.2	5173.8	1497	15.0	312.0	166.0
20	300	10400	39.2	799.4	5094.6	1998	20.0	307.0	166.0
30	470	18900	33.6	938.0	4956.0	3000	30.0	297.0	167.0
40	629	26850	29.1	1049.4	4844.6	4001	40.0	287.0	169.0
50	787	34750	25.5	1138.5	4755.5	4997	50.0	277.0	172.0
60	934	42100	22.9	1232.9	4691.2	6002	60.0	267.0	176.0
70	1051	47950	21.0	1249.9	4644.1	7000	70.0	257.0	181.0
80	1161	53450	19.8	1279.6	4614.4	8001	80.0	247.0	187.0
90	1220	56400	18.9	1301.9	4592.1	9002	90.0	237.0	194.0
100	1348	62800	18.4	1314.2	4579.8	10000	100.0	227.0	202.0

Test no. 10

SHEAR DATA (çont.)

No.	Deviatoric stress kPa	Volumetric stress kPa	Void ratio e	Axial strain %	Volumetric strain %	Deviatoric strain %	$\frac{(\sigma_1-\sigma_3)}{\sigma_{conf}}$	$\frac{(\sigma_1-\sigma_3)}{\sigma_m}$
11	0.0	1034.2	0.470	0.0	0.0	0.0	0.000	0.000
12	44.5	1049.0	0.469	0.3	0.1	0.4	0.043	0.042
13	75.8	1059.5	0.469	0.6	0.1	0.9	0.073	0.072
14	87.6	1063.4	0.468	0.9	0.1	1.3	0.085	0.082
15	253.3	1118.6	0.467	1.3	0.2	1.9	0.245	0.226
20	626.7	1243.1	0.444	2.9	1.8	3.5	0.606	0.504
30	1132.6	1411.7	0.405	6.0	4.4	6.8	1.095	0.802
40	1590.6	1564.4	0.373	9.2	6.6	10.5	1.538	1.017
50	2024.1	1708.9	0.348	12.3	8.3	14.3	1.957	1.184
60	2396.1	1832.9	0.330	15.5	9.6	18.5	2.317	1.307
70	2653.5	1918.7	0.316	18.7	10.5	22.8	2.566	1.383
80	2861.1	1987.9	0.308	21.8	11.0	27.2	2.767	1.427
90	2910.8	2004.5	0.302	25.0	11.5	31.8	2.815	1.452
100	3112.7	2071.8	0.298	28.2	11.7	36.5	3.010	1.502

Test no. 11

State of specimen	N
Date tested	23/4/81
Confining pressure	2758 kPa
Initial volume	5894 cc
Initial height	327 mm
Weight of specimen	10.5 kg
Water content	1.0 %
Volume of solids	3779 cc

COMPRESSION DATA

Pressure kPa	Time interval	Volume change reading	Volume change cc	corr. Volume cc	Void Ratio e
103	5 min	67.8	0.0	5894.0	0.560
345	5 min	66.2	39.6	5854.4	0.549
552	5 min	64.0	94.1	5800.0	0.535
827	5 min	61.2	163.4	5730.7	0.516
1103	5 min	58.9	220.3	5673.7	0.501
1379	5 min	56.2	287.1	5606.9	0.484
1792	5 min	53.6	351.5	5542.6	0.467
2137	5 min	51.4	405.9	5488.1	0.452
2517	5 min	49.0	465.3	5428.7	0.436
2758	5 min	46.8	519.8	5374.3	0.422
2758	1.5 h	42.8	618.8	5275.3	0.396

SHEAR DATA

No.	Load cell reading	Force N	Volume change read.	Volume change cc	corr. Volume cc	Axial read.	Height change mm	corr. Height mm	corr. Area cm
7	252	0	42.7	621.2	5272.8	700	7.0	320.0	165.0
8	267	750	42.7	621.2	5272.8	800	8.0	319.0	165.0
9	311	2950	42.5	626.2	5267.8	898	9.0	318.0	166.0
10	339	4350	42.3	631.1	5262.9	1000	10.0	317.0	166.0
11	371	5950	42.0	638.6	5255.5	1100	11.0	316.0	166.0
15	772	26000	39.5	700.4	5193.6	1500	15.0	312.0	167.0
20	1067	40750	36.4	777.2	5116.9	1998	20.0	307.0	167.0
25	1342	54500	33.5	848.9	5045.1	2498	25.0	302.0	167.0
30	1566	65700	31.0	910.8	4983.2	3000	30.0	297.0	168.0
35	1824	78600	29.3	952.9	4941.1	3498	35.0	292.0	169.0
40	2042	89500	27.0	1009.8	4884.2	4000	40.0	287.0	170.0
45	2250	99900	25.3	1051.9	4842.1	4499	45.0	282.0	172.0
50	2458	110300	24.0	1084.1	4810.0	5000	50.0	277.0	174.0
55	2598	117300	22.7	1116.2	4777.8	5502	55.0	272.0	176.0
60	2784	126600	21.7	1141.0	4753.0	6002	60.0	267.0	178.0
65	2920	13300	20.8	1163.3	4730.8	6497	65.0	262.0	181.0
70	3084	141600	20.1	1180.6	4713.4	6997	70.0	257.0	183.0
75	3196	147200	19.5	1195.4	4698.6	7500	75.0	252.0	187.0
80	3310	152900	19.0	1207.8	4686.2	8000	80.0	247.0	190.0
85	3364	155600	18.6	1217.7	4676.3	8497	85.0	242.0	193.0
90	3454	160100	18.3	1225.1	4668.9	9002	90.0	237.0	197.0
95	3580	166400	18.1	1230.1	4663.9	9500	95.0	232.0	201.0
100	3564	165600	17.9	1235.0	4659.0	10000	100.0	227.0	205.0

Test no. 11

SHEAR DATA (cont.)

No.	Deviatoric stress kPa	Volumetric stress kPa	Void ratio e	Axial strain %	Volumetric strain %	Deviatoric strain %	$\frac{(\sigma_1 - \sigma_3)}{\sigma_{conf}}$	$\frac{(\sigma_1 - \sigma_3)}{\sigma_m}$
7	0.0	2757.9	0.395	0.0	0.0	0.0	0.000	0.000
8	45.4	2773.0	0.395	0.3	0.0	0.5	0.017	0.016
9	178.1	2817.3	0.394	0.6	0.1	0.9	0.065	0.063
10	262.0	2845.2	0.393	0.9	0.2	1.3	0.095	0.092
11	357.8	2877.2	0.391	1.3	0.3	1.8	0.130	0.124
15	1561.9	3278.5	0.374	2.5	1.5	3.0	0.566	0.476
20	2444.9	3572.9	0.354	4.1	3.0	4.7	0.887	0.684
25	3262.4	3845.4	0.335	5.6	4.3	6.3	1.183	0.848
30	3915.7	4063.1	0.319	7.2	5.5	8.1	1.420	0.964
35	4644.9	4306.2	0.307	8.8	6.3	10.1	1.684	1.078
40	5259.1	4510.9	0.292	10.3	7.4	11.8	1.907	1.166
45	5818.1	4697.3	0.281	11.9	8.2	13.8	2.110	1.239
50	6352.1	4875.3	0.273	13.4	8.8	15.7	2.303	1.303
55	6677.9	4983.9	0.264	15.0	9.4	17.8	2.421	1.340
60	7111.7	5128.5	0.258	16.6	9.9	20.2	2.579	1.387
65	7388.0	5220.6	0.252	18.1	10.3	22.0	2.679	1.415
70	7720.8	5331.5	0.247	19.7	10.6	24.3	2.800	1.448
75	7894.8	5389.5	0.243	21.3	10.9	26.5	2.863	1.465
80	8059.1	5444.3	0.240	22.8	11.1	28.7	2.922	1.480
85	8052.4	5442.0	0.237	24.4	11.3	31.0	2.920	1.480
90	8127.0	5466.9	0.235	25.9	11.5	33.1	2.947	1.487
95	8277.3	5517.0	0.234	27.5	11.6	35.5	3.001	1.500
100	8068.6	5447.4	0.233	29.1	11.6	37.9	2.926	1.481

Test no.	7
State of specimen	N
Date tested	3/4/81
Confining pressure	1896 kPa
Initial volume	5894 cc
Initial height	327 mm
Weight of specimen	10.5 kg
Water content	0.5 %
Volume of solids	3780 cc

COMPRESSION DATA

Pressure kPa	Time interval	Volume change reading	Volume change cc	corr. Volume cc	Void Ratio e
103	5 min	43.3	0.0	5894.0	0.559
241	5 min	42.3	24.8	5869.2	0.553
483	5 min	42.2	27.2	5866.8	0.552
690	5 min	38.6	116.3	5777.7	0.528
1000	5 min	36.0	180.7	5713.3	0.511
1241	5 min	34.1	227.7	5666.3	0.499
1410	5 min	32.8	259.9	5634.1	0.490
1655	5 min	31.1	302.0	5592.0	0.479
1823	5 min	29.7	336.6	5557.4	0.470
1896	5 min	28.9	356.4	5537.6	0.465
1896	1.5 h	25.5	440.6	5453.4	0.443

SHEAR DATA

No.	Load cell reading	Force N	Volume change read.	Volume change cc	corr. Volume cc	Axial read.	Height change mm	corr. Height mm	corr. Area cm
5	19	0	42.3	445.5	5448.5	500	5.0	322.0	169.0
6	43	1200	42.2	448.0	5446.0	600	6.0	321.0	170.0
7	134	5730	42.0	452.9	5441.1	694	6.9	320.1	170.0
8	238	10950	41.0	477.7	5416.3	798	8.0	319.0	170.0
10	363	17200	39.7	509.9	5384.2	997	10.0	317.0	170.0
20	877	42900	33.5	663.5	5230.7	1997	20.0	307.0	170.0
30	1278	62950	28.9	777.2	5116.9	2999	30.0	297.0	172.0
40	1619	80000	25.3	866.3	5027.8	4000	40.0	287.0	175.0
50	1868	92450	23.0	923.2	4970.8	5000	50.0	277.0	180.0
60	2094	103250	21.2	967.7	4926.3	6000	60.0	267.0	185.0
70	2298	72650	12.3	759.8	4896.6	7000	70.0	257.0	200.0
80	2398	118950	19.2	1017.2	4876.8	7999	80.0	247.0	197.0
90	2500	126550	18.6	1032.1	4861.9	8992	89.0	237.1	205.0
100	2626	130350	18.3	1039.5	4854.5	10001	100.0	227.0	214.0

Test no. 7

SHEAR DATA (cont.)

No.	Deviatoric stress kPa	Volumetric stress kPa	Void ratio e	Axial strain %	Volumetric strain %	Deviatoric strain %	$\frac{(\sigma_1-\sigma_3)}{\sigma_{conf}}$	$\frac{(\sigma_1-\sigma_3)}{\sigma_m}$
5	0.0	1896.1	0.444	0.0	0.0	0.0	0.000	0.000
6	70.6	1919.6	0.441	0.3	0.1	0.4	0.037	0.037
7	337.1	2008.5	0.439	0.6	0.1	0.9	0.178	0.168
8	644.1	2110.8	0.433	0.9	0.6	1.1	0.340	0.305
10	1011.8	2233.4	0.424	1.6	1.2	1.8	0.534	0.453
20	2523.5	2737.3	0.384	4.6	4.0	4.9	1.331	0.922
30	3718.0	3135.4	0.354	7.8	6.1	8.7	1.961	1.186
40	4571.4	3419.9	0.330	10.9	7.7	12.5	2.411	1.337
50	5136.1	3608.1	0.315	14.0	8.8	16.6	2.709	1.424
60	5581.1	3756.5	0.303	17.1	9.6	20.9	2.944	1.486
70	5966.0	3884.8	0.295	20.2	10.1	25.3	3.147	1.536
80	6038.1	3908.8	0.290	23.3	10.5	29.7	3.185	1.545
90	6173.2	3953.8	0.286	26.4	10.8	34.2	3.256	1.561
100	6091.1	3926.5	0.284	29.5	10.9	38.8	3.212	1.551

Test no. 8

State of specimen	N
Date tested	7/4/81
Confining pressure	1034 kPa
Initial volume	5894 cc
Initial height	327 mm
Weight of specimen	10.3 kg
Water content	1.7 %
Volume of solids	3665 cc

COMPRESSION DATA

Pressure kPa	Time interval	Volume change reading	Volume change cc	corr. Volume cc	Void Ratio e
103	5 min	43.0	0.0	5894.0	0.608
206	5 min	42.6	9.9	5884.1	0.606
345	5 min	41.2	44.6	5849.4	0.596
483	5 min	40.0	74.3	5819.7	0.588
724	5 min	37.6	133.7	5760.3	0.572
827	5 min	36.5	160.9	5733.1	0.564
1034	5 min	34.4	212.9	5681.2	0.550
1034	1.5 h	34.2	217.8	5676.2	0.549

SHEAR DATA

No.	Load cell reading	Force N	Volume change read.	Volume change cc	corr. Volume cc	Axial read.	Height change mm	corr. Height mm	corr. Area cm
3	92	0	34.2	217.8	5676.2	300	3.0	324.0	175.0
4	191	4950	33.5	235.1	5658.9	400	4.0	323.0	175.0
5	253	8050	32.8	252.5	5641.5	500	5.0	322.0	175.0
6	304	10600	32.0	272.2	5621.7	600	6.0	321.0	175.0
10	469	18850	29.2	341.6	5552.4	1000	10.0	317.0	175.0
20	772	34000	23.9	472.5	5421.3	2000	20.0	307.0	177.0
30	984	44600	20.0	569.3	5324.7	3000	30.0	297.0	179.0
40	1146	52700	17.0	643.5	5250.5	4004	40.0	287.0	183.0
50	1298	60300	15.0	693.0	5201.0	5000	50.0	277.0	188.0
60	1423	66550	13.5	730.1	5163.9	6000	60.0	267.0	193.0
67	1506	70700	12.6	752.4	5141.6	6700	67.0	260.0	198.0
70	1545	72650	12.3	759.8	5134.2	7000	70.0	257.0	200.0
73	1551	72950	12.0	767.3	5126.8	7300	73.0	254.0	202.0
80	1572	74000	11.6	777.2	5116.8	8000	80.0	247.0	207.0
90	1607	75750	11.3	784.6	5109.4	9000	90.0	237.0	216.0
100	1683	79550	10.8	797.0	5097.0	10005	100.1	226.9	225.0

Test no. 8

SHEAR DATA (cont.)

No.	Deviatoric stress kPa	Volumetric stress kPa	Void ratio e	Axial strain %	Volumetric strain %	Deviatoric strain %	$\frac{(\sigma_1-\sigma_3)}{\sigma_{conf}}$	$\frac{(\sigma_1-\sigma_3)}{\sigma_m}$
3	0.0	1034.2	0.549	0.0	0.0	0.0	0.000	0.000
4	282.9	1128.5	0.544	0.3	0.3	0.3	0.274	0.251
5	460.0	1187.5	0.539	0.6	0.6	0.6	0.445	0.387
6	605.7	1236.1	0.534	0.9	1.0	0.9	0.586	0.490
10	1076.2	1392.9	0.515	2.2	2.2	2.2	1.041	0.773
20	1925.4	1676.0	0.479	5.3	4.5	5.7	1.862	1.149
30	2487.7	1863.4	0.453	8.3	6.2	9.4	2.405	1.335
40	2880.7	1994.4	0.433	11.4	7.5	13.4	2.785	1.444
50	3211.5	2104.7	0.419	14.5	8.4	17.6	3.105	1.526
60	3441.0	2181.2	0.409	17.6	9.0	21.9	3.327	1.578
67	3575.2	2225.9	0.403	19.8	9.4	25.0	3.457	1.606
70	3636.6	2246.4	0.401	20.7	9.6	26.3	3.516	1.619
73	3614.2	2238.9	0.399	22.5	9.7	28.9	3.495	1.614
80	3572.1	2224.9	0.396	23.8	9.9	30.8	3.454	1.606
90	3513.7	2205.4	0.394	26.9	10.0	35.4	3.398	1.593
100	3541.3	2214.6	0.391	30.0	10.2	39.9	3.424	1.599

Test no. 13

State of specimen	NW
Date tested	2/5/81
Confining pressure	2758 kPa
Initial volume	5894 cc
Initial height	327 mm
Weight of specimen	10.1 kg
Water content	3.8 %
Volume of solids	3642 cc

COMPRESSION-DATA

Pressure kPa	Time interval	Volume change reading	Volume change cc	corr. Volume cc	Void Ratio e
103	5 min	71.9	0.0	5894.0	0.618
310	5 min	69.1	69.3	5824.7	0.599
758	5 min	62.7	227.7	5666.3	0.556
1103	5 min	59.1	316.8	5577.2	0.531
1379	5 min	56.5	381.2	5512.9	0.514
1825	5 min	52.8	472.2	5421.3	0.489
2137	5 min	50.3	534.6	5359.4	0.472
2448	5 min	48.5	579.2	5314.9	0.459
2758	5 min	46.7	623.7	5270.3	0.447
2758	1.5 h	42.7	722.7	5171.3	0.420

SHEAR DATA

No.	Load cell reading	Force N	Volume change read.	Volume change cc	corr. Volume cc	Axial read.	Height change mm	corr. Height mm	corr. Area cm^2
8	242	0	42.7	722.7	5171.3	800	8.0	319.0	162.0
9	294	2600	42.6	725.2	5168.8	900	9.0	318.0	163.0
10	330	4400	42.6	725.2	5168.8	1000	10.0	317.0	163.0
11	352	5500	42.6	725.2	5168.8	1096	11.0	316.0	164.0
12	360	5900	42.2	735.1	5158.9	1201	12.0	315.0	164.0
13	392	7500	42.1	737.6	5156.5	1295	13.0	314.0	164.0
14	394	7600	41.9	742.5	5151.5	1400	14.0	313.0	165.0
15	586	17200	41.2	759.8	5134.2	1500	15.0	312.0	165.0
20	913	33550	38.5	826.7	5067.4	2003	20.0	307.0	165.0
25	1205	48150	35.9	891.0	5003.0	2500	25.0	302.0	166.0
30	1458	60800	33.7	945.5	4948.5	3000	30.0	297.0	167.0
35	1718	73800	31.7	995.0	4899.0	3500	35.0	292.0	168.0
40	1911	83450	30.0	1037.0	4857.0	4000	40.0	287.0	169.0
45	2124	94100	28.7	1069.2	4824.8	4498	45.0	282.0	171.0
50	2290	102400	27.5	1098.9	4795.1	5000	50.0	277.0	173.0
55	2442	110000	26.5	1123.7	4770.3	5499	55.0	272.0	175.0
60	2602	118000	25.9	1138.5	4755.5	5998	60.0	267.0	178.0
65	2704	123100	25.3	1153.4	4740.6	6499	65.0	262.0	181.0
70	2780	126900	24.9	1163.3	4730.7	7000	70.0	257.0	184.0
75	2900	132900	24.6	1170.7	4723.3	7498	75.0	252.0	187.0
80	2982	137000	24.4	1175.6	4718.4	7998	80.0	247.0	191.0
85	3040	139900	24.3	1178.1	4715.9	8500	85.0	242.0	195.0
90	3104	143100	24.2	1180.6	4713.4	9000	90.0	237.0	199.0
95	3144	145100	24.1	1183.1	4710.9	9498	95.0	232.0	203.0
100	3230	149400	24.0	1185.5	4708.5	10000	100.0	227.0	207.0

Test no. 13

SHEAR DATA (cont.)

No.	Deviatoric stress kPa	Volumetric stress kPa	Void ratio e	Axial strain %	Volumetric strain %	Deviatoric strain %	$(\sigma_1-\sigma_3)/\sigma_{conf}$	$(\sigma_1-\sigma_3)/\sigma_m$
8	0.0	2757.9	0.420	0.0	0.0	0.0	0.000	0.000
9	160.0	2811.2	0.419	0.3	0.1	0.4	0.058	0.057
10	269.9	2847.9	0.419	0.6	0.1	0.9	0.098	0.095
11	336.3	2870.0	0.419	0.9	0.1	1.3	0.122	0.117
12	360.3	2878.0	0.417	1.3	0.2	1.9	0.131	0.125
13	456.7	2910.1	0.416	1.6	0.3	2.3	0.166	0.157
14	461.8	2911.8	0.415	1.9	0.4	2.7	0.168	0.159
15	1045.2	3106.3	0.410	2.2	0.7	3.0	0.379	0.337
20	2032.6	3435.4	0.391	3.8	2.0	4.7	0.737	0.592
25	2906.5	3726.7	0.374	5.3	3.3	6.3	1.054	0.780
30	3649.1	3974.3	0.359	6.9	4.3	8.2	1.323	0.918
35	4398.7	4224.1	0.345	8.5	5.3	10.1	1.595	1.041
40	4939.1	4401.6	0.334	10.0	6.1	12.0	1.788	1.122
45	5500.0	4591.2	0.325	11.6	6.7	14.1	1.994	1.198
50	5915.4	4729.7	0.317	13.1	7.3	16.0	2.145	1.251
55	6272.1	4848.6	0.310	14.7	7.8	18.2	2.274	1.294
60	6625.2	4966.3	0.306	16.3	8.0	20.5	2.402	1.334
65	6803.3	5025.7	0.302	17.9	8.3	22.7	2.467	1.354
70	6893.9	5055.9	0.299	19.4	8.5	24.9	2.500	1.364
75	7090.5	5121.4	0.297	21.0	8.7	27.2	2.571	1.385
80	7171.7	5148.5	0.296	22.6	8.8	29.5	2.600	1.393
85	7179.1	5150.9	0.295	24.1	8.8	31.8	2.603	1.394
90	7195.3	5156.3	0.294	25.7	8.9	34.1	2.609	1.395
95	7145.7	5139.8	0.294	27.3	8.9	36.5	2.591	1.390
100	7202.7	5158.8	0.293	28.8	9.0	38.7	2.612	1.396

Test no. 5

State of specimen	NW
Date tested	12/3/81
Confining pressure	1896 kPa
Initial volume	5894 cc
Initial height	327 mm
Weight of specimen	10.3 kg
Water content	1.1 %
Volume of solids	3711 cc

COMPRESSION DATA

Pressure kPa	Time interval	Volume change reading	Volume change cc	corr. Volume cc	Void Ratio e
103	5 min	69.6	0.0	5894.0	0.588
207	5 min	69.2	9.9	5885.0	0.586
330	5 min	66.2	84.2	5809.8	0.566
483	5 min	63.1	160.9	5733.1	0.545
724	5 min	59.2	257.4	5636.6	0.519
931	5 min	56.0	336.6	5557.4	0.498
1172	5 min	52.0	435.6	5458.4	0.471
1345	5 min	50.5	472.7	5421.3	0.461
1551	5 min	48.5	522.2	5371.8	0.448
1792	5 min	46.3	576.7	5317.3	0.483
1896	5 min	45.4	599.0	5295.0	0.427
1896	1.5 h	43.0	658.4	5235.6	0.411

SHEAR DATA

No.	Load cell reading	Force N	Volume change read.	Volume change cc	corr. Volume cc	Axial read.	Height change mm	corr. Height mm	corr. Area cm
10	179	0	42.9	660.8	5233.2	1000	10.0	317.0	165.0
13	196	196	42.8	663.3	5230.7	1300	13.0	315.0	167.0
14	220	2050	42.7	665.8	5286.6	1398	14.0	313.0	167.0
20	612	21650	39.2	752.4	5141.6	1995	20.0	307.0	168.0
30	1006	41350	33.7	888.5	5005.5	2992	30.0	297.0	169.0
40	1356	58850	29.7	987.5	4906.5	3998	40.0	287.0	171.0
50	1634	72750	26.9	1056.8	4837.2	5003	50.0	277.0	175.0
60	1811	81600	25.1	1111.4	4792.3	6000	60.0	267.0	180.0
70	1980	90050	24.0	1128.6	4765.4	7005	70.1	256.9	186.0
80	2124	97250	23.2	1148.4	4745.6	7996	80.0	247.0	192.0
90	2184	100250	22.7	1160.8	4733.3	8994	90.0	237.0	200.0
100	2280	105050	22.4	1168.2	4725.7	10001	100.0	227.0	208.0

Test no. 5

SHEAR DATA (cont.)

No.	Deviatoric stress kPa	Volumetric stress kPa	Void ratio e	Axial strain %	Volumetric strain %	Deviatoric strain %	$\frac{(\sigma_1 - \sigma_3)}{\sigma_{conf}}$	$\frac{(\sigma_1 - \sigma_3)}{\sigma_m}$
10	0.0	1896.1	0.404	0.0	0.0	0.0	0.000	0.000
13	50.9	1913.1	0.410	0.3	0.1	0.4	0.027	0.027
14	122.8	1937.0	0.403	0.6	0.1	0.9	0.065	0.063
20	1288.7	2325.7	0.386	2.5	1.8	2.9	0.680	0.511
30	2446.7	2711.7	0.349	5.7	4.4	6.4	1.290	0.902
40	3441.5	3043.3	0.322	8.9	6.2	10.3	1.815	1.131
50	4157.1	3281.8	0.304	12.1	7.6	14.4	2.192	1.267
60	4533.3	3407.2	0.292	15.2	8.4	18.6	2.391	1.331
70	4841.4	3509.9	0.284	18.4	8.9	23.2	2.553	1.379
80	5065.1	3584.5	0.279	21.6	9.3	27.8	2.671	1.413
90	5012.5	3566.9	0.276	24.8	9.6	32.4	2.644	1.405
100	5050.5	3579.6	0.273	27.9	9.7	37.0	2.664	1.411

Test no. 9

State of specimen	NW
Date tested	10/4/81
Confining pressure	1034 kPa
Initial volume	5894 cc
Initial height	327 mm
Weight of specimen	10.3 kg
Water content	3.4 %
Volume of solids	3706 cc

COMPRESSION DATA

Pressure kPa	Time interval	Volume change reading	Volume change cc	corr. Volume cc	Void Ratio e
103	5 min	64.6	0.0	5894.0	0.591
207	5 min	63.8	19.8	5874.2	0.585
345	5 min	59.8	118.8	5775.2	0.558
483	5 min	56.2	207.9	5686.1	0.534
690	5 min	53.6	272.3	5621.8	0.517
931	5 min	47.0	435.6	5458.4	0.473
1034	5 min	45.0	485.1	5408.9	0.460
1034	5 min	42.9	572.2	5366.8	0.448

SHEAR DATA

No.	Load cell reading	Force N	Volume change read.	Volume change cc	corr. Volume cc	Axial read.	Height change mm	corr. Height mm	corr. Area cm
9	85	0	42.8	529.7	5364.4	900	9.0	318.0	167.0
10	113	1400	42.7	532.1	5361.9	1000	10.0	317.0	169.0
11	126	2050	42.2	544.5	5349.5	1100	11.0	316.0	169.0
12	193	5400	42.0	549.5	5344.5	1185	11.9	315.1	171.0
11	371	5950	42.0	638.6	5255.5	1100	11.0	316.0	166.0
12	193	5400	42.0	549.5	5344.5	1185	11.9	315.1	170.0
13	237	7600	41.8	554.4	5339.6	1298	13.0	314.0	170.0
20	392	15350	37.0	673.2	5220.8	2000	20.0	307.0	170.0
30	583	24900	31.6	806.9	5087.2	3000	30.0	297.0	171.0
40	746	33050	27.5	908.3	4985.7	3997	40.0	287.0	174.0
50	905	41000	24.3	987.5	4906.5	4998	50.0	277.0	177.0
60	1031	47300	22.0	1044.5	4849.5	6000	60.0	267.0	182.0
70	1150	53250	20.4	1084.1	4809.9	6998	70.0	257.0	187.0
80	1243	57900	19.4	1108.8	4785.2	8000	80.0	247.0	194.0
90	1323	61900	18.7	1126.1	4767.9	8998	90.0	237.0	201.0
100	1348	63150	18.4	1133.6	4760.4	9999	100.0	227.0	210.0

Test no. 9

SHEAR DATA (cont.)

No.	Deviatoric stress kPa	Volumetric stress kPa	Void ratio e	Axial strain %	Volumetric strain %	Deviatoric strain %	$\frac{(\sigma_1-\sigma_3)}{\sigma_{conf}}$	$\frac{(\sigma_1-\sigma_3)}{\sigma_m}$
9	0.0	1034.2	0.448	0.0	0.0	0.0	0.000	0.000
10	82.8	1061.8	0.447	0.3	0.1	0.4	0.080	0.078
11	121.3	1074.6	0.444	0.6	0.3	0.8	0.117	0.113
12	315.8	1139.5	0.442	0.9	0.4	1.2	0.305	0.277
13	447.1	1183.2	0.441	1.3	0.5	1.7	0.432	0.378
20	902.9	1335.2	0.409	3.5	2.7	3.9	0.873	0.676
30	1453.7	1518.8	0.373	6.6	5.2	7.3	1.406	0.957
40	1899.4	1667.3	0.345	9.7	7.1	11.0	1.837	1.139
50	2314.7	1805.8	0.324	12.9	8.5	15.1	2.238	1.282
60	2604.2	1902.3	0.309	16.0	9.6	19.2	2.518	1.369
70	2845.2	1982.6	0.298	19.2	10.3	23.7	2.751	1.435
80	2988.7	2030.4	0.291	22.3	10.8	28.1	2.890	1.472
90	3076.9	2059.8	0.287	25.5	11.1	32.7	2.975	1.494
100	3011.3	2038.0	0.285	28.6	11.3	37.3	2.912	1.478

Test 18

State of specimen	PD
Date tested	19/5/81
Confining pressure	1896 kPa
Initial volume	5894 cc
Initial height	327 mm
Weight of specimen	10.9 kg
Water content	0.7 %
Volume of solids	3945 cc

COMPRESSION DATA

Pressure kPa	Time interval	Volume change reading	Volume change cc	corr. Volume cc	Void Ratio e
103	5 min	58.1	0.0	5894.0	0.494
345	5 min	55.0	76.7	5817.3	0.475
690	5 min	52.7	133.7	5760.3	0.460
1034	5 min	50.1	198.0	5696.0	0.444
1379	5 min	48.8	230.2	5663.8	0.436
1896	5 min	46.3	295.1	5601.9	0.420
1896	1.5 h	43.0	373.7	5520.3	0.399

SHEAR DATA

No.	Load cell reading	Force N	Volume change read.	Volume change cc	corr. Volume cc	Axial read.	Height change mm	corr. Height mm.	corr. Area cm^2
5	173	0	42.8	378.7	5515.3	500	5.0	322.0	171.0
6	177	200	42.8	378.7	5515.3	600	6.0	321.0	172.0
7	194	1050	42.8	378.7	5515.3	700	7.0	320.0	172.0
8	228	2750	42.7	381.2	5512.8	800	8.0	319.0	173.0
9	341	8400	42.6	383.6	5510.4	900	9.0	318.0	173.0
10	475	15100	42.4	388.6	5505.4	1000	10.0	317.0	174.0
11	589	20800	42.3	391.1	5502.9	1100	11.0	316.0	174.0
15	1052	43950	41.3	415.8	5478.2	1500	15.0	312.0	176.0
16	1165	49600	41.1	420.8	5473.2	1600	16.0	311.0	176.0
18	1388	60750	40.7	430.7	5463.4	1800	18.0	309.0	177.0
20	1609	71800	40.3	440.6	5453.4	2000	20.0	307.0	178.0
25	2090	95850	39.2	467.8	5334.6	2500	25.0	302.0	180.0
30	2408	111750	38.2	492.5	5401.5	3000	30.0	297.0	182.0
35	2604	121550	37.3	514.8	5379.2	3500	35.0	292.0	184.0
40	2694	126050	36.9	529.7	5364.3	4000	40.0	287.0	187.0
45	2728	127750	36.2	542.0	5352.0	4500	45.0	282.0	190.0
50	2744	128550	36.0	547.0	5347.0	5000	50.0	277.0	193.0
55	2796	131150	35.9	549.5	5344.5	5500	55.0	272.0	197.0
60	2788	130750	35.8	551.9	5342.1	6000	60.0	267.0	200.0
65	2790	130850	35.8	551.9	5342.1	6500	65.0	262.0	204.0
70	2822	132450	36.0	547.0	5347.0	7000	70.0	257.0	208.0
75	2880	135350	36.1	544.5	5349.5	7500	75.0	252.0	212.0
80	2884	135550	36.2	542.0	5352.0	8000	80.0	247.0	217.0
85	2874	135050	36.4	537.1	5356.9	8500	85.0	242.0	221.0
90	2920	137350	36.5	534.6	5359.4	9000	90.0	237.0	226.0
95	2974	140050	36.8	527.2	5366.8	9500	95.0	232.0	231.0
99	2942	138450	36.9	524.7	5369.3	9900	99.0	228.0	236.0

Test no. 18

SHEAR DATA (cont.)

No.	Deviatoric stress kPa	Volumetric stress kPa	Void ratio e	Axial strain %	Volumetric strain %	Deviatoric strain %	$\frac{(\sigma_1 - \sigma_3)}{\sigma_{conf}}$	$\frac{(\sigma_1 - \sigma_3)}{\sigma_m}$
5	0.0	1896.1	0.398	0.0	0.0	0.0	0.000	0.000
6	11.6	1900.0	0.398	0.3	0.0	0.5	0.006	0.000
7	60.9	1916.4	0.398	0.6	0.0	0.9	0.032	0.032
8	159.1	1949.1	0.397	0.9	0.1	1.3	0.084	0.082
9	484.8	2057.7	0.397	1.2	0.1	1.8	0.258	0.236
10	869.5	2185.9	0.395	1.6	0.2	2.3	0.459	0.400
11	1194.4	2294.2	0.395	1.9	0.2	2.8	0.630	0.521
15	2503.1	2730.5	0.389	3.1	0.7	4.3	1.320	0.917
16	2818.4	2835.6	0.387	3.4	0.8	4.7	1.486	0.994
18	3435.9	3041.4	0.385	4.0	0.9	5.6	1.812	1.130
20	4042.0	3243.4	0.382	4.7	1.1	6.5	2.132	1.246
25	5334.6	3674.3	0.375	6.2	1.6	8.5	2.813	1.452
30	6144.6	3944.3	0.369	7.8	2.1	10.7	3.241	1.558
35	6598.1	4095.5	0.363	9.3	2.5	12.7	3.480	1.611
40	6743.9	4144.1	0.360	10.9	2.7	15.0	3.557	1.627
45	6731.3	4139.9	0.357	12.4	3.0	17.1	3.550	1.626
50	6659.5	4115.9	0.355	14.0	3.1	19.5	3.512	1.618
55	6674.6	4121.0	0.355	15.5	3.1	21.7	3.520	1.620
60	6535.0	4074.4	0.354	17.1	3.1	24.1	3.447	1.604
65	6417.5	4035.3	0.354	18.6	3.1	26.4	3.385	1.590
70	6366.1	4018.1	0.355	20.2	3.1	28.8	3.358	1.584
75	6376.0	4021.4	0.356	21.7	3.0	31.1	3.363	1.591
80	6255.8	3981.4	0.357	23.3	3.0	33.5	3.299	1.571
85	6100.9	3929.7	0.358	24.9	2.9	35.9	3.218	1.553
90	6073.8	3920.7	0.358	26.4	2.8	38.2	3.203	1.549
95	6054.2	3914.2	0.360	28.0	2.7	40.7	3.193	1.547
99	5879.1	3855.8	0.361	29.2	2.7	42.5	3.101	1.525

Test 19

State of specimen	PW
Date tested	22/5/81
Confining pressure	1896 kPa
Initial volume	5894 cc
Initial height	327 mm
Weight of specimen	11.7 kg
Water content	20.7 %
Volume of solids	4219 cc

COMPRESSION DATA

Pressure kPa	Time interval	Volume change reading	Volume change cc	corr. Volume cc	Void Ratio e
103	5 min	50.0	0.0	5894.0	0.397
345	5 min	47.8	54.5	5839.5	0.384
690	5 min	45.2	118.8	5775.2	0.369
1034	5 min	43.7	155.9	5738.1	0.360
1379	5 min	42.6	183.2	5710.8	0.354
1896	5 min	41.6	207.9	5686.1	0.348
1896	1.5 h	40.0	247.5	5646.5	0.339

SHEAR DATA

No.	Load cell reading	Force N	Volume change read.	Volume change cc	corr. Volume cc	Axial read.	Height change mm	corr. Height mm	corr. Area cm^2
8	156	0	39.2	267.3	5626.7	800	8.0	319.0	176.0
9	167	550	39.2	267.3	5626.7	900	9.0	318.0	177.0
10	310	7700	39.1	269.8	5624.2	1000	10.0	317.0	177.0
11	391	11750	38.9	274.7	5619.3	1100	11.0	316.0	178.0
15	473	15850	38.4	287.1	5606.9	1500	15.0	312.0	180.0
20	526	18500	38.0	297.0	5597.0	2000	20.0	307.0	182.0
25	581	21250	37.5	309.4	5584.6	2500	25.0	302.0	185.0
30	624	23400	37.0	321.8	5572.3	3000	30.0	297.0	188.0
35	693	268550	36.5	334.1	5559.9	3500	35.0	292.0	190.0
40	727	285550	36.0	346.5	5547.5	4000	40.0	287.0	193.0
45	780	31200	35.5	358.9	5535.1	4500	45.0	282.0	196.0
50	853	34850	34.9	373.7	5520.3	5000	50.0	277.0	199.0
55	905	37450	34.4	386.1	5507.9	5500	55.0	272.0	203.0
60	941	39250	34.0	396.0	5498.0	6000	60.0	267.0	206.0
65	962	40300	33.2	415.8	5478.2	6500	65.0	262.0	209.0
70	1042	44300	33.1	418.3	5475.7	7000	70.0	257.0	213.0
75	1075	45950	32.9	423.2	5470.8	7500	75.0	252.0	217.0
80	1143	48850	32.9	423.2	5470.8	8000	80.0	247.0	222.0
85	1123	48350	32.8	427.7	5468.3	8500	85.0	242.0	226.0
90	1247	54550	32.7	428.2	5465.8	9000	90.0	237.0	231.0
95	1292	56800	32.7	428.2	5465.8	9500	95.0	232.0	236.0
100	1343	59350	32.7	428.2	5465.8	10000	100.0	227.0	241.0

Test no. 19

SHEAR DATA (cont.)

No.	Deviatoric stress kPa	Volumetric stress kPa	Void ratio e	Axial strain %	Volumetric strain %	Deviatoric strain %	$\frac{(\sigma_1-\sigma_3)}{\sigma_{conf}}$	$\frac{(\sigma_1-\sigma_3)}{\sigma_m}$
8	0.0	1896.1	0.334	0.0	0.0	0.0	0.000	0.000
9	31.1	1906.5	0.334	0.3	0.0	0.5	0.016	0.016
10	434.0	2040.8	0.333	0.6	0.1	0.9	0.229	0.213
11	660.8	2116.4	0.332	0.9	0.1	1.3	0.349	0.312
12	799.5	2162.6	0.331	1.3	0.2	1.9	0.422	0.370
13	830.5	2172.9	0.331	1.6	0.2	2.3	0.438	0.382
14	856.1	2181.5	0.330	1.9	0.3	2.7	0.452	0.392
15	882.0	2190.1	0.329	2.2	0.4	3.1	0.465	0.413
20	1014.7	2234.3	0.327	3.8	0.5	5.5	0.535	0.454
25	1149.1	2279.1	0.324	5.3	0.8	7.6	0.606	0.504
30	1247.2	2311.8	0.321	6.9	1.0	9.9	0.658	0.540
35	1410.1	2366.1	0.318	8.5	1.2	12.2	0.744	0.596
40	1477.0	2388.4	0.315	10.0	1.4	14.3	0.779	0.618
45	1589.6	2426.0	0.312	11.6	1.6	16.6	0.838	0.655
50	1748.7	2479.0	0.309	13.2	1.9	18.9	0.922	0.705
55	1849.4	2512.6	0.306	14.7	2.1	21.0	0.975	0.736
60	1906.1	2531.5	0.303	16.3	2.3	23.3	1.005	0.753
65	1927.4	2538.6	0.299	17.9	2.6	25.6	1.017	0.759
70	2079.2	2589.2	0.298	19.4	2.7	27.8	1.097	0.803
75	2116.6	2601.6	0.297	21.0	2.8	30.1	1.116	0.814
80	2205.5	2631.3	0.297	22.6	2.8	32.5	1.163	0.838
85	2139.7	2609.3	0.296	24.1	2.9	34.7	1.129	0.820
90	2365.3	2684.5	0.296	25.7	2.9	37.1	1.248	0.881
95	2410.9	2699.7	0.296	27.3	2.9	39.5	1.272	0.893
100	2464.9	2717.7	0.296	28.8	2.9	41.8	1.300	0.907

Test 17

State of specimen	AW
Date tested	15/5/81
Confining pressure	1896 kPa
Initial volume	5894 cc
Initial height	327 mm
Weight of specimen	10.5 kg
Water content	4.7 %
Volume of solids	3772 cc

COMPRESSION DATA

Pressure kPa	Time interval	Volume change reading	Volume change cc	corr. Volume cc	Void Ratio e
103	5 min	74.4	0.0	5894.0	0.563
345	5 min	68.4	148.5	5745.5	0.523
690	5 min	60.5	344.0	5550.0	0.472
1034	5 min	54.6	490.1	5403.9	0.433
1379	5 min	50.5	591.5	5302.5	0.406
1896	5 min	45.6	712.8	5181.2	0.374
1896	1.5 h	43.0	777.2	5116.8	0.357

SHEAR DATA

No.	Load cell reading	Force N	Volume change read.	Volume change cc.	corr. Volume cc	Axial read.	Height change mm	corr. Height mm	corr. Area cm^2
10	172	0	42.6	787.1	5106.9	1000	10.0	317.0	161.0
11	198	1300	42.5	789.5	5104.5	1100	11.0	316.0	162.0
12	213	2050	42.5	789.5	5104.5	1200	12.0	315.0	162.0
13	230	2900	42.3	794.5	5099.5	1300	13.0	314.0	162.0
14	234	3100	42.3	794.5	5099.5	1400	14.0	313.0	163.0
15	243	3550	42.3	794.5	5099.5	1500	15.0	312.0	164.0
16	265	4650	42.1	799.4	5094.6	1600	16.0	311.0	164.0
17	278	5300	41.8	806.9	5087.1	1700	17.0	310.0	164.0
18	356	9200	41.4	816.8	5077.3	1800	18.0	309.0	164.0
19	439	13350	40.6	836.6	5057.4	1900	19.0	308.0	164.0
20	487	15750	40.3	844.0	5050.0	2000	20.0	307.0	165.0
25	664	24600	37.4	915.8	4978.2	2500	25.0	302.0	165.0
30	871	34950	34.8	980.1	4913.9	3000	30.0	297.0	166.0
35	1047	43750	32.6	1034.6	4859.4	3500	35.0	292.0	166.0
40	1215	52150	30.7	1081.6	4812.4	4000	40.0	287.0	168.0
45	1372	60000	28.9	1126.1	4767.9	4500	45.0	282.0	169.0
50	1511	66950	27.6	1158.3	4735.7	5000	50.0	277.0	171.0
55	1625	72650	26.3	1190.5	4703.5	5500	55.0	272.0	173.0
60	1732	78000	25.3	1215.2	4678.8	6000	60.0	267.0	175.0
65	1822	82500	24.6	1232.6	4661.5	6500	65.0	262.0	178.0
70	1922	87500	24.0	1247.4	4646.6	7000	70.0	257.0	181.0
75	1965	89650	23.5	1259.8	4634.2	7500	75.0	252.0	184.0
80	2048	93800	23.1	1269.7	4624.3	8000	80.0	247.0	187.0
85	2072	95000	22.8	1277.1	4616.9	8500	85.0	242.0	191.0
90	2090	95900	22.6	1282.1	4611.9	9000	90.0	237.0	195.0
95	2166	99700	22.3	1289.5	4604.5	9500	95.0	232.0	199.0
100	2196	101200	22.2	1292.0	4602.0	10000	100.0	227.0	203.0

Test no. 17

SHEAR DATA (cont.)

No.	Deviatoric stress kPa	Volumetric stress kPa	Void ratio e	Axial strain %	Volumetric strain %	Deviatoric strain %	$(\sigma_1-\sigma_3)/\sigma_{conf}$	Norm. Vol. stress
10	0.0	1896.1	0.354	0.0	0.0	0.0	0.000	1.000
11	80.5	1922.9	0.353	0.3	0.1	0.4	0.043	1.014
12	126.5	1938.3	0.353	0.6	0.1	0.9	0.067	1.022
13	178.6	1955.6	0.352	1.0	0.2	1.4	0.094	1.031
14	190.3	1959.5	0.352	1.3	0.2	1.9	0.100	1.033
15	217.2	1968.5	0.352	1.6	0.2	2.3	0.115	1.038
16	283.9	1990.7	0.351	1.9	0.2	2.8	0.150	1.050
17	323.0	2003.8	0.349	2.2	0.4	3.1	0.170	1.057
18	559.9	2082.7	0.346	2.5	0.6	3.5	0.295	1.098
19	813.0	2167.1	0.341	2.8	1.0	3.7	0.429	1.143
20	957.5	2215.3	0.339	3.2	1.1	4.3	0.505	1.168
25	1492.3	2393.5	0.320	4.7	2.5	5.8	0.787	1.262
30	2112.4	2600.2	0.303	6.3	3.8	7.6	1.114	1.371
35	2628.9	2772.4	0.289	7.9	4.8	9.5	1.387	1.462
40	3110.1	2932.8	0.276	9.5	5.8	11.4	1.640	1.547
45	3548.8	3079.0	0.264	11.0	6.6	13.2	1.872	1.624
50	3916.0	3201.4	0.256	12.6	7.3	15.3	2.065	1.688
55	4201.3	3296.5	0.247	14.2	7.9	17.4	2.216	1.739
60	4451.2	3379.8	0.241	15.8	8.4	19.5	2.348	1.783
65	4637.0	3441.8	0.236	17.4	8.7	21.8	2.446	1.815
70	4839.6	3509.3	0.232	18.9	9.0	23.9	2.552	1.851
75	4875.0	3521.1	0.229	20.5	9.3	26.1	2.571	1.857
80	5010.2	3566.2	0.226	22.0	9.5	28.3	2.642	1.881
85	4979.5	3555.9	0.224	23.7	9.6	30.8	2.626	1.875
90	4928.1	3538.8	0.223	25.2	9.7	33.0	2.599	1.866
95	5023.4	3570.6	0.221	26.8	9.8	35.3	2.649	1.883
100	4991.8	3560.0	0.220	28.4	9.9	37.7	2.632	1.878

APPENDIX C

MISCELLANEOUS

C1 Membrane Correction

Membrane correction factors were obtained using the method outlined by Bishop and Henkel (1962). The correction, σ_r, to the measured compression strength of the specimen is

$$\sigma_r = \frac{\pi D.M.\varepsilon(1-\varepsilon)}{a_o}$$

where D is the initial diameter of the specimen, M is the compression modulus of the rubber membrane, per unit width, ϵ is the axial strain, and a_o the initial cross-sectional area of the specimen.

According to Bishop and Henkel (1962), the compression modulus M cannot be measured directly on a thin membrane, but its value may be reasonably assumed to be similar to that measured in extension.

Three 150 mm membranes were used in the tests. The correction factors are as follows:

Type of membrane	Thickness	Correction factor at 20 % strain
standard	0.3 mm	0.153 kPa
latex covered	1.8 mm	0.703 kPa
neoprene	0.8 mm	0.806 kPa
Total		1.7 kPa

C2 Calibration of Load Cell

The load cell used in the experiments was calibrated against a certified-accurate Tinius-Olsen Universal Testing Machine. A known load was applied to the load cell and the corresponding reading was recorded. A graph of known load versus load cell reading was plotted in order to obtain the relationship between these two values. The graph is shown in Figure C1. The relationship is as follows:

$$\text{Load Cell} \times 50 = \text{Applied Load (Newtons)}$$

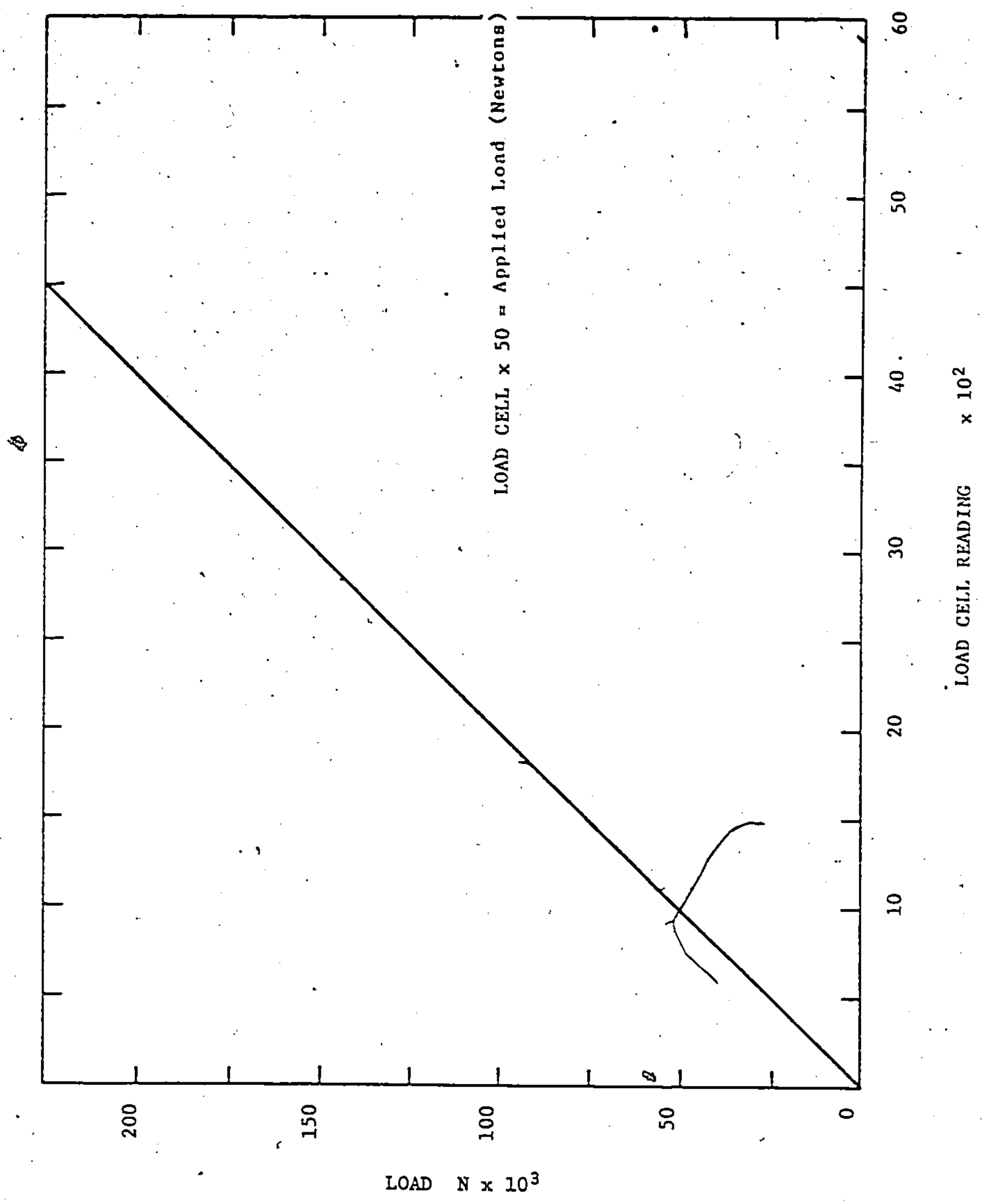

Figure C1 Load Cell Calibration.

C3 Slaking Characteristics of Queenston Shale

The slaking Characteristics of Quenston Shale are presented in Figure C2. The graph shows the water content of specimens of shale after different saturation times. According to Morgenstern an Eigenbrod (1974), all materials eventually reach a final water content equal to their liquid limits. Queenston Shale reaches an almost constant value of 8 % water content, although its liquid limit is 20.2.

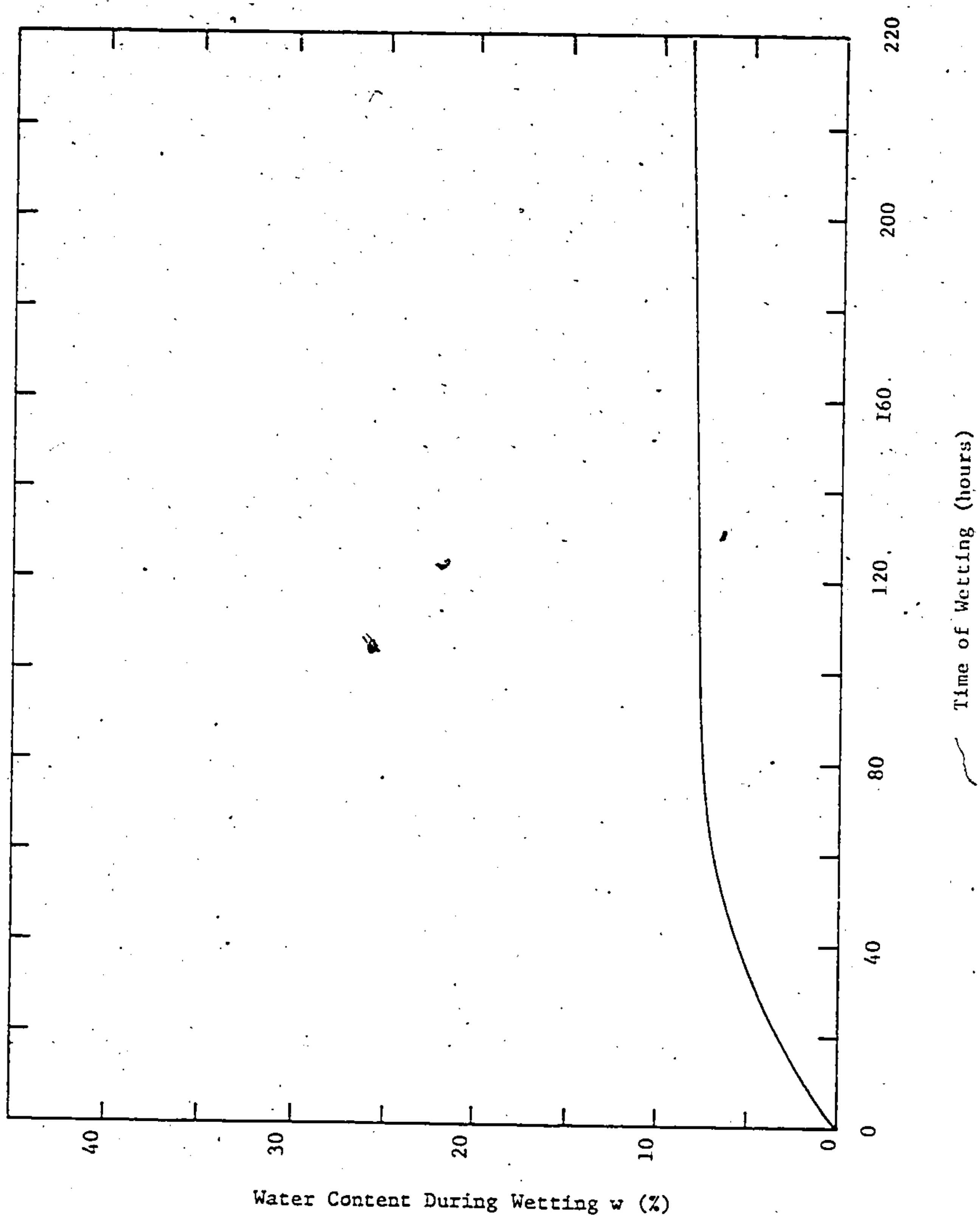

Figure C2 Change of water content with time of wetting.
(According to Morgenstern and Eigenbrod 1974)

C4 X-ray Diffraction of Queenston Shale

X-ray Diffraction is a method for identification of fine-grained soil minerals. It consists of bombarding a finely ground sample of material with electrons. When the electrons reach the minerals on the atomic level, they either knock specific electrons from energy levels within the atoms, or lose their energy in the intense electrical fields surrounding the atomic nuclei. The result is two kinds of radiation. The first, due to electron displacement, is a specific radiation uniquely defining the bombarded mineral. The second, due to the loss of energy in the electrical field, results in an easily recognized background radiation dependent on the intensity and voltage of the source of electron bombardment.

Figure C3 shows the X-ray pattern of Queenston Shale. The 2θ angle corresponds to the wavelength of the minerals. The material is composed mainly of quartz, illite, mica, kaolin, chlorite, hematite, pyrite, and some carbonates.

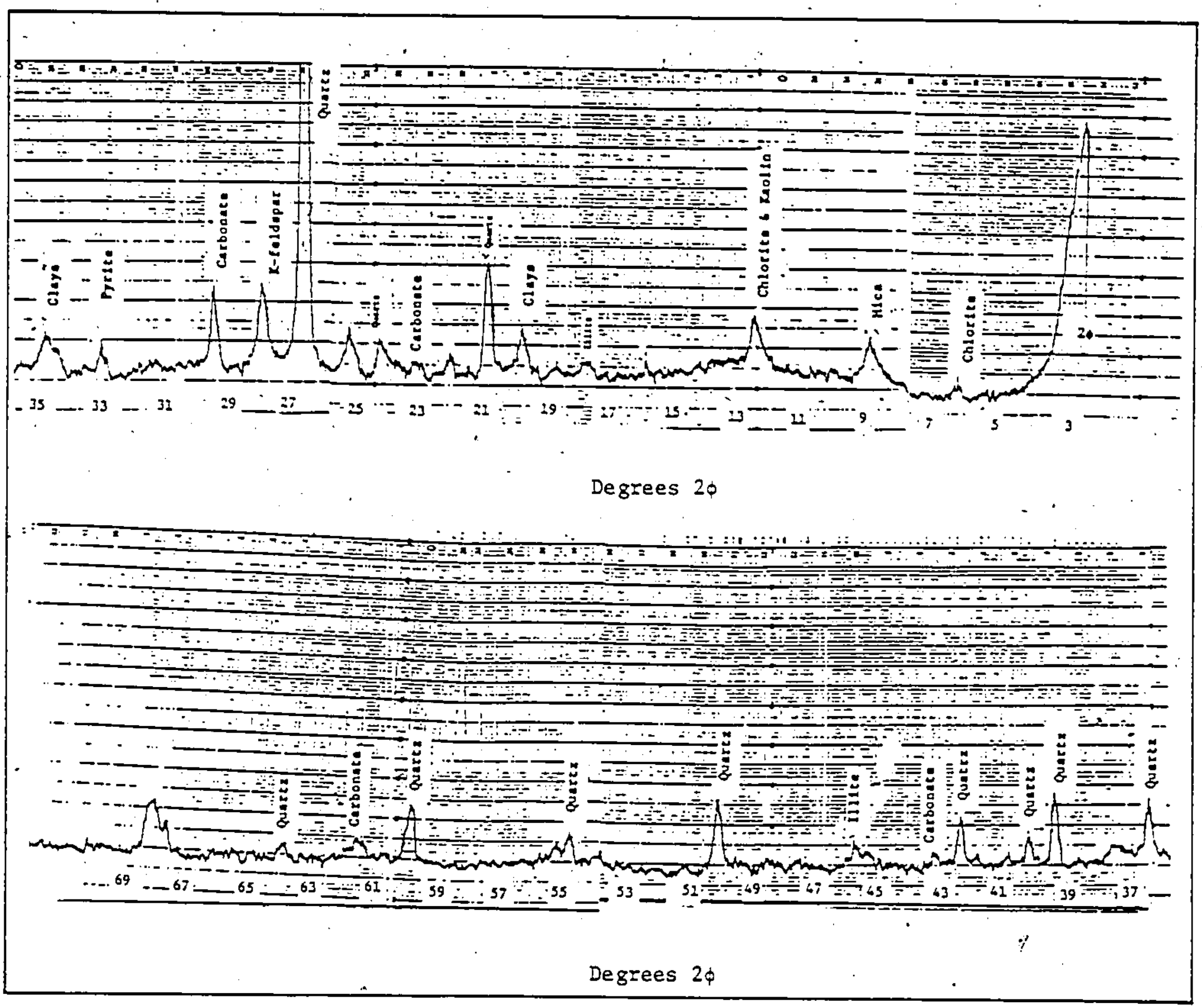

Figure C3 X-ray Diffraction Pattern of Queenston Shale.

C5 Janbu's (1967) Tangent Modulus Curves

The graphs using Janbu's (1967) method for dry weathered (25D), saturated weathered (25W), dry natural (N), saturated natural (NW), dry powdered (PD), and saturated powdered (PW) specimens are presented in the following pages.

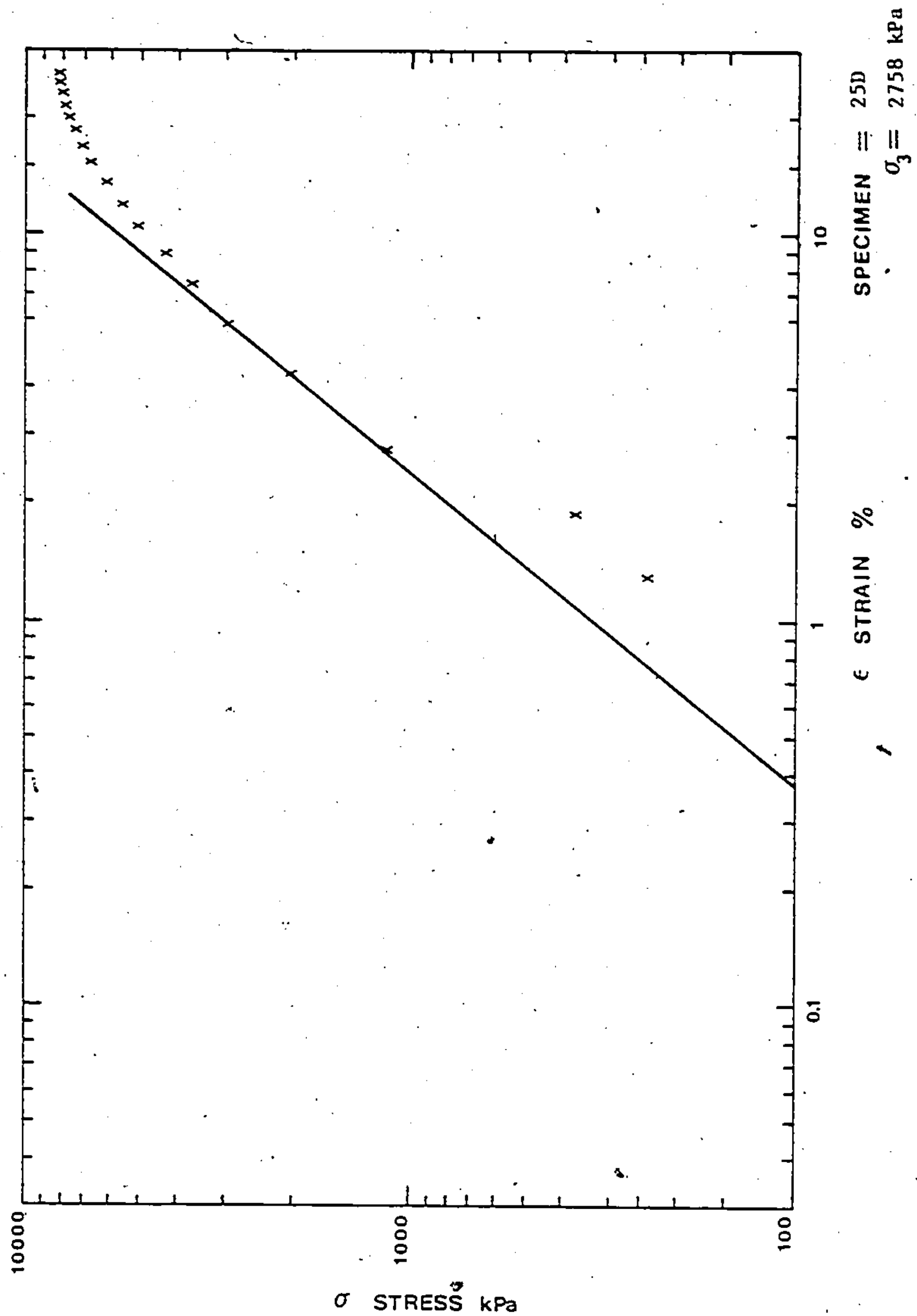

Figure C4 a) Tangent modulus curve.

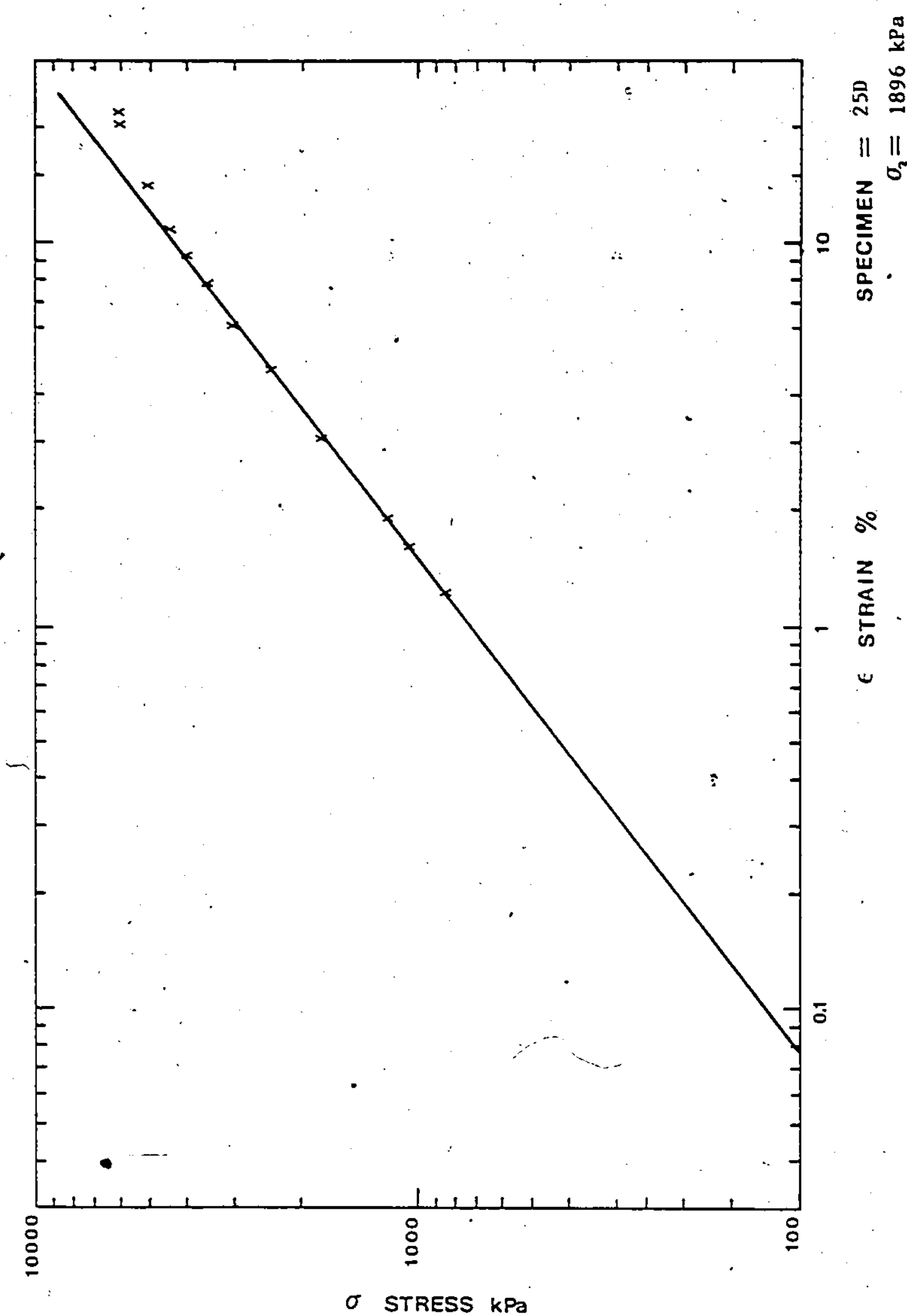

Figure C4 b) Tangent modulus curve.

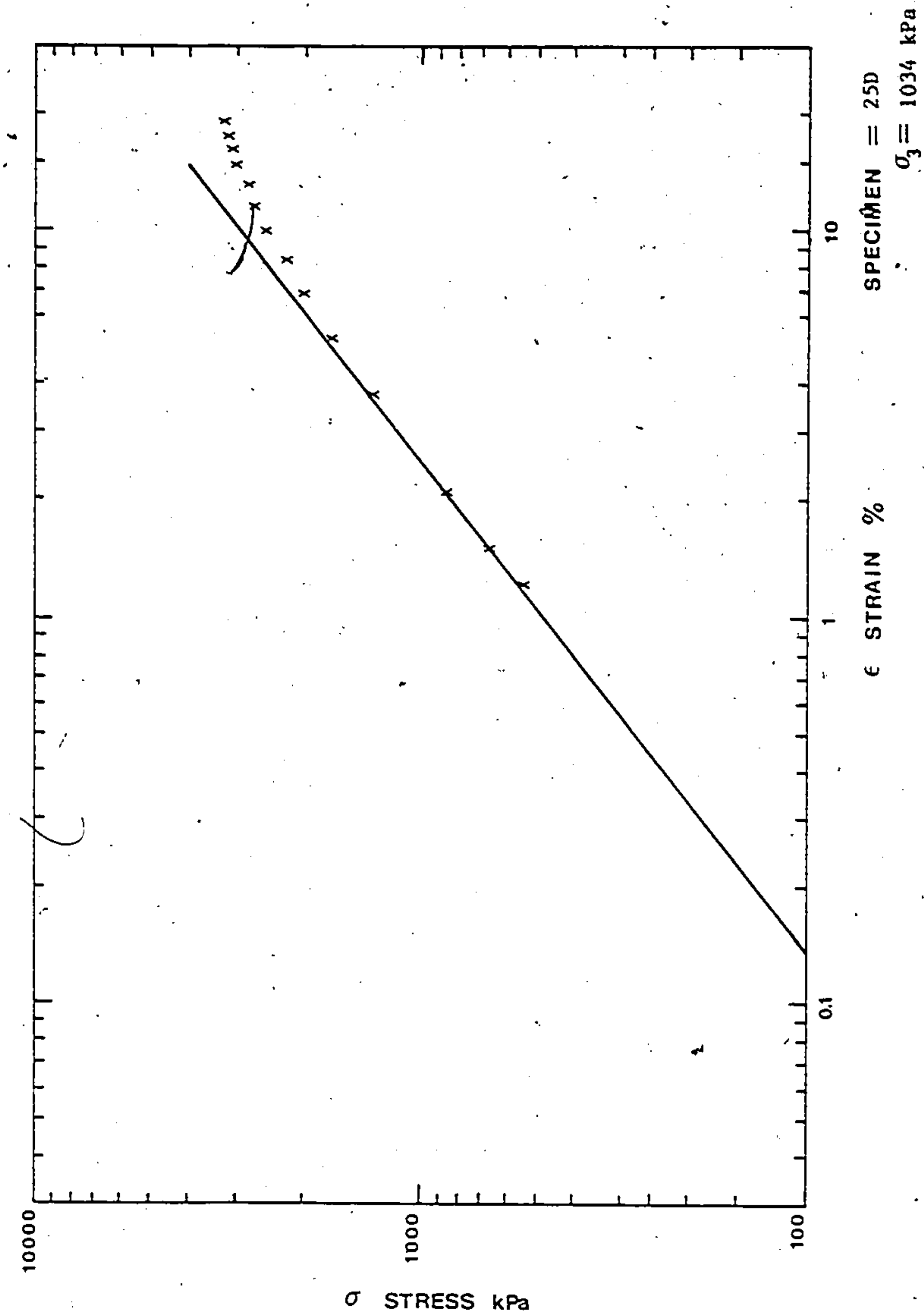

Figure C4 c) Tangent modulus curve.

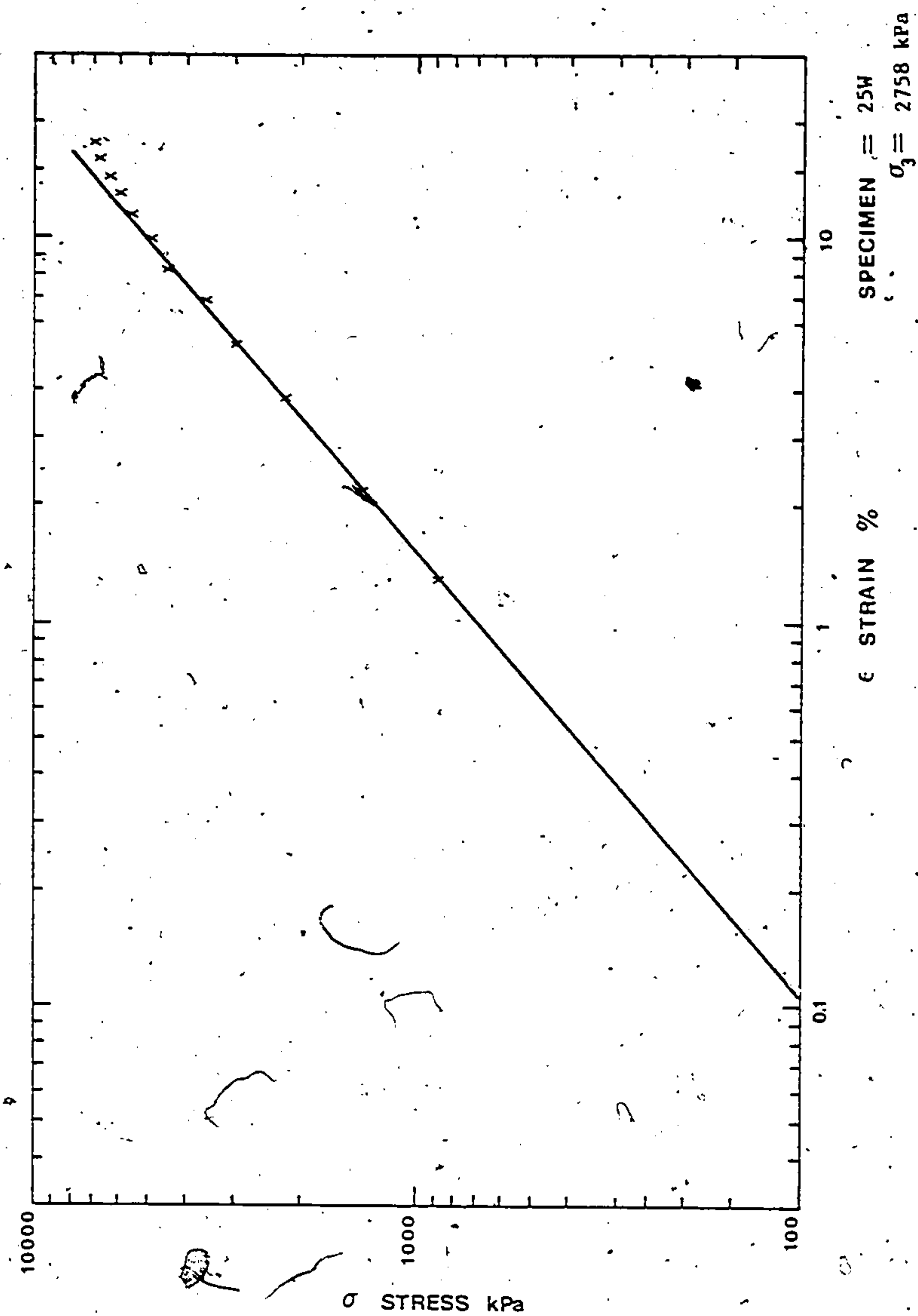

Figure C4 d) Tangent modulus curve.

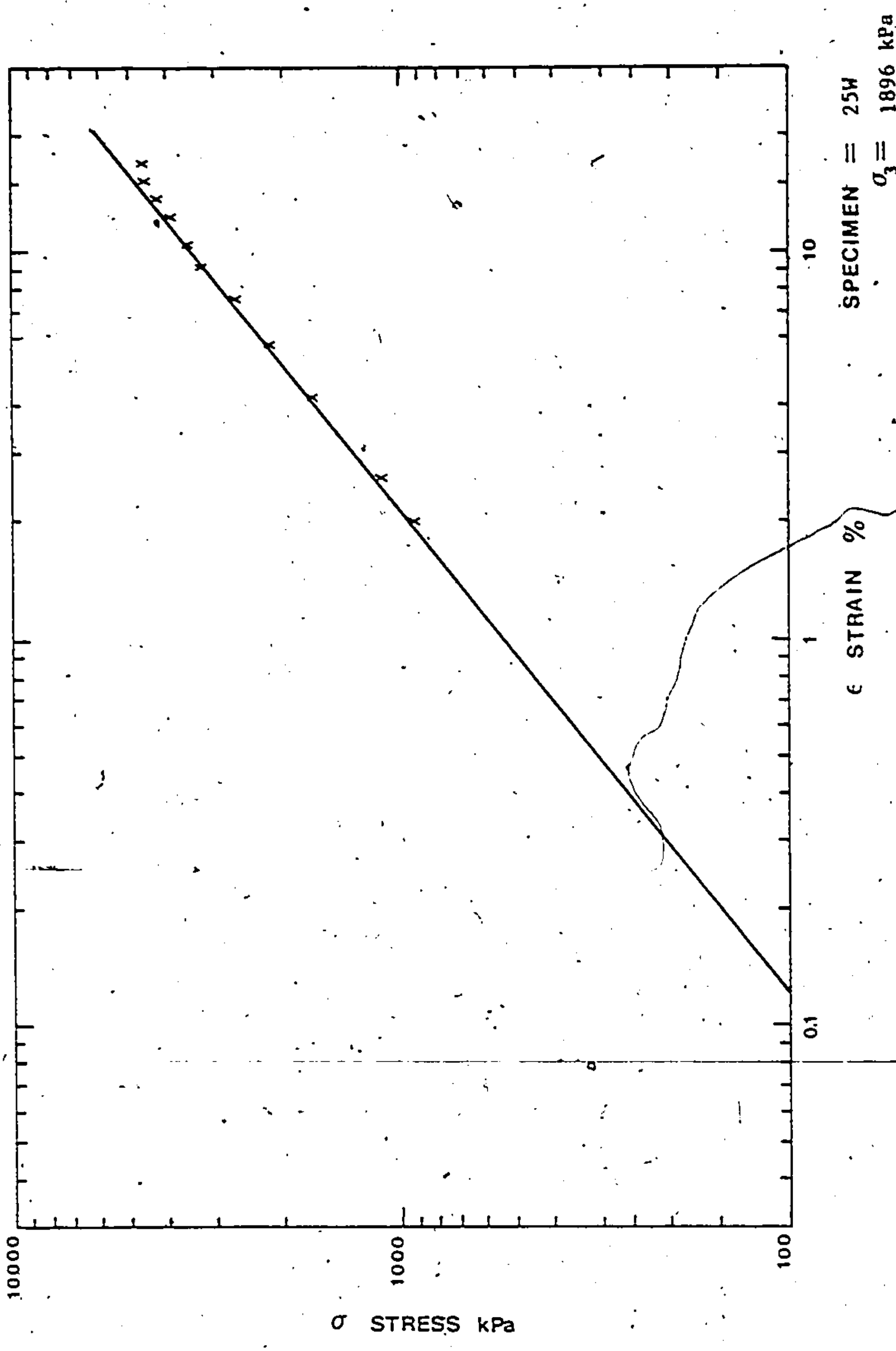

Figure C4 e) Tangent modulus curve.

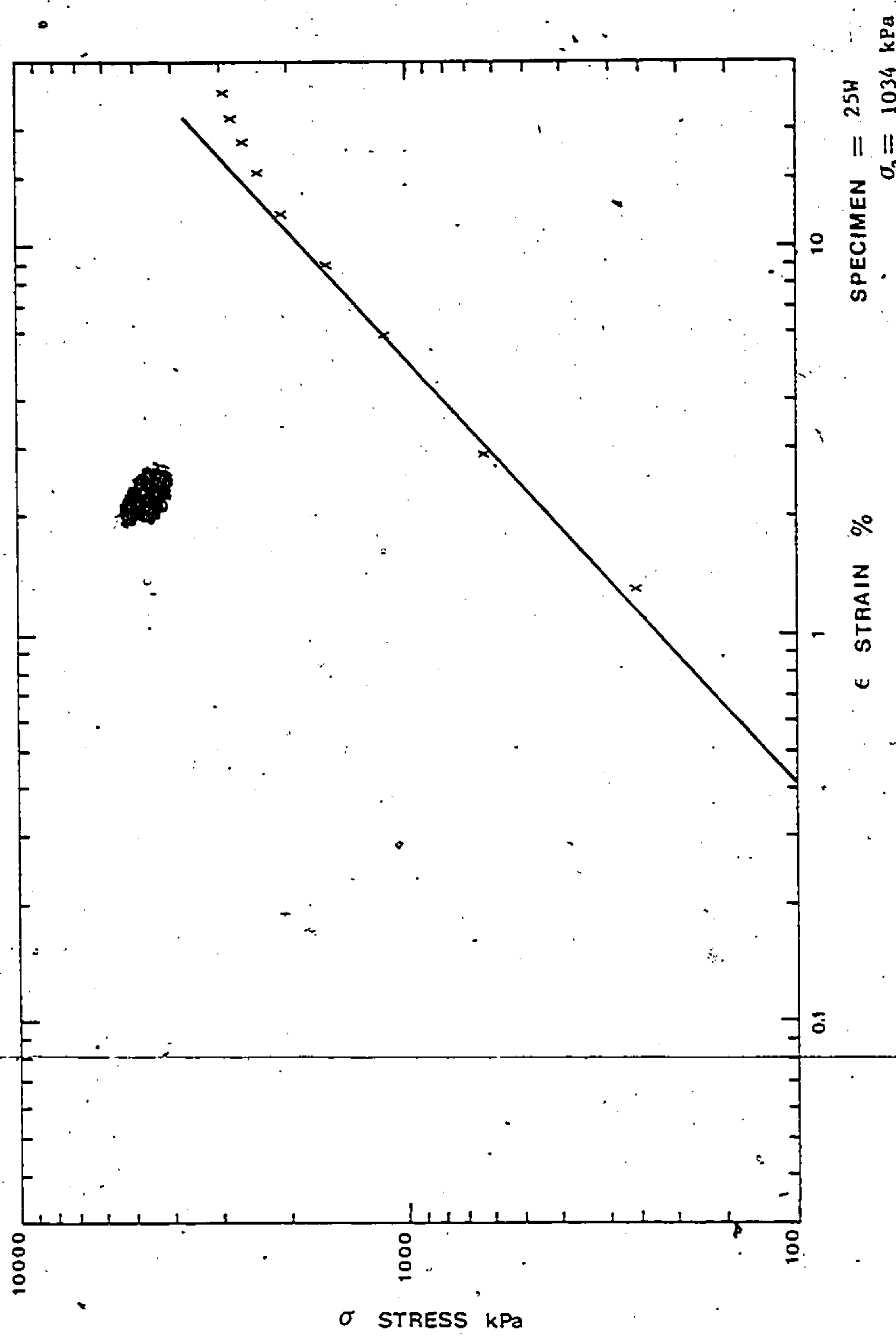

Figure C4 f) Tangent modulus curve.

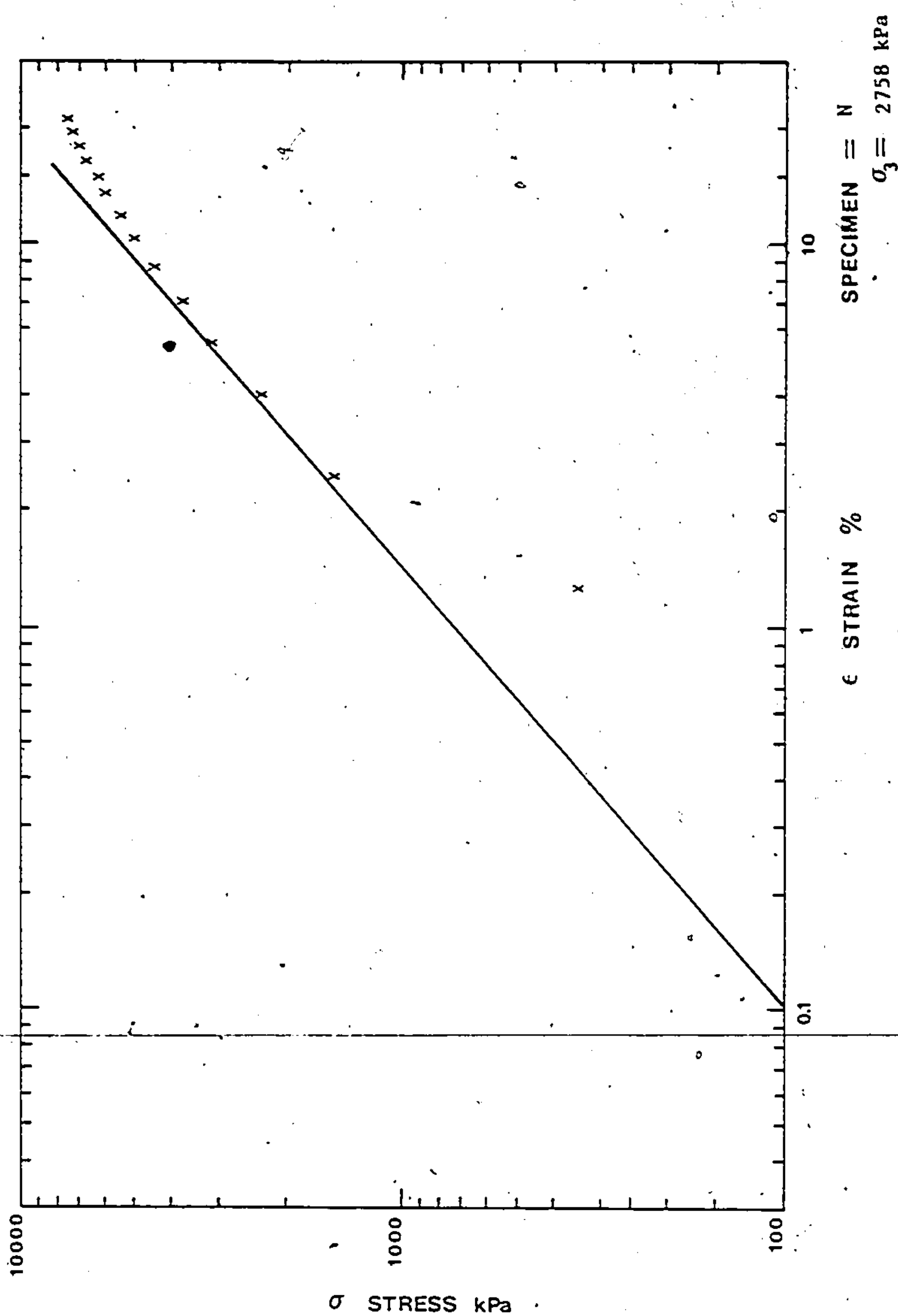

Figure C4 g) Tangent modulus curve.

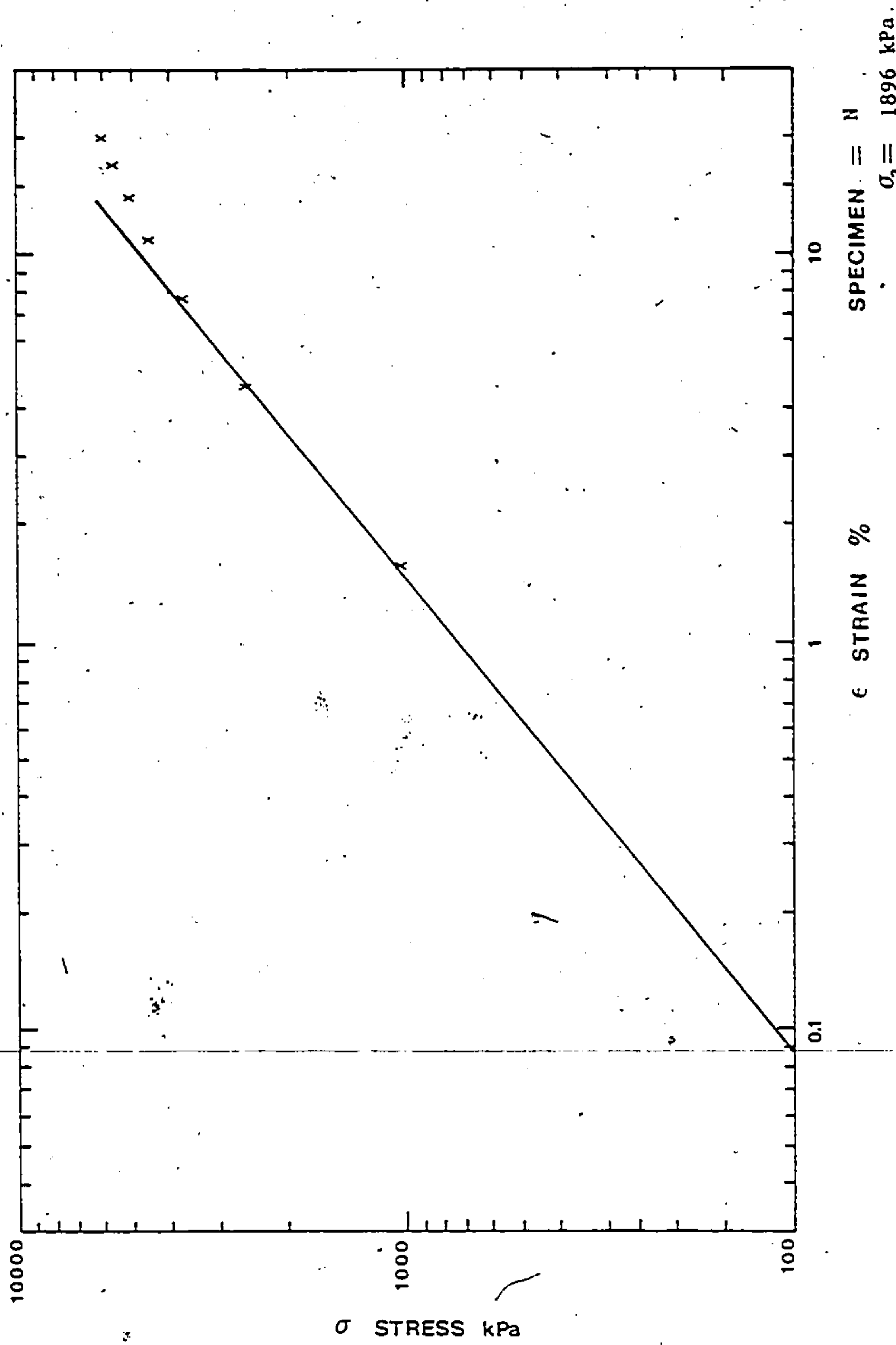

Figure C4 h) Tangent modulus curve.

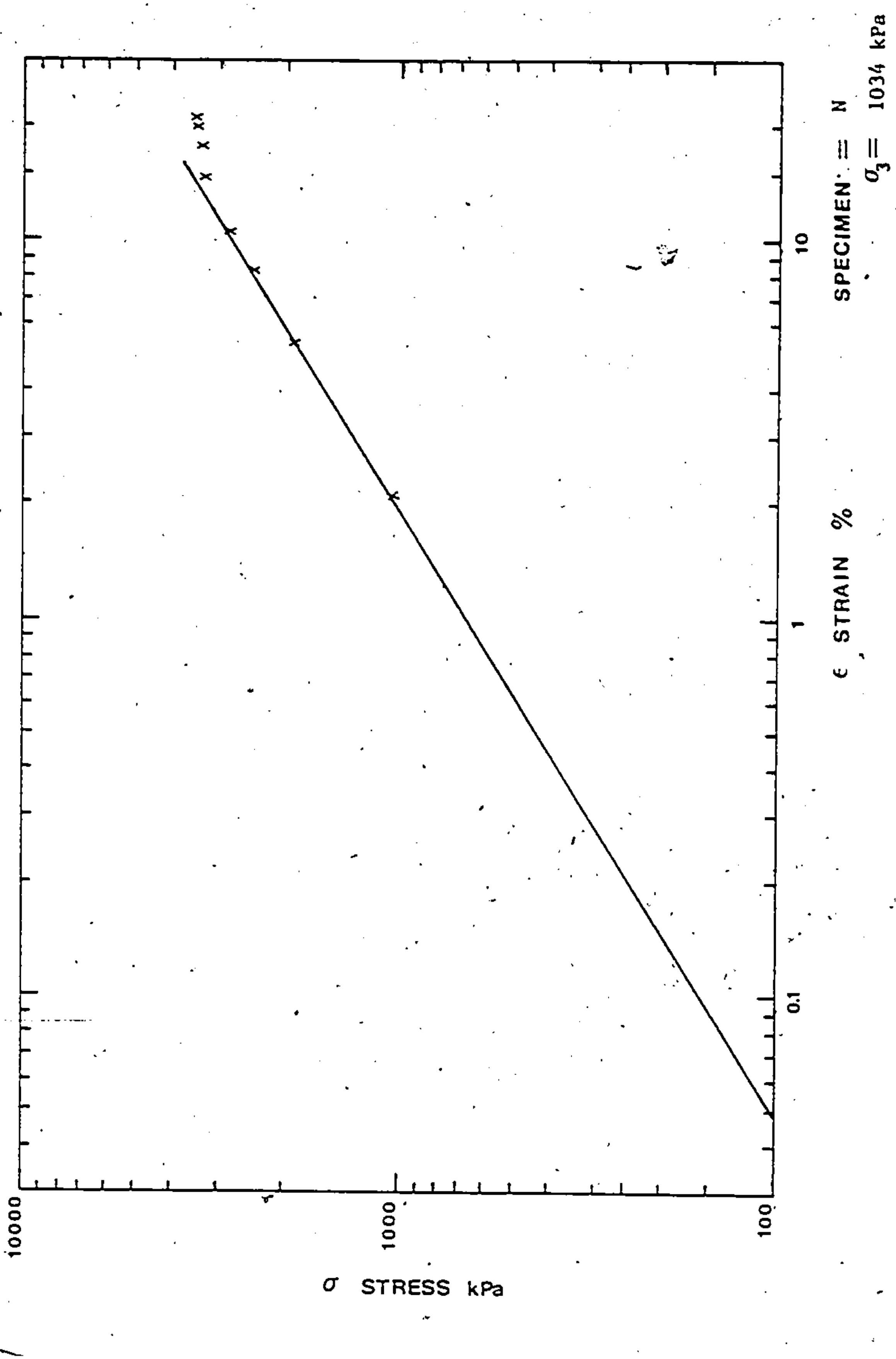

Figure C4 i) Tangent modulus curve.

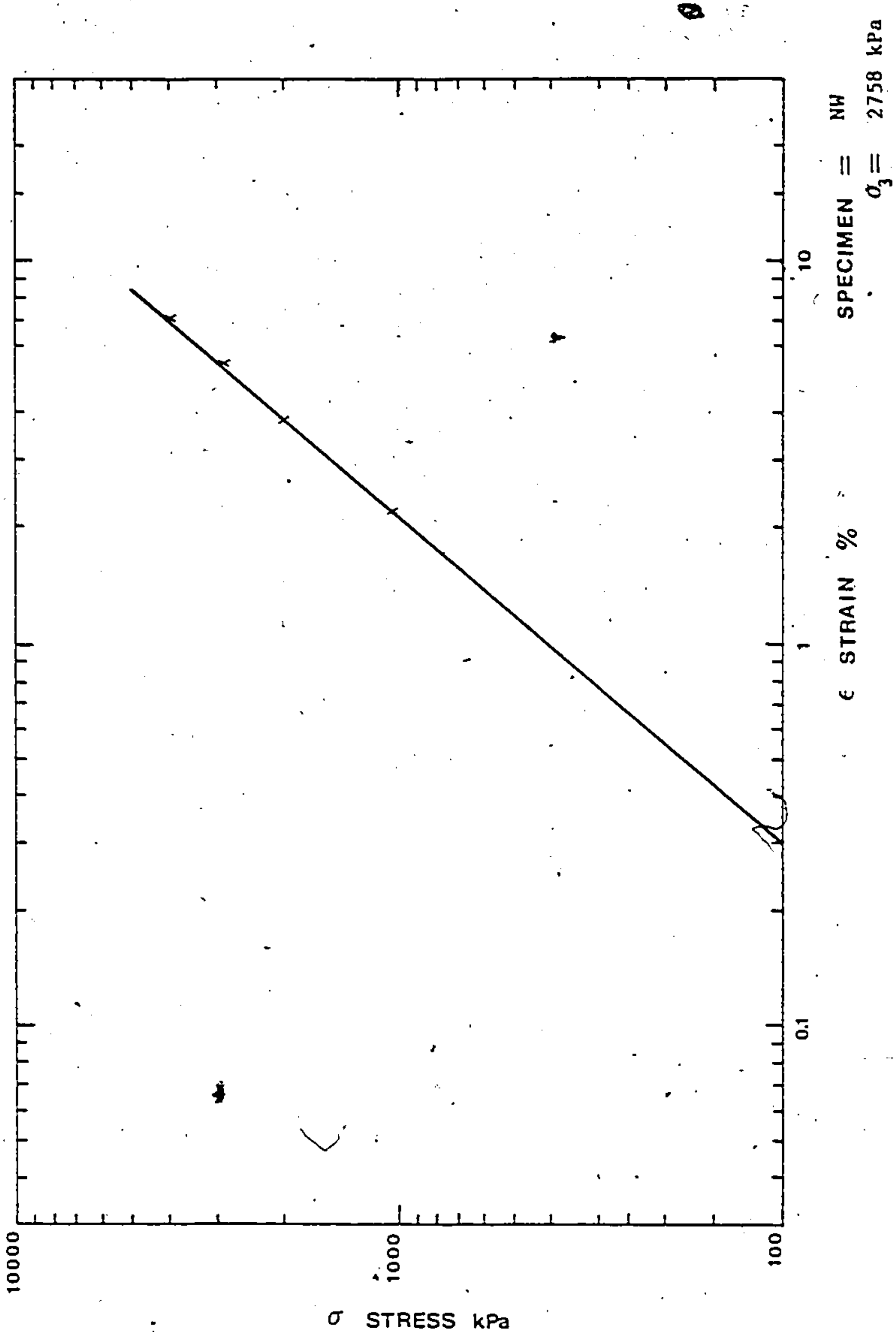

Figure C4 j) Tangent modulus curve.

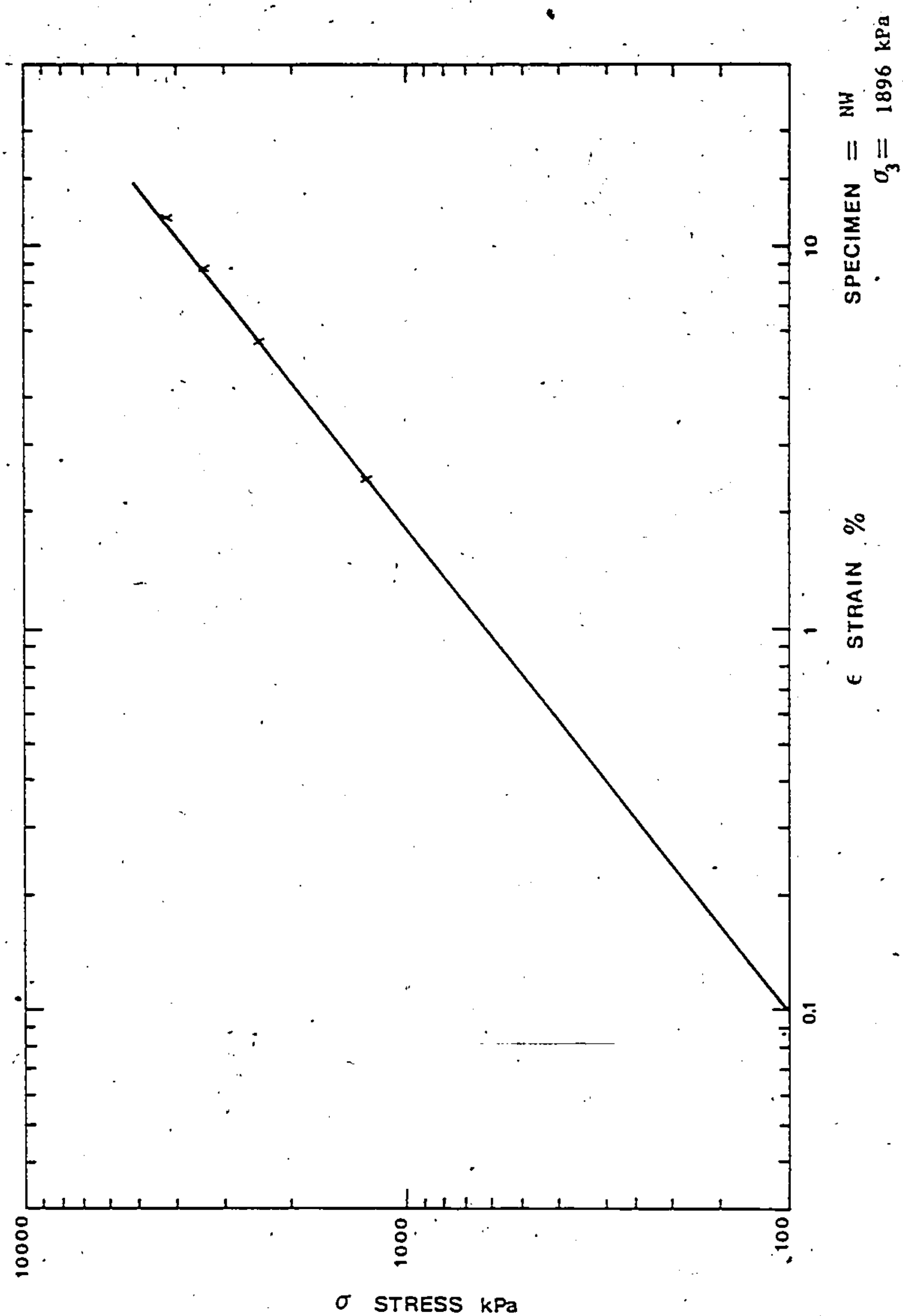

Figure C4 k) Tangent modulus curve.

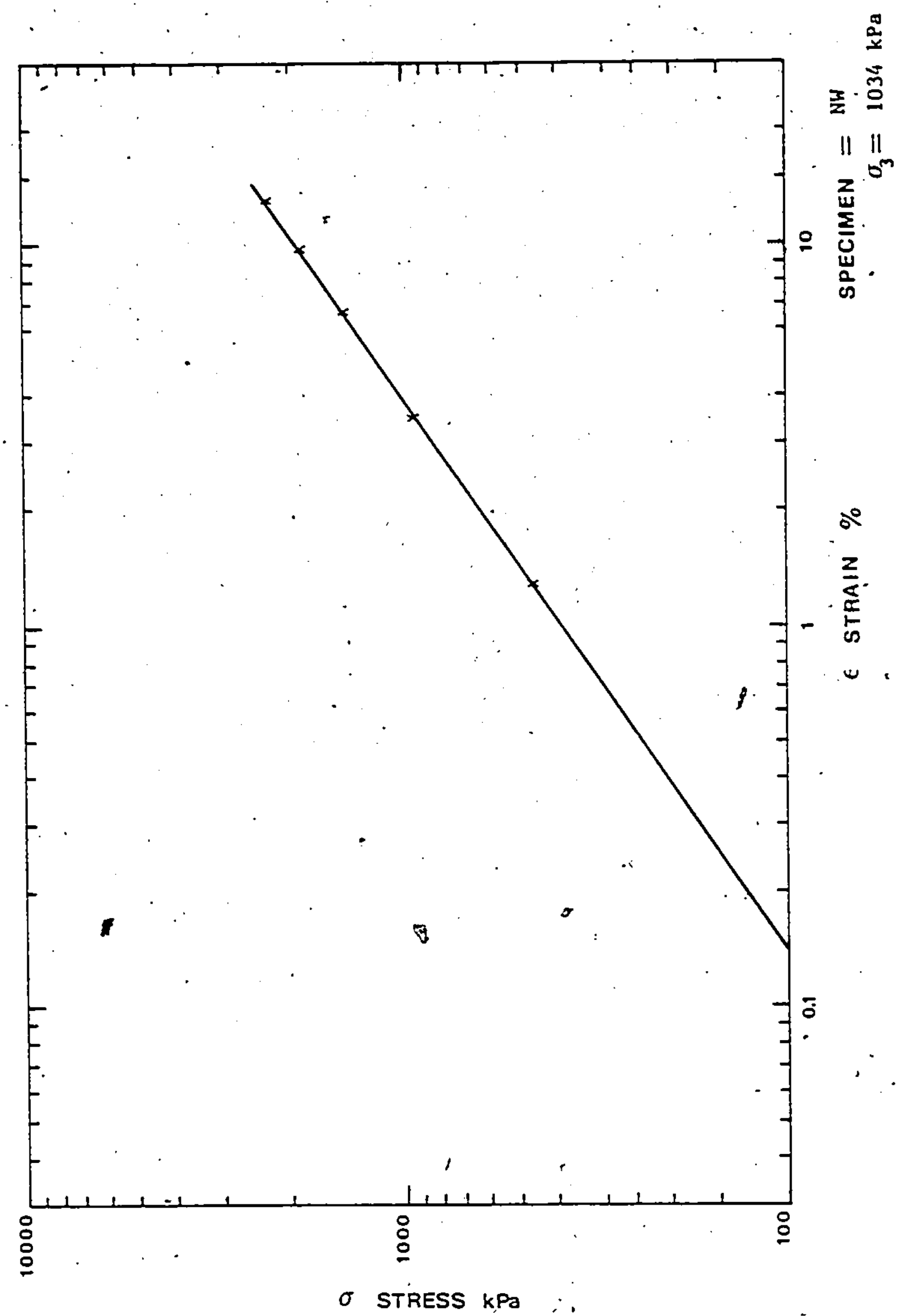

Figure C4 1) Tangent modulus curve.

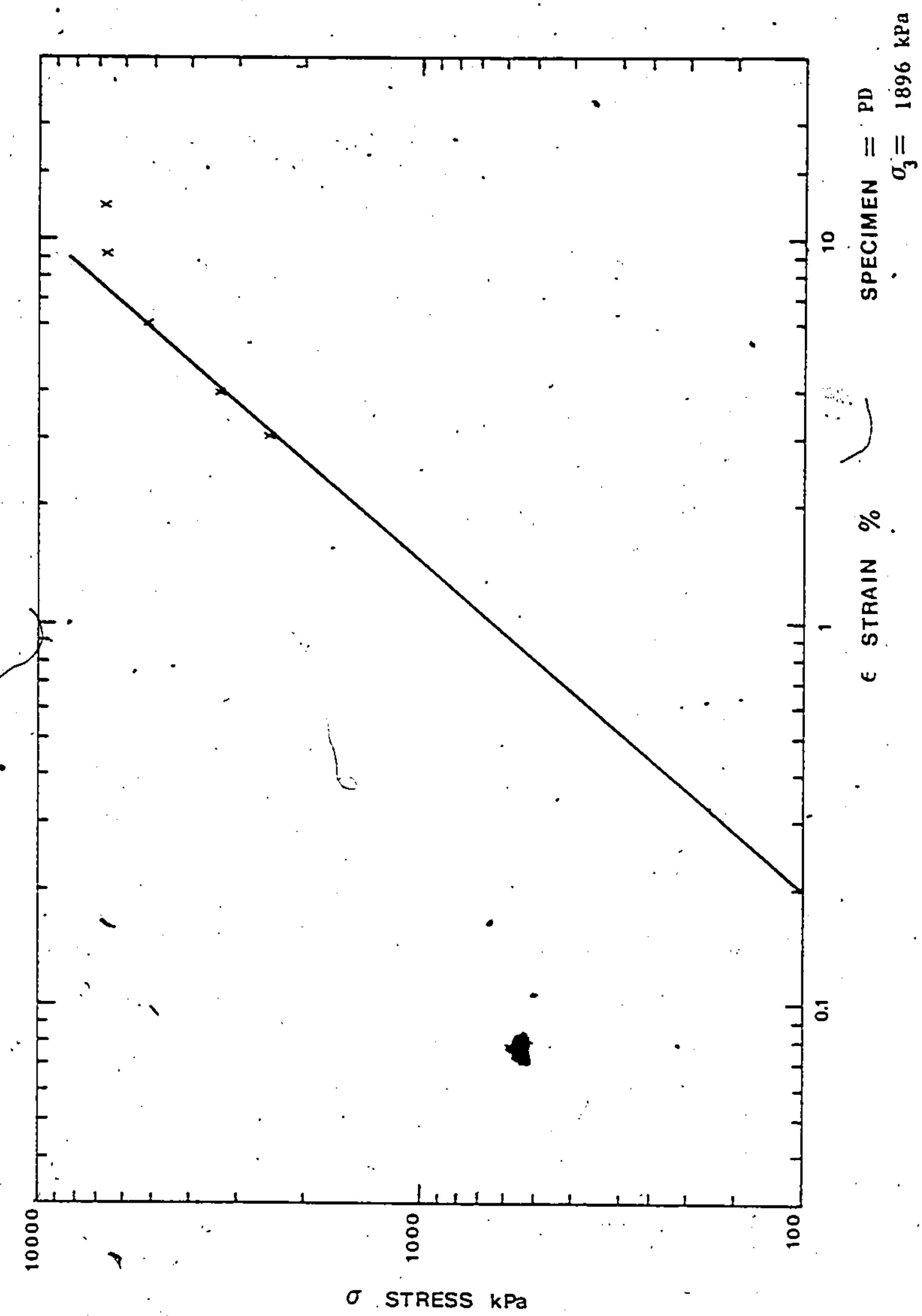

Figure C4 m) Tangent modulus curve.

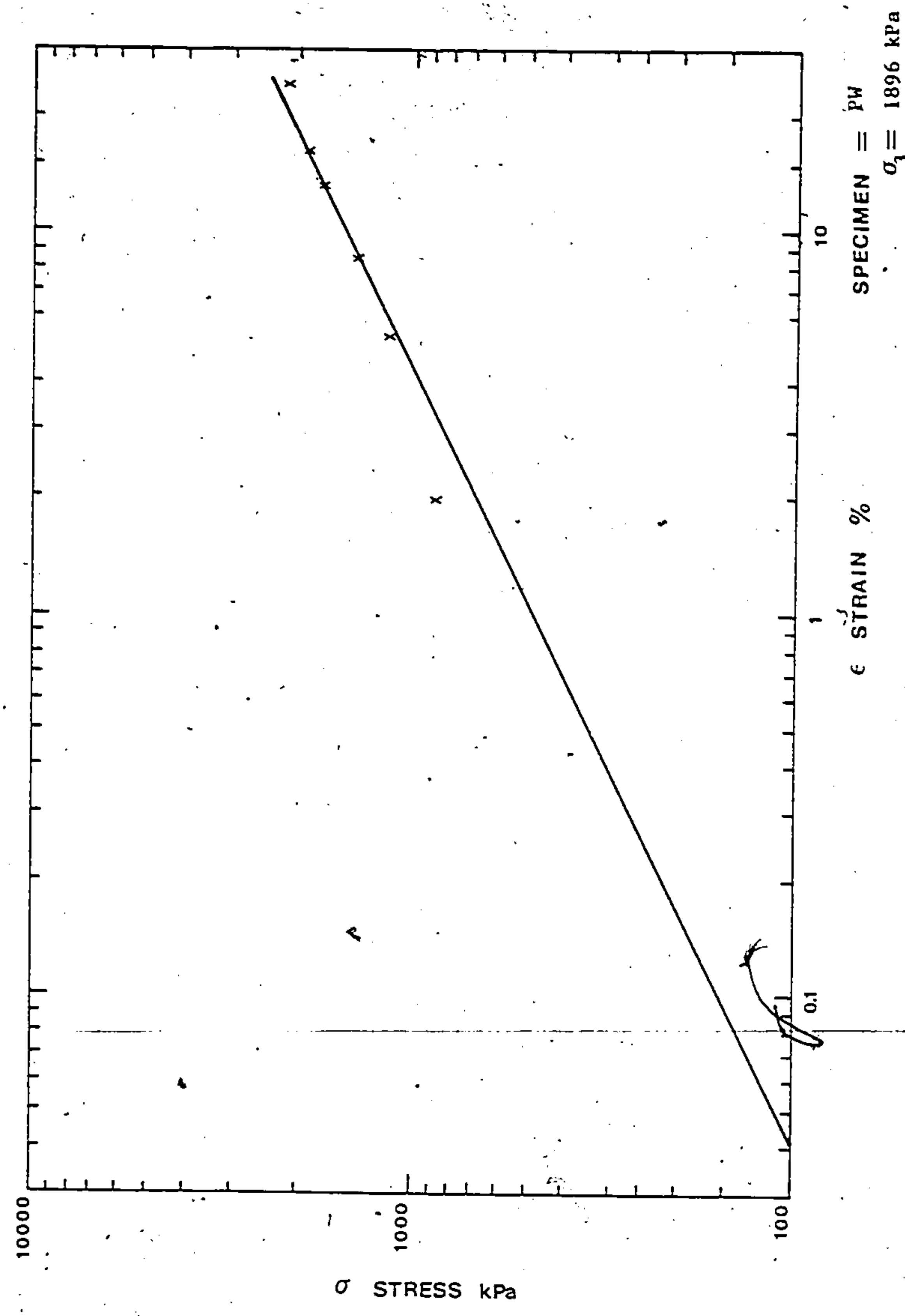

Figure C4 n) Tangent modulus curve.

APPENDIX D

VOLUME CHANGE CORRECTION EQUATIONS

D.1 Taylor (1948)

In order to determine the volume change component of shear strength of a dense sand in a direct shear test, Taylor (1948) derived the following expression:

$$\tau_e = \sigma_n \cdot dh/dx \qquad \text{-D.1}$$

in which τ_e is the shear stress required to provide energy for expansion, σ_n is the applied normal stress, dx is the increment of shear deformation, and dh is the corresponding increment in thickness of the sample.

D.2 Bishop (1954)

Bishop (1954) derived a corresponding expression

$$\sigma_e = \sigma_3 \cdot d\epsilon_{vol}/d\epsilon_a \qquad \text{-D.2}$$

in which σ_3 is the confining pressure, $d\epsilon_{vol}$ is the increment of volumetric strain, and $d\epsilon_a$ is the increment of axial strain, to determine the portion of the applied deviator stress in a triaxial compression test which must be applied to provide energy for sample expansion.

D.3 Rowe (1962)

Rowe (1962) derived an alternate expression for correcting the deviator stress for volume change effects. The expression is as follows:

$$\sigma_c = \sigma_1 \cdot 1/(1 + d\epsilon_{vol}/d\epsilon_a) \qquad \text{D.3}$$

where σ_1 is the maximum principal stress, $d\epsilon_{vol}$ is the increment of volumetric strain, and $d\epsilon_a$ is the increment of axial strain.